

Flexible Continuous Controlled Smart Antenna Platform

Author

Liu Yao

Supervisor

Dr. Paul O'Leary

Michael McCarthy

A report submitted toward the award of
Master of Science in Electronic Engineering

Department of Engineering Technology

Waterford Institute of Technology,

Ireland.

June 2012.

Declaration

I hereby declare that this report is entirely my own work and does not contain material previously published by any other author, except where due reference or acknowledgement has been made. Furthermore, I declare that this report has not previously been submitted to any other institution for any other academic award.

Lin Yao

Acknowledgements

I would like to thank Dr. Paul O'Leary and Michael McCarthy for their direction, assistance and guidance. Their help was not only related to academic issues but also to daily life and bureaucracy. This project could never have been completed without their knowledge, patience, kindness and selflessness.

I also wish to thank Dr. Paul Barry, Prof. Fu, Dr. Mícheál ÓhEigeartaigh and Helen Kang for their efforts related to bureaucratic procedures.

Special thanks should be given to my student colleagues who helped me in many ways.

Finally, words alone cannot express the thanks I owe to Ms. Zhang, my mother, and Mr. Liu, my father, for their financial support and encouragement.

Abstract

This thesis introduces the origin and subsequent development of smart antennas, up to the present day status of R&D test platform research. A novel, flexible, low-cost, easy-to-use platform prototype was developed and is described in this thesis. The prototype is based on quadrature modulators, D/A quadrature control converters and low-speed synthesis control. The prototype was put to the test with four antenna elements at a 2.4GHz operating frequency. A set of test results demonstrated the validity of the platform. This research will be of benefit in digital beamforming algorithm research, MIMO technology or software defined radio techniques.

Contents

1	Introduction	8
1.1	Thesis Outline	9
2	Literature Review	11
2.1	Background	11
2.2	Application of smart antenna technology	12
2.3	The advantages and challenges of smart antennas	14
2.3.1	The advantages of smart antenna	14
2.3.2	Challenges	15
2.4	The present situation of research	16
2.4.1	Europe	16
2.4.2	Japan	17
2.4.3	United States	17
2.4.4	Canada	19
2.4.5	China	19
2.4.6	Summary	20
2.5	Digital Beam Forming	21
2.5.1	Beam switching mode	21
2.5.2	Adaptive Beamforming	22
2.6	Study on smart antenna calibration technology	25
2.6.1	Injected signal calibration system	26
2.6.2	Blind calibration system	27
2.6.3	Wireless signal feed in calibration system	28
3	Smart Antenna Theory	31
3.1	Antenna Arrays	31
3.2	Pattern Multiplication Theorem	31
3.3	Uniform N-Element Linear Array	34

3.4	Grating lobes	36
3.5	Conclusion	38
4	Test Platform Design	39
4.1	System Design Overview	39
4.2	Phase Shifter	39
4.2.1	Switched line phase shifter	39
4.2.2	Quadrature Modulator Phase Shifter	40
4.2.3	Quadrature Modulator AD 8346	41
4.3	Local Oscillator Design	43
4.3.1	Power Divider Introduction	43
4.3.2	Resistive divider	43
4.3.3	Reactive power divider	46
4.3.4	Practical Wilkinson Power Divider	49
4.4	I,Q Input Control Circuits	50
4.4.1	DAC Selection	50
4.4.2	REF19x Series Voltage Reference	52
4.5	Radiation Units	53
4.6	Controlling Unit	56
4.6.1	Microcontroller ATmega128L	56
4.6.2	PCD8544 LCD Display	56
4.6.3	Software	57
5	Platform Tests	60
5.1	Calibration	60
5.2	Gain measurement methods	60
5.2.1	Standard-gain horn antenna comparison method	60
5.2.2	Two-antenna method	62
5.2.3	Three-antenna method	62
5.2.4	Comparison	62
5.3	Beam angle platform test	63
6	Summary & Future Work	68
6.1	Conclusion	68
6.2	Future work	69
	Appendix A Graphics	70

Appendix B ATmega128 C code	79
B.1 5110cmd.h	79
B.2 5110cmd.c	81
B.3 AD5308.h	91
B.4 AD5308.c	92
B.5 global.h	95
B.6 main.c	96
Appendix C Matlab Scripts	101
C.1 main.m	101
C.2 get_amplitude.m	103
C.3 get_phase.m	104
C.4 movephase.m	105
C.5 readcsvfile.m	106
C.6 calibration.m	108
C.7 nonlinear_main.m	110
C.8 arrayfactor.m	112
C.9 pointingdirection.m	113
C.10 drawing.m	114
C.11 semipolar_dB.m	115
C.12 patchparacalutor.m	122

Chapter 1

Introduction

The rapid development of wireless communication technology simultaneously allows people greater freedom as well as greater connectivity. Compared to the single voice communication services of the past, the demand for high quality wireless services, such as multimedia data exchange and internet access, has pushed development forward. Due to the increased demands, user capacity has become insufficient and quality of service has suffered. Smart antenna technology is a potential optimal solution to achieve this.

However, smart antenna technology is still in the research stage. Various implementation techniques are possible, requiring a lot of experiments to be performed and verified to match the theoretical results. Relying only on simulations is not reliable without practical experimentation to confirm the findings. In the case of this thesis, an efficient and low cost testbed will be developed to meet this end.

The steps taken are as follows:

1. An in-depth analysis and research was undertaken based on smart antenna theory.
2. Several modules were designed, based on a four-channel (four-antennas) test platform.
3. Simulations of a four-channel test platform were also carried out in an attempt to characterize the performance.
4. Combine all of the modules mentioned above to complete the test platform.
5. The platform was characterized and tests planned for target beam angles.

The work is divided into the following five parts:

- Design a Wilkinson power divider with Agilent Advanced Design System (ADS), to split an externally supplied signal, which will act as the smart antenna system Local Oscillator (LO).

- The Wilkinson power divider outputs are then fed into quadrature modulators, each digitally controlling (via dedicated Digital to Analogue Converters (DACs)) the phase of the signal feed to the associated antenna.
- For each DAC, noise minimization interface circuits were developed.
- Develop a simple patch antenna array as the antenna radiation units.
- Programme an on-chip system controller for Digital Beam Forming and LCD display of status and other information.

The experimental results demonstrated that the beam and the control of the beam are both very similar to the results predicted by theoretical analysis. With further research and improvements, the results achieved indicate that the technique is worth pursuing both in terms of cost, phase angle selection and improved continuity in phase angle transition.

1.1 Thesis Outline

This chapter briefly describes the motivation, work completed and the structure of this thesis. Chapter 2 contains a literature review, which gives a broader picture of the area to which this work belongs, as well as describing the current state-of-the-art for this technology. It presents a brief introduction to smart antenna technology and its advantages and drawbacks. The current international research on smart antennas is described. This chapter also gives two key features of smart antennas. One is Digital Beam Forming (DBF), including beam-switching mode and adaptive beamforming mode. The other feature described is calibration, including injected signal calibration, blind calibration and wireless signal feed-in calibration systems.

A theoretical description of antenna arrays can be found in Chapter 3, where the theoretical combination equation is presented and the key influencing parameters identified. The Array Factor (AF) and Grating lobes for uniformly-spaced identical elements of equal magnitude with a linearly progressive current phase difference has been analysed and is shown in diagrams.

In chapter 4, the platform design is described in detail. Firstly, two types of phase shifter are compared, the switched-line shifter and the quadrature modulator shifter. The local oscillator circuit (including a Wilkinson power divider) was simulated in Agilent's ADS, is presented in the following section. The fourth section compared three A/D converter candidates and gives a I/Q voltage control circuit based on the AD5308 and the REF192 2.5V voltage reference chip. A simple patch antenna was developed and simulated in ADS in section 5. Several simulation results shown identify important parameters such as gain, directivity and associated

S-parameters. The last section gives the software structure, consisting of a lookup table, a calibration unit, an LCD display driver, etc.

Chapter 5 describes the platform validity tests, using a Vector Network Analyser (VNA) and spectrum analyser, using Tektronix Digital Phosphor Technology to highlight the flexibility and continuity in phase angle selection. The first section shows the calibration process for the quadrature modulator. A series of normalized Matlab graphics and several snapshots from the spectrum analyser present supporting result.

The last chapter makes some recommendation on future work, based on the test results, the experience gained and the potential application of a successful future development.

Chapter 2

Literature Review

2.1 Background

As a primary means of personal communication in the future, mobile communication will play an increasingly important role in the global communications business. With the rapid growth of the number of mobile communication users and the increasing requirements of people for communication bandwidth and sustained quality, mobile communication networks still have to maintain high quality of service. However, there are currently two main challenges in mobile communication[1]. First, with the increase in mobile users, spectrum resources are increasingly limited. Second, due to multi-path channel effects (attenuation, fading and delay spread) the desired signal will experience degradation before reaching the receiver antenna. In addition, interference from other users greatly limits the system's ability to maintain communication quality. The two issues (declining resources in the face of increasing demand) are the principal, contradictory challenges in the development of mobile communication technology. Effective means are required to address the spectrum constraint and to improve service quality and capacity.

In order to solve the problem of system capacity, the second generation of digital cellular systems uses multiple access techniques, namely Time Division Multiple Access (TDMA) and Code Division Multiple Access (CDMA). In order to improve communication quality, modulation, channel coding and signal processing equalization techniques, RAKE receiver (CDMA system) synchronization, cellular division/spatial demarcation techniques and sector antennas, were all introduced. All of these techniques are now widely used in the second generation systems. While each of these systems does play their part, as solutions they represented early, low-cost, basic use of the channel as a function of time, frequency and space.

Smart antenna technology is introduced in this context as a possible efficiency increase in time, frequency and space solution for mobile communications. Theoretical and experimental data

show that the line-of-sight (LOS)/dominant path receiver signal, the other multi-path versions and also any interfering signals usually each have a different direction of arrival (DOA) to the receiver antenna. If the LOS/dominant path DOA can be emphasized with a higher gain, then the receiver antenna can offer an additional degree of freedom, to improve system capacity and to simultaneously combat fading and suppress interference. Through such spatial selection, smart antenna technology can effectively expand the system capacity and greatly improve the communication quality. It has been widely accepted that smart antenna technology could be a key technology in the third generation mobile communication systems, and it is therefore attracting a lot of attention. Almost all Third Generation Radio Transmission Technology (3GRTT) standards submitted to International Telecommunication Union (ITU) include smart antenna technology. As early as the ITU meeting in March 2000, it was suggested that smart antenna technology, used in the CDMA system should be pursued[2], and the meeting in August 2000 had a formal discussion of applying smart antenna technology in CDMA systems[3]. It can be expected, therefore, that smart antenna technology could occupy a very important position in mobile communication systems in the future.

It is often difficult for a smart antenna adaptive process to both capture and track the user signal dynamically. An important verification technique is to establish a hardware platform to replicate the required performance in an actual environment. This thesis mainly studies the design and implementation of a hardware platform for the radio frequency (RF) front-end, which can be used to efficiently and smoothly implement smart antenna technology.

2.2 Application of smart antenna technology

Smart antenna technology has a history of over five decades[4]. In the intervening period, as wireless communication technology developed and expanded, smart antenna technology made good progress, and can now be found in concept or in practice in most areas of mobile wireless communications, such as mobile digital television, mobile satellite communications, mobile terminals and mobile phone communications.

Mobile digital television

Applying smart antenna in vehicular High Definition TeleVision (HDTV) and combining with time domain signal processing can, not only improve resistance to fading and interference, but also greatly improve the reliability of signal reception by using multipath mitigation signal processing technology(section 2.3.1). Smart antenna technology can swiftly identify interference directions and place nulls in their directions. This minimizes the effect from pulse signal interference to the receivers[5].

Smart antenna for mobile satellite communications

Mobile satellite communication currently uses a smart antenna for L-band (1 to 2GHz) communications. The typical antenna consists of a $4 * 4$ square planar array, formed by 16 ring micro-strip antennas, and its RF frequency, digital-analog sampling rate and resolution are 1.542 GHz, 128 KHz and 8-bit respectively. An FPGA was selected for digital signal processing, and the Constant Modulus Algorithm (CMA) chosen as the adaptive algorithm. System tests[6] show that it can generate 16 directional time division waves covering the entire upper half space, and automatically capture and track satellite signals based on the maximum gain beam.

Smart antennas for mobile terminals

Limited by factors like physical terminal size, the array element space used in mobile terminals cannot be large. As a consequence coupling between the antennas can be strong and this mutual coupling can make the multi-antenna system receiving efficiency decline. Secondly, the gain of the antenna system depends on the correlation coefficient between each of the diversity-offering antennas. The smaller the correlation coefficient is, the higher will be the diversity effect and thus the overall gain. It should be noted that the theory and implementation of smart antennas for mobile terminals is different from that of other types of smart antennas[7]. Each element's space and size is limited, as well as a lower algorithmic complexity requirement, for lower power consumption. In other words, performance and mobility should be balanced. Experiments [8] show that by applying smart antennas in mobile terminals, along with a maximum SINR beamforming algorithm, an average Signal to Interference-plus-Noise Ratio (SINR) gain of 0.176 to 3.335dB can be obtained.

Smart antennas for mobile phone communications

The introduction of smart antenna technology into mobile communication systems means more types of service and better performance can be offered to more users. The following information will explain the needs of smart antenna technology applications from two perspectives, that of the mobile communications network operator and that of the mobile users.

1. First of all, from the mobile communications network operator's point of view, adding extra base stations has been used as a means for expansion. This is not economic and is inefficient for a mature network. In areas requiring very large capacity, the traditional method of cell division is gradually becoming less feasible. However, replacing the ordinary antenna in base stations with a smart antenna both expands the system coverage area and also the spectrum reutilization rate in the cell[9]. Operator investment and operating costs can therefore be reduced, tempered only by the cost difference between the purchase and operation of a smart antenna compared with a conventional cell an-

tenna. The introduction of smart antenna technology in base stations can improve the communication link performance, which makes it easier for operators to provide new services such as a variety of extra data services. Additionally, the system improvement means more active users are offered enhanced path gain, which greatly improves the efficiency of the system.

2. Secondly, from the mobile user's point of view, they can get improved call quality, because smart antennas can improve both signal-to-interference and signal-to-noise ratios and reduce the impact of delay spread. Moreover, spatial domain or space-time domain combined processes can be used to improve the performance of links by applying narrow, time selective beams to track users[10]. Smart antennas can improve the antenna direction gain, which means that the device can work at lower power, which can in turn prolong mobile phone talk time and standby time. It would also greatly reduce the electromagnetic radiation, reducing potential effects on the human body.

In short, the potential benefits to mobile communications offered by smart antenna technology cannot be replicated by any other technology, so the case for its implementation is compelling for both mobile network operators and also mobile users. It seems definite now that smart antenna technology will play an increasingly important role in the future development of mobile communications[11].

2.3 The advantages and challenges of smart antennas

2.3.1 The advantages of smart antenna

With the introduction of the fourth dimensional multiple access method, namely spatial division multiple access in smart antenna technology, while using the same time slot, the same frequency or the same code, user devices and base stations can still spatially select any one of the signal's multipaths and significantly reduce interference. Therefore, smart antenna technology can improve the performance of mobile communication system in many ways, including improving the spectrum utilization, reducing fading impact, reducing power and related costs, enhancing the security of communications and knowing the approximate position of the mobile terminal.

Improve spectrum utilization

Replacing the ordinary base station antennas with smart antennas improves frequency reuse rate within a cell, so that system capacity can be added without establishing new base stations or at least by establishing fewer extra base stations. The interfering beams (due to frequency reuse) from all other directions will be reduced by the smart antenna spatial filter.

By adjusting the weight of antenna elements, optimizing the antenna array distribution and pointing the null to the interference direction, smart antennas can greatly increase the array's output signal-to-interference ratio, improve system quality and system reliability. As for a CDMA system with soft capacity, the improvement of signal-to-interference ratio also means the system capacity can increase.

Reduce fading impact

One of the main problems for wireless communications is the fading of signals. Ordinary omni-directional antenna or even directional antennas often suffer signal distortion due to fading. If smart antennas are used to control the receiving direction and also to adjust the antenna gain direction adaptively, the gain in the direction of delay paths can be minimized, to reduce the effect of signal fading. In addition, smart antennas can also be used in diversity reception to reduce the fading.

Reduce power and reduce costs

Smart antennas can optimize the transmission for each particular user, which reduces the required transmitter and receiver power.

Enhance the security of communications

In traditional wireless communication technology, the user's air interface wireless signals can be readily intercepted. However, with the use of smart antenna technology, due to the directional nature of the beam, the user's signals can only be received in a much more limited space, which improves the communication security. However the system is now potentially more vulnerable to signal jamming.

Mobile terminal position

Most cellular mobile communication systems can only determine the cell where the mobile user is, but with the use of smart antenna technology, the approximate position of the person holding the mobile phone can be determined at any time, which is not only convenient for users and network managers but could offer opportunities to develop new business. Of course, this has implications for privacy.

2.3.2 Challenges

Smart antenna technology will play an important role in enhancing the performance and reducing the cost of any mobile communication system. However, smart antennas also bring new challenges. These include the calibration of the smart antenna, the combination of the smart antenna and other anti-interference technology, the speed of beamforming, device complexity, the frame structure and related physical layer technology and shared downlink channel. In order to achieve further development and improvement of smart antenna technology, the problems must be solved gradually through standard development and product design.

2.4 The present situation of research

In the early 1990s, smart antennas originated from adaptive antennas applied in military radar and sonar systems. The initial research was in radar antenna arrays, to improve the system performance and electronic warfare capacity of radar. In the 1950s, to enhance satellite communications signals, the USA began to study adaptive antennas. In the early stages, adaptive antenna studies were mainly in radar systems, and its beam forming network consisted only of microwave devices. The concept of modern day smart antennas was developed by some scholars in the late 1980s to early 1990s[12].

Smart antennas applied in mobile communications, especially in cellular mobile communications, generally refers to multi-antenna array modules, which can process technology through digital signal processing and generate multiple spatial beams to different users. All beams automatically are individually aligned to their respective user's direction of arrival, but also aligned antenna nulls to interference directions, so that the performance of mobile communication systems can be enhanced (such as co-channel interference (CCI), coverage and system capacity, etc.). As software simulation has its limitations, the accuracy and reliability of simulation results can be relatively poor. Therefore, to study smart antenna technology, many countries conducted a considerable amount of theoretical research, and at the same time established a series of technical test platforms and experimental system to undertake more in-depth and practical research.

2.4.1 Europe

The Commission of European Communications (CEC), in the RACE (Research into Advanced Communication in Europe) program, implemented the first stage study on smart antenna technology, and the study was called TSUNAMI (The Technology in Smart antenna for Universal Advanced Mobile Infrastructure), carried out by Germany, Britain, Denmark and Spain. The project established a smart antenna test model based on DECT base stations and began field tests in 1995. The antenna consisted of 8 array elements, with the working frequency of 1.89GHz. The space between array elements was adjustable and array elements distribution could be linear, circular or planar array, which achieved a smart antenna through a digital beamforming method and by using a special integrated circuit chip, the DBF1108 from ERA Technology Co., Ltd. The system developed the Multi-User Signal Identification and Classification algorithm (MUSIC) to automatically recognize the received signal's direction of arrival. The adaptive algorithm used both the normalized least mean square algorithm (NLMS) and the recursive least squares (RLS) algorithm[13].

Various experiments have verified the correct functioning of the smart antenna. A four-

element adaptive antenna array (i.e., Temporal Reference Beamforming (TRB)) test bed with a Direct Matrix Inversion (DMI) algorithm was designed by AT&T, Holmdel, NJ [14][15] for evaluation of the SA concept in an IS-136 system operating at 850 MHz/1.9 GHz. A 5-dB higher gain was achieved at 10^{-2} bit error rate (BER) in a Rayleigh fading environment. Field test results show that circular and planar antenna arrays are suitable for the indoor communications environment, but a simple linear array is more appropriate for an urban environment [16]. The CEC continued the second phase study on smart antenna technology in ACTS (Advanced Communication Technologies and Services) program, focusing on the following aspects: an optimal beam forming algorithm, system protocol studies and system performance evaluation, a combination of multi-user detection and adaptive antenna, space-time channel characteristics estimation, optimization of micro-cellular structure and field tests [17].

2.4.2 Japan

The ATR Optical Communications Research Institute developed a multi-beam smart antenna based on a beam-space processing approach [18]. The antenna array layout was a planar array of 16 elements, with a half-wavelength spacing and a working frequency of 1.545 GHz. The signals received by array elements first experience modulus transformation, and then experience Fast Fourier transform processing and finally form orthogonal beams. During the process, a constant modulus algorithm and a maximum ratio combination (MRC) algorithm are used respectively. Digital signal processing is finished by 10 FPGAs, and the entire circuit board size is 23.3 x 34.0 (cm). Field tests confirmed the functioning of a multi-beam smart antenna using a modulus algorithm.

ATR researchers have proposed the concept of a Software Antenna as shown in Figure 2.1 [19] below.

Depending on different user environments, the factors (such as noise, co-channel interference or ISI) affecting system performance are different. Different software algorithms are applied in the different environments. For example, when noise is the main factor, a multi-beam maximum ratio combination algorithm is used; when co-channel interference is a major factor, the multi-beam constant modulus algorithm is used; the least mean square (LMS) algorithm and maximum likelihood successive estimation (MLSE) are used to offset the ISI, based on which algorithm diversity is provided.

2.4.3 United States

The United States is a world leader in smart antenna technology research, and many telecommunications equipment manufacturers have launched their own products, from which

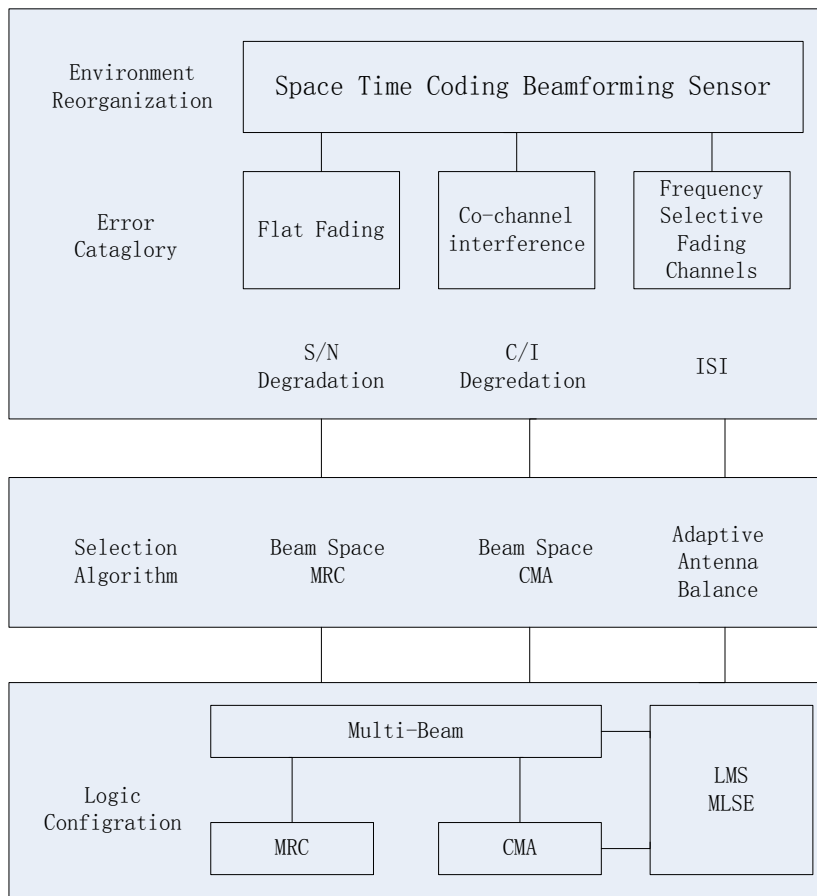


Figure 2.1: Concept of Software Antenna

ArrayComm may be considered a good representative with wide global collaboration[20]. ArrayComm is a world-renowned communications technology company with mature adaptive smart antenna technology and has a number of patented technologies at a world leading level. ArrayComm Company has a number of adaptive smart antenna products, among which the IntelliCell technology can improve the signal quality and spectrum utilization rate, increase the system capacity and coverage and improve the data transmission rate, so that the best voice quality can be obtained. Through adaptive processing algorithms, the IntelliCell processor can modify the weighted parameters and make hundreds of adjustment per second to the amplitude, phase and arrival angle, thus achieving both the uplink and downlink beamforming processing. The technology has been applied in more than 75,000 base stations all over the world, and offered high-quality wireless broadband services for 4.5 million wireless users. The technology supports third generation (3G) mobile communication of various air interface standards (IMT-2000 WCDMA, CDMA2000, TD-SCDMA) and has obvious advantages over the traditional mobile communication system in the capacity, data transmission rate, coverage

and service quality. It is said that IntelliCell can reduce 50% of the base stations required, so that the equipment costs and operating costs can be reduced[21].

Virginia Institute of Technology and Virginia Tech Antenna Group (VTAG) and the Mobile Portable Wireless Research Group (MPRG) from Virginia Polytechnic Institute conducted a study and performance tests on a mobile smart antenna and developed a hand-held antenna array test platform (HAAT), vector multipath communication simulator (VMPS), and broadband VIPER measurement system[22]. The test results show that applying adaptive array beamforming technology of 4-element antenna array in mobile terminal can achieve interference suppression of up to 40dB. The Wireless Communications Research Centre in Canada (CRC) conducted research on a mobile smart antenna SA100 used in satellite communications and a mobile smart antenna SA300 used in cellular communications[23]. The working frequency band of the SA300 is 1.85-1.90GHz, and the SA300 can generate 16 beams of equal intervals within a 360-degree range with each beam's 3dB bandwidth of 60 degrees and the antenna transmit power being 2W.

2.4.4 Canada

Canada's McMaster University has developed a four-antenna array, and conducted research on CMA Constant Module Algorithm [24] .

2.4.5 China

As for the study on smart antennas, China started late, but still had some success. For example, Beijing Xinwei developed the smart antenna system applied in McWiLL (Multi-Carrier Wireless Information Local Loop)[25]. The smart antenna of Xinwei Corporation applies a ring adaptive array of 8 elements with a working frequency of 1785-1805MHz, using a time division duplex mode and receiving interval of 10ms so that the beamforming gain can be as high as 18 dB for the link budget in downlink. For a conventional antenna system to reach the same coverage as the smart antenna system with eight 2W amplifier, the power level of the amplifier has to be increased by 64 times to 128W. However, this system can only work in a wireless local loop (WLL), and is restricted by user location and mobile rate.

Another point worth mentioning relates to the TD-SCDMA proposal submitted to the ITU by the Chinese Academy of Post and Telecommunication Science Technology in 1998 on behalf of the Chinese Telecommunications Department and also the CDMA TDD technology (low chip rate options), one of the standards of the third international generation of mobile communications and, finally, the first CDMA communication system using smart antenna as a core technology, which won widespread recognition and support outside China. The rel-

evant standards were developed[26]. Some Chinese universities and research institutes, like Tsinghua University, Xi'an Jiaotong University, China University of Science and Technology, Xi'an University of Electronic Science and Technology, Northern Jiaotong University, Beijing University of Posts and Telecommunications Research Institute of Science and Technology, have successfully launched theoretical studies on smart antennas [27]. Some large telecommunications equipment manufacturers such as Datang Telecom, Huawei, and ZTE have also invested a lot of manpower and material resources in research and development; the national "863" program, the national Natural Science Foundation, and the Doctoral Fund also support corresponding units for theoretical and technological platform research. For various reasons, China's study on smart antenna technology is still at the theoretical research and technology tracking stage. The smart antenna has a very attractive future, with so many countries having invested a great deal of manpower and material resources to study the technology, and made some achievements. Generally speaking, the present research programme has addressed the following two problems:

1. Research demonstrated that smart antennas are feasible and effective in different mobile communication systems. A test platform has been developed and under certain conditions (from the current situation, the smart antennas are gradually applied in the fixed wireless access system) smart antenna technology has been achieved and the powerful advantage that smart antennas showed in improving performance of mobile communication system has been verified.
2. A study on the basic structure and functional modules of a smart antenna has been conducted, and some performance metrics and adaptive smart antenna beamforming algorithms have been produced.

2.4.6 Summary

Smart antennas is a relatively new technology in mobile communications, and it is now still at the development stage with many unsolved problems, among which particularly prominent is the problem of the tracking speeds of smart antennas. Smart antennas adjust the array element weights according to certain performance metrics' criteria and use an adaptive algorithm capable of achieving the capture and tracking of users. The adaptive algorithm is at the core of, and key to, the success of smart antenna technology. Due to the complicated mobile communication environment and existing chip processing speed constraints, adaptive algorithms now have the problems of both large computation, without achieving the acquisition and tracking of mobile users at all times, which is the major problem limiting the application of smart antennas. Looking for fast adaptive algorithms has therefore become the focus of

some study on smart antenna technology.

2.5 Digital Beam Forming

Digital beam forming (DBF) has many equivalent names such as: spatial adaptive filtering, adaptive arrays, adaptive antennas and smart antennas. *Smart* vividly describes the function of spatial adaptive filtering, that is, that it can adjust parameters adaptively, according to actual conditions to achieve a treatment predefined by the chosen algorithm. It has a certain degree of intelligence, and is very different in nature from traditional antennas, where parameters are fixed. Spatial adaptive filtering implies the use of beams of certain shape to restrict unwanted interference in the direction in which the desired signals are traveling. It is also called beamforming and can also be achieved digitally on base stations.

Spatial adaptive filtering can in turn be sub-divided into digital independent beamforming, optimum beamforming and adaptive beamforming. Digital independent beamforming is designed based on system requirements without any knowledge of the array's input signal. Digital independent beamforming can include multiple beams and shaped beams. Multiple beams are also called *switched beams* and are widely used in communications and radar systems. Optimum beamforming is designed based on prior knowledge of the signal interference environment and some optimizing principles are used, such as Minimum Mean Square Error, MaxSNR, Linearly Constrained Minimum Variance, Least Squares Method, Maximum-Likelihood. Adaptive beamforming is designed based on a real-time input signal, an interference signal vector and uses an adaptive algorithm for processing. Strictly speaking, spatial adaptive filtering is only related to adaptive beamforming. However, since the switching-beam method is easy to implement, it is widely used in communications.

2.5.1 Beam switching mode

The current cellular communication space can be divided into three 120 degree sectors, which can be considered as a three-beam switching system. Beam switching smart antennas further divide such macro-sectors into several micro-sectors by using a beam that is narrower than the 120 degree sector. When the mobile station goes into the macro-sector, the switching beam system detects the signal strength and selects the beam receiving the strongest signal for the user.

When the mobile station crosses the micro-sector, the mobile station switches automatically from one beam to another beam, as shown in Figure 2.2. Due to the narrow beam assigned to the user, the beam switching mode, to a certain extent, improves the signal-to-interference noise ratio (SINR) and anti-interference capability is therefore strengthened. Meanwhile, be-

cause of its simple structure, low construction cost, low investment risk, no need for direction-of-arrival (DOA) estimation, the beam switching mode is widely used. The direction of all beams of a beam switching smart antenna is fixed, and their beamwidths change with the number of antenna array elements. For mobile users, base stations select different beams to obtain the maximum received signal strength.

However, a user's signal may not be in the center of a fixed beam. When the user's signal is at the edge of a beam and the interference signal is in the center, the reception is most affected. Therefore, multiple beam switching antennas cannot always achieve the best signal reception. Meanwhile, multiple beam antennas cannot distinguish between the useful signal and the interference signals in the main lobe, and cannot handle diversity combination of multipath components. When there is lateral movement of the user with respect to the base station, the gain change caused by overlapping beams will cause great fluctuations of the received signal power.

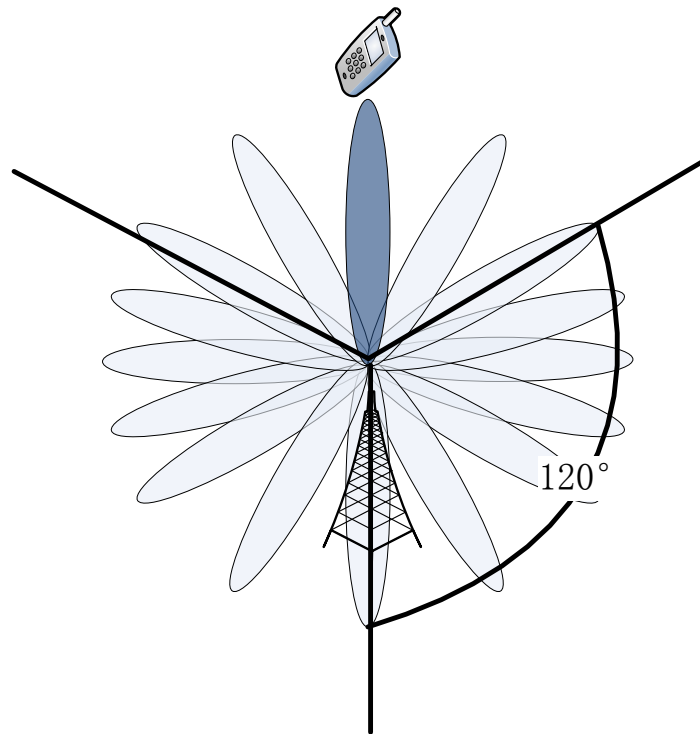


Figure 2.2: Beam Switching Mode

2.5.2 Adaptive Beamforming

Adaptive beamforming mode smart antennas (also called adaptive smart antennas) is a more likely candidate for the title of smart antenna, as they can achieve optimal signal reception.

They mainly consist of antenna arrays and a real-time adaptive signal receiver processor, which forms a closed loop, feedback control system. Through the use of an adaptive beamforming algorithm, it can automatically adjust the antenna array beam pattern making it form nulls in the interference direction and aligning the main beam to the desired signal to enhance anti-interference. The typical beam is shown in Figure 2.3. Due to increased expected signal gain and also interference suppression, adaptive smart antennas greatly increase the SINR, which permits the system capacity and spectrum utilization to increase. Theoretically, a smart antenna with M array elements can form M independent beams and reduce the interference of $M - 1$ different Directions-Of-Arrival (DOAs).

After decades of development, adaptive beamforming technology has gradually matured. The existing adaptive beamforming algorithms can be divided into three categories: beamforming based on a reference signal, beamforming based on the beam DOA, and blind beamforming based on signal structure characteristics.

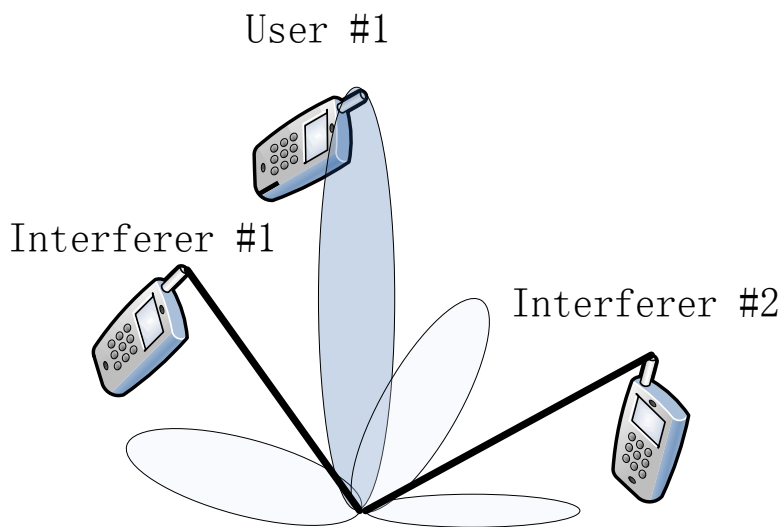


Figure 2.3: Adaptive Mode

1. Beamforming based on a reference signal. The algorithm requires that the transmitter sends a training sequence or pilot signal to the receiver to generate a receiver reference signal. The 2G-GSM system uses a special code training sequence, and the 3G-UMTS system users can use a user-specific pilot channel. For adaptive beamforming, the Least Mean Squares (LMS), Recursive Least Squares (RLS) and Direct Matrix Inversion (DMI) algorithms can be used. Without needing to determine the DOA of a signal, these algorithms are robust, with no need for correction, and they can combine with

multi-path acquisition to reduce fading effects. This approach generally requires precise synchronization and high update rates. Frequency-division duplex (FDD) cannot receive information from the uplink to determine the weight vector of the downlink beam.

2. DOA-based beamforming. These algorithms require the support of DOA estimation techniques, and require no information on the inference signal. The algorithms include DOA estimation and DOA-based beam adjustment. DOA estimation is very important in DOA-based beamforming techniques. Currently, there are a variety of DOA estimation algorithms, such as Multiple Signal Classification (MUSIC) and Estimation Signal Parameters via Rotational Invariance Techniques (ESPRIT), which form weights based on Linearly Constrained Minimum Variance (LCMV), after estimating the direction vector. In order to improve accuracy, better weights can be gained based on an eigenspace algorithm. These algorithms have a common feature that the direction of each incident wave is first estimated, and meanwhile a beamformer is produced for recovery of the signal from the direction. Generally, these algorithms require an accurately matched phase splitter or array manifold, but in a real system inaccuracies (principally due to manifold error) are probable, which requires that the array must be corrected via calibration. Another advantage of such an algorithm is that it is very suitable for a frequency division duplex system.
3. Blind beamforming algorithm. The purpose of a blind beamforming algorithm and the non-blind algorithm is similar, that is, to determine a set of weights for the best quality of the receiving signal. Without requiring training sequences, a blind beamforming algorithm achieves the same function based on time, space, code structure or the array manifold. The main advantages of the blind beamforming technology are: the beamformer has no relationship with the channel spatial property and the array correction. As long as the desired signal has characteristics different from those of the noise and interference, the array direction vector of the desired signal can be estimated. This can then be used as a direction vector for adaptive beamforming. Usually, the typical statistical properties of a signal include non-Gaussian and cyclo-stationarity, and typical uncertainties include constant modulus and finite symbol set characteristics. This constitutes a new beamforming algorithm, a blind beamforming algorithm. The typical blind beamforming algorithm is the constant modulus algorithm (CMA).

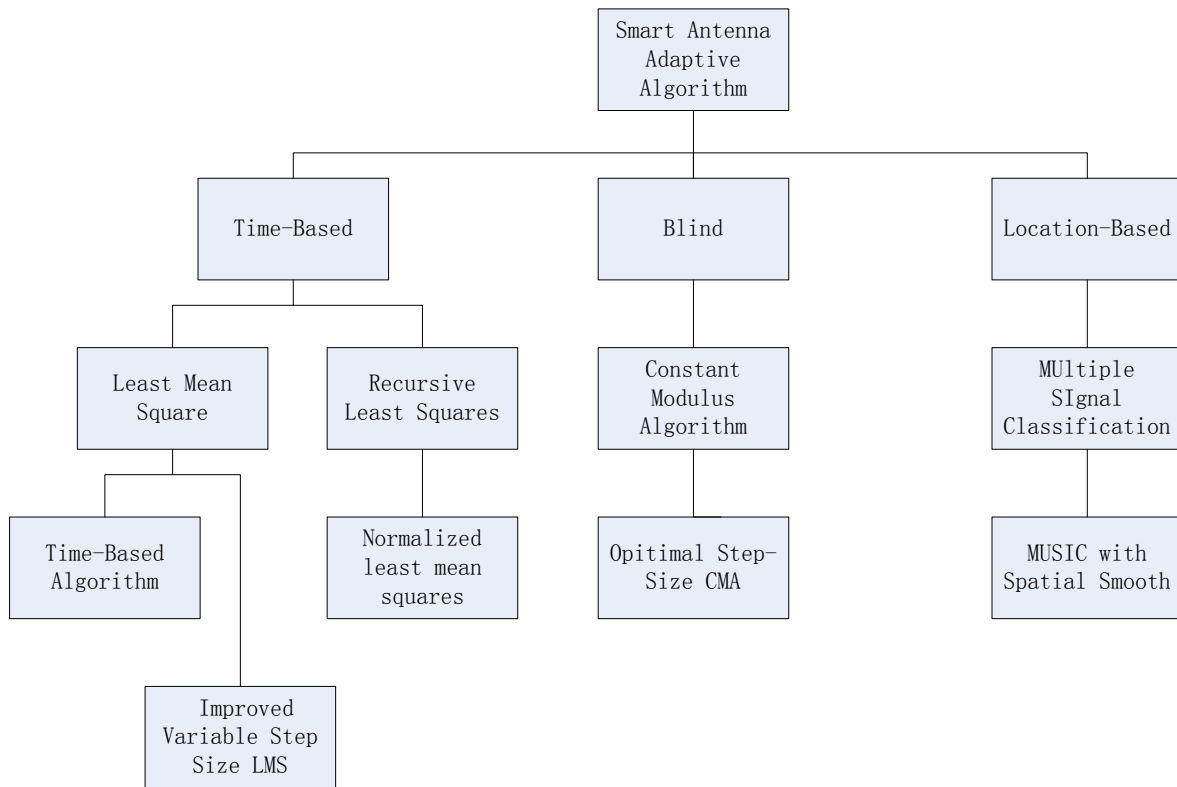


Figure 2.4: Adaptive Algorithm Classification

2.6 Study on smart antenna calibration technology

Usually, the DBF algorithm assumes, for the antenna array, that the space between channels stays consistent, without amplitude or phase errors. The location of the antenna array must be completely the same as in the model and there is no error between antenna elements and no mutual coupling between each other. These assumptions are necessary when using the algorithm because it helps reduce the complexity of the model, allowing the research to focus on the DBF algorithm. However, in the process of actual implementation of the DBF system, many non-ideal factors influence performance. These include processing errors in the antenna array elements, antenna array position errors, the RF circuits of each channel have different reactions to changing environmental factors (such as temperature and humidity), which in turn cause channel amplitude and phase errors. There is also usually mutual coupling between array elements, which means consistent assumptions are difficult to meet, thus affecting the DBF algorithm performance. When daily temperature variation is between 14-27 degrees Celsius, the channel amplitude variation can be as high as 1.76dB and the phase variation can be up to 180 degrees, at which point the DBF algorithm can no longer operate. In order to put a DBF antenna into practice, it is therefore necessary to develop an appropriate

calibration system.

For a mobile communication system, array antennas can be usually used at a fixed location, namely at the base station. Since the base station is usually unmanned, the DBF calibration system must be able to run automatically at the appropriate time, but in order not to affect the correct system operation the calibration time must be both short enough and have real-time ability. For example, for the WCDMA 3G standards, the length of a wireless frame is 10ms, so the calibration time should be confined to within 10ms. Radar systems usually have many array elements. Taking the Digital Array Radar[28] for example, it was a digital array radar, with 224 array elements designed by the Lincoln Laboratory, using digital beam forming technology, for U.S. Navy 21st century operational requirements. In order to capture the target in time, there are stringent requirements for the calibration system accuracy and real time ability. Therefore, the development of an effective, real-time calibration system is a critical step in putting DBF technology into practice.

Figure 2.4 gives an overview classification of the various possible adaptive algorithms.

2.6.1 Injected signal calibration system

In the literature [29], K. Fukino and others used an injected calibration signal calibration system as shown in Figure 2.5. The calibration signal generator generates a calibration signal with the same carrier frequency in the uplink and the same code rate and with an actual dedicated physical channel (DPCH). Then the calibration signals are injected into each RF receiver circuit in turn, through multi-channel switches. After the transmission through the RF circuits, amplitude and phase shift caused by each RF circuit (the circuit's impulse response) can be estimated, by comparing the output signal with the calibration signal generator output. Then the calibration parameters can be calculated. In order not to affect normal operation, the input calibration signal power should be adaptively adjusted based on the total real-time received power. This method can be implemented any time calibration is needed. The disadvantage of this technique is that the calibration of all channels must be conducted one by one. Therefore, significant time must be spent if the array size is large, and the antenna element's error and array position error cannot be corrected. When the technique is applied, amplitude and phase fluctuations of RF circuits during the calibrated period will be ignored. If the fluctuations are significant this will have an impact on performance, and the longer the working time between calibrations is, the greater the consequent impact is.

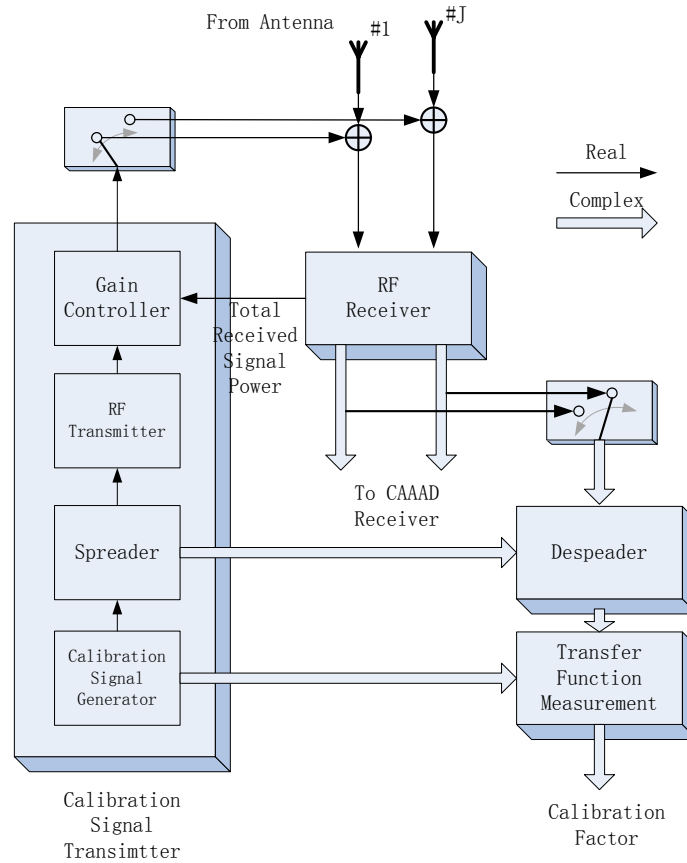


Figure 2.5: Injection Calibration System[29]

2.6.2 Blind calibration system

Injecting the signal itself brings interference for the system, so some researchers proposed a method of blind signal calibration[30]. Advantages of this approach are:

1. There is no need for an additional reference signal, avoiding the introduction of undesired signal amplitude shift and phase shift when feeding each channel. There is no interference from the introduction of the reference signal.
2. The uplink (Figure 2.6) and downlink (Figure 2.7) can be corrected using the same method.
3. Fast convergence facilitates tracking for changes in amplitude and phase.

The signals received by all antennas form a reference signal $r(n)$. After being corrected in RF channels, the combined signal $y(n)$ is outputted into an adaptive antenna processing unit.

The corrector adjusts $w(n)$ making the square of the output error $e(n)$ as small as possible. Here the weights are adjusted using normalized least mean square algorithm (NLMS).

In the downlink, the output of the adaptive processing unit is the reference signal $r(n)$, before calibration, and the signal before the transmitting antenna array is $y(n)$. The weight updater applies the same algorithm to that used in the uplink to update the weights, so that the square of the output error, $e(n)$, is as small as possible.

This calibration algorithm has a fast convergence. The uplink can achieve a calibration with 150 samples, and the downlink can also achieve a calibration with 500 samples, which meet the requirements of dynamic calibration (calibrating during signal transmitting process without interruption).

2.6.3 Wireless signal feed in calibration system

Although antenna error, position error and the mutual coupling error are not the main sources of error, it is still desired that the calibration system calibrate this error.

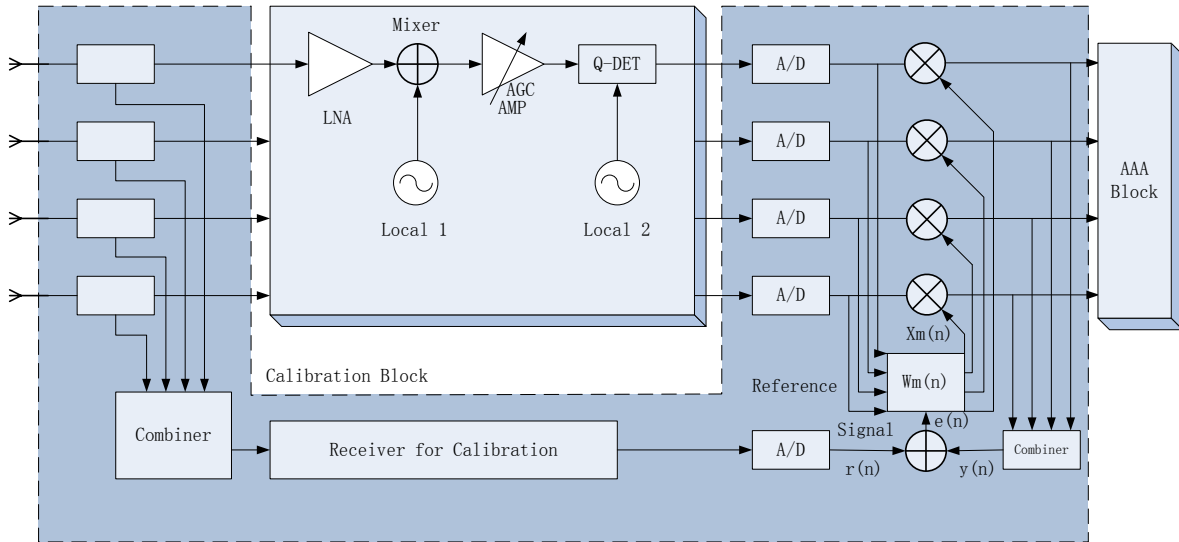


Figure 2.6: Blind Signal Calibration Uplink[30]

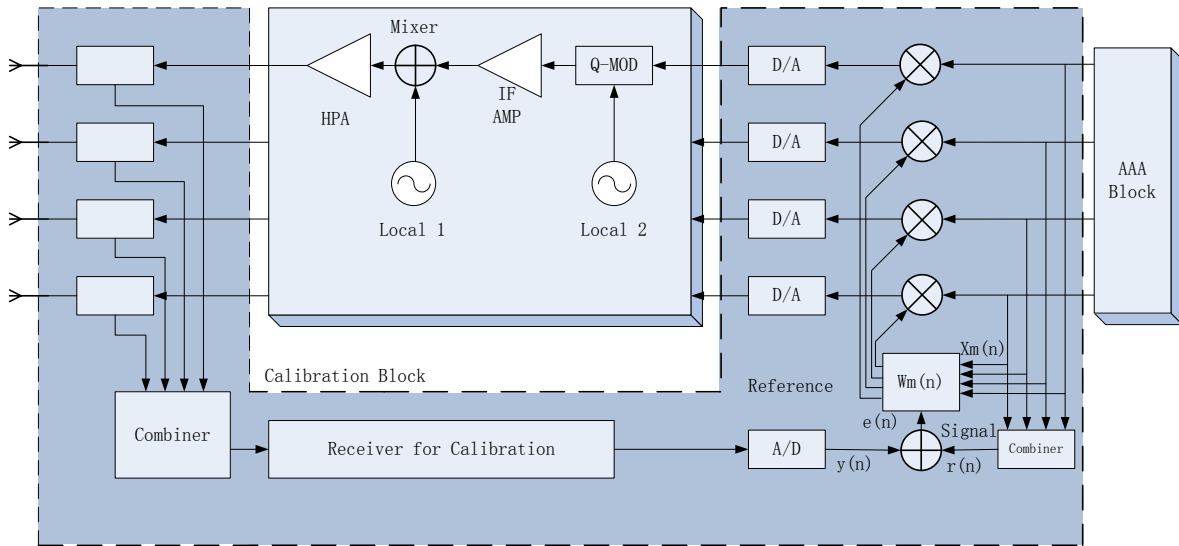


Figure 2.7: Blind Signal Calibration Downlink[30]

In literature [31], a wireless signal calibration feedthrough system was introduced as shown in Figure 2.8. The signals transmitted by an antenna array at a fixed location in the array's far field region are received by all antennas, down converted and then an A/D converts them into a digital signal, and are then inputted to an FPGA. The FPGA calculates the amplitude and time delay of each channel. Taking one channel as a reference, the time delay should be adjusted for each other channel. The amplitudes are all normalized to the maximum value. After the channel error parameters are obtained, they can be applied in the DBF process, to achieve the array error calibration.

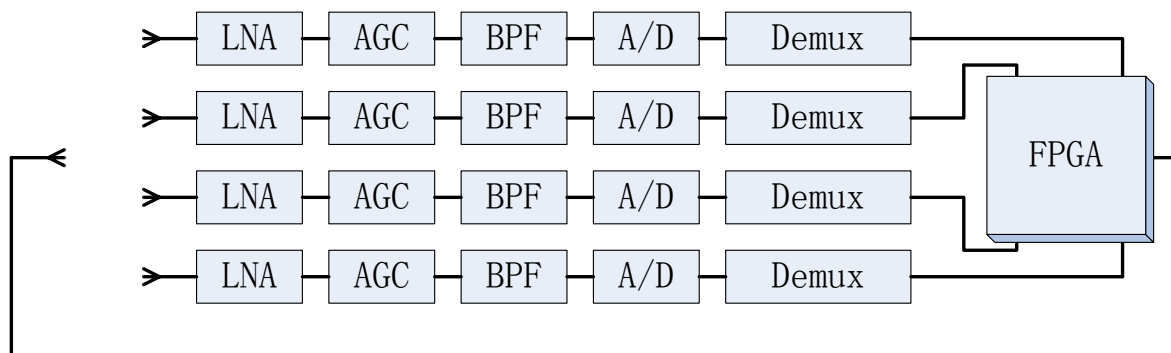


Figure 2.8: Wireless signal feed in calibration system[31]

Figure 2.9 shows a channel calibration circuit implemented in a FPGA. The core of the circuit is a 1024-point FFT converting the time domain signal into the frequency domain and obtain-

ing the corresponding transmitted calibration signal frequency components. The component amplitude and phase will be stored for calculating array calibration factors.

The 1024-point FFT consumes a lot of hardware resources, so for an 8-element linear array [31], two Xilinx Virtex-E FPGA level chip (XCV1000E, equivalent to 1.5 million logic cells in the circuit) were used to achieve the 8-channel FFT. The whole calibration system consumes 5 FPGA chips.

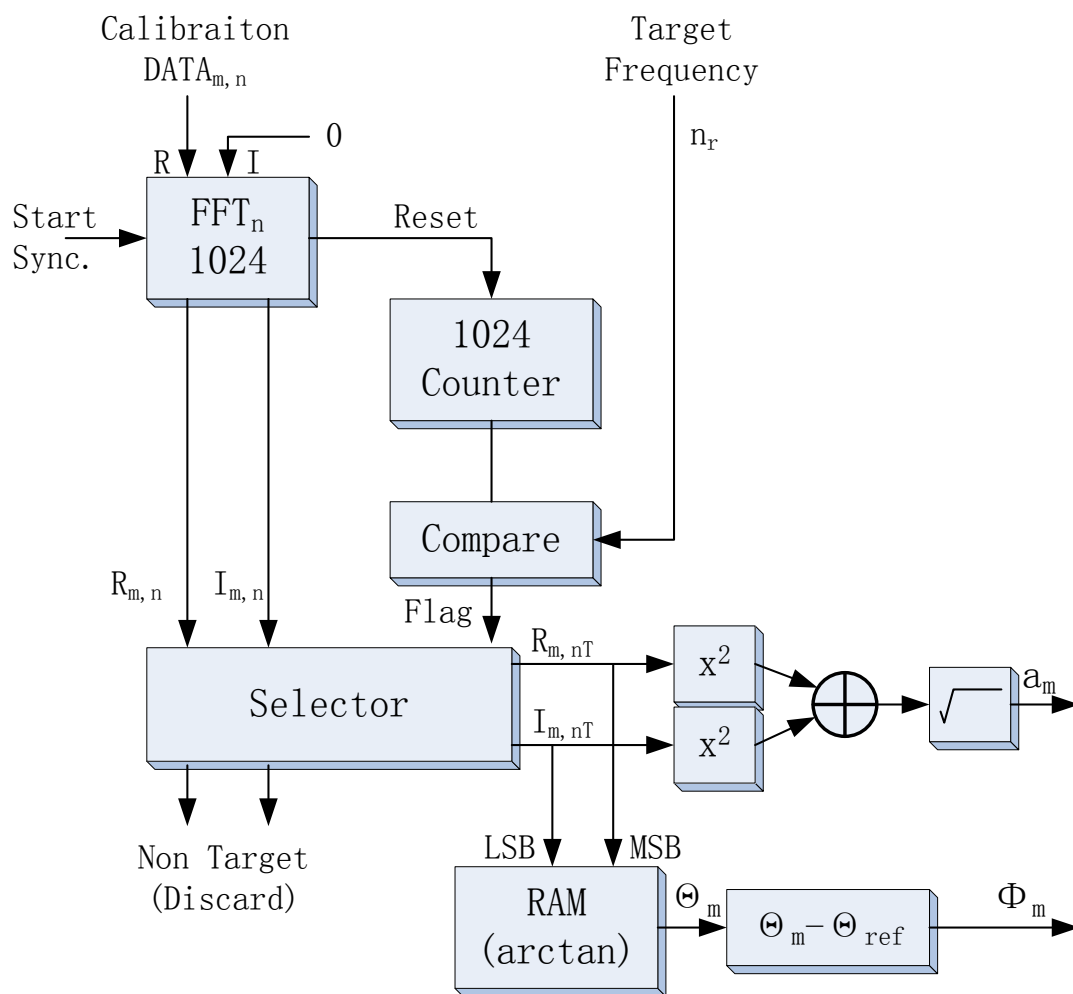


Figure 2.9: FPGA Calibration Circuit[31]

Chapter 3

Smart Antenna Theory

3.1 Antenna Arrays

Individual antennas can be configured into various patterns, such as a straight line (linear array), a circle or a 2-dimensional array. Traditional means of directing antennas was only through mechanical movement. Now, alternatively, phase arrays can control the antenna direction simply by careful element phase excitation.

Various antenna array parameters can be changed to form certain desired radiation patterns. These are usually fixed, such as the individual antenna pattern, the antenna configuration, the antenna spacing and parameters that can be varied, such as the antenna excitation amplitude and the antenna excitation phase.

3.2 Pattern Multiplication Theorem

The radiation pattern of an antenna array can be predicted with pattern multiplication theory, which can be represented by Figure 3.2.

$$\textit{Array Pattern} = \textit{Array Element Pattern} \times \textit{Array Factor}(AF) \quad (3.1)$$

- **Array element pattern** - the radiation pattern of the individual array element.
- **Array factor** - a function based only on the configuration of the array and the excitation of the elements.

We assume that the elements of the array are uniformly-spaced with a separation distance d . In the far field, the line connecting the radiation source and the receiver can be considered

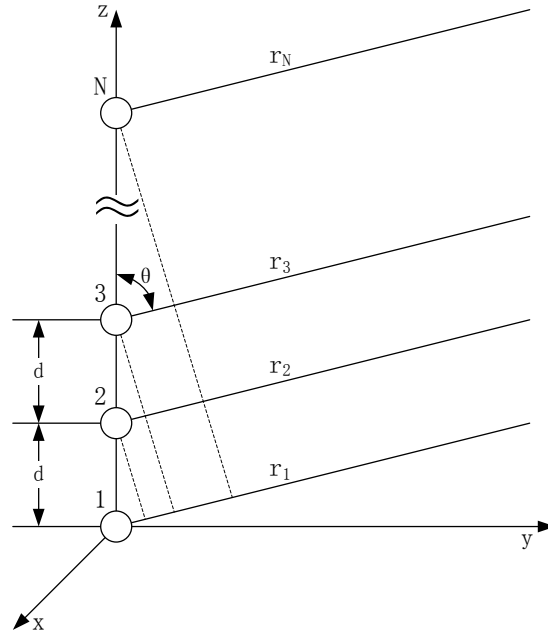


Figure 3.1: Elements Configuration

as parallel. In this case, the distance difference between two adjacent elements is decided by: $d \cos \theta$

$$\begin{aligned}
 r_1 &= r \\
 r_2 &= r - d \cos \theta \\
 r_3 &= r - 2d \cos \theta \\
 &\vdots \\
 r_N &= r - (N - 1)d \cos \theta
 \end{aligned} \tag{3.2}$$

where N is the number of elements

Here the electrical current magnitudes at each array element are assumed to be equal and the current, I_0 , in the array element located at the origin is used as the phase reference (zero phase). If each element is denoted by the antenna number as a subscript, then the current in

each antenna, I_1 to I_N , is:

$$\begin{aligned}
 I_1 &= I_0 \\
 I_2 &= I_0 e^{j\Phi_2} \\
 I_3 &= I_0 e^{j\Phi_3} \\
 &\vdots \\
 I_N &= I_0 e^{j\Phi_N}
 \end{aligned} \tag{3.3}$$

Φ is the phase difference using the first element as a reference.

Therefore, for example, Φ_k = phase difference between the k^{th} antenna and the first antenna that acts as a reference.

Each individual antenna's far field electric field is then:

$$\begin{aligned}
 E_{\theta 1} &\approx E_0 \\
 E_{\theta 2} &\approx E_0 e^{j(\phi_2 + kdcos\theta)} \\
 E_{\theta 3} &\approx E_0 e^{j(\phi_3 + 2kdcos\theta)} \\
 &\vdots \\
 E_{\theta N} &\approx E_0 e^{j(\phi_N + (N-1)kdcos\theta)}
 \end{aligned} \tag{3.4}$$

Finally, the overall antenna array far field electric field is found:

$$\begin{aligned}
 E_\theta &= E_{\theta 1} + E_{\theta 2} + E_{\theta 3} + \dots + E_{\theta N} \\
 &= E_0 + E_0 e^{j(\Phi_2 + kdcos\theta)} + E_0 e^{j(\Phi_3 + 2kdcos\theta)} + \dots + E_0 e^{j(\Phi_N + (N-1)kdcos\theta)} \\
 &= E_0 [1 + e^{j(\Phi_2 + kdcos\theta)} + e^{j(\Phi_3 + 2kdcos\theta)} + \dots + e^{j(\Phi_N + (N-1)kdcos\theta)}] \\
 &= E_0 [AF]
 \end{aligned} \tag{3.5}$$

where k = wave number.

$$k = \frac{2\pi}{\lambda} \tag{3.6}$$

And the Array Factor (AF) is

$$AF = 1 + e^{j(\Phi_2 + kdcos\theta)} + e^{j(\Phi_3 + 2kdcos\theta)} + \dots + e^{j(\Phi_N + (N-1)kdcos\theta)} \tag{3.7}$$

(Array factor for a uniformly-spaced N-element linear array)

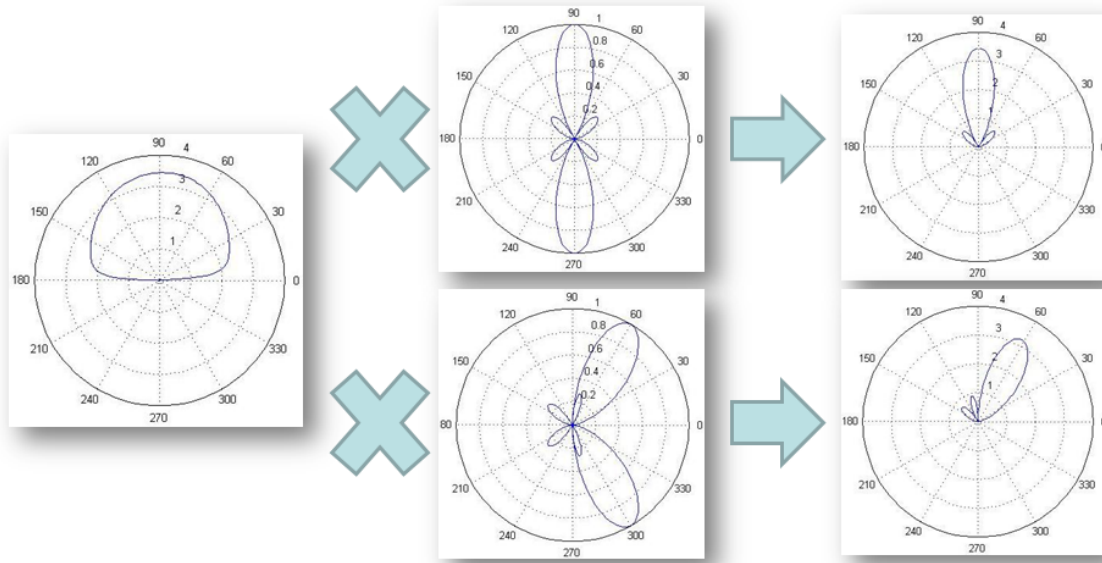


Figure 3.2: Pattern Multiplication Theorem

3.3 Uniform N-Element Linear Array

A uniform array is defined by uniformly-spaced identical elements of equal magnitude with a linearly progressive current phase difference, α , from element to element[32].

$$\begin{aligned}
 \Phi_1 &= 0 \\
 \Phi_2 &= \alpha \\
 \Phi_3 &= 2\alpha \\
 &\vdots \\
 \Phi_N &= (N - 1)\alpha
 \end{aligned}
 \tag{3.8}$$

Inserting this linear phase progression into the formula for the general N-element array gives:

$$\begin{aligned}
 AF &= 1 + e^{j(\Phi_2 + kd\cos\theta)} + e^{j(\Phi_3 + 2kd\cos\theta)} + \dots + e^{j(\Phi_N + (N-1)kd\cos\theta)} \\
 &= 1 + e^{j\Psi} + e^{j2\Psi} + \dots + e^{j(N-1)\Psi} \\
 &= \sum_{n=1}^n e^{j(n-1)\Psi} \quad (\Psi = \alpha + kd\cos\theta)
 \end{aligned}
 \tag{3.9}$$

The function Ψ is defined as the array phase function and is a function of the element spacing, phase shift, frequency and elevation angle. If the array factor is multiplied by $e^{j\Psi}$, the result is

$$(AF)e^{j\Psi} = e^{j\Psi} + e^{j2\Psi} + \dots + e^{jN\Psi}
 \tag{3.10}$$

Subtracting the array factor from the Equation 3.10 gives:

$$AF(e^{j\Psi} - 1) = e^{jN\Psi} - 1 \quad (3.11)$$

$$\begin{aligned} AF &= \frac{e^{jN\Psi} - 1}{e^{j\Psi} - 1} \\ &= \frac{e^{jN\frac{\Psi}{2}} \cdot e^{jN\frac{\Psi}{2}} - e^{-jN\frac{\Psi}{2}} \cdot e^{-jN\frac{\Psi}{2}}}{e^{j\frac{\Psi}{2}} \cdot e^{j\frac{\Psi}{2}} - e^{-j\frac{\Psi}{2}} \cdot e^{-j\frac{\Psi}{2}}} \\ &= e^{j(N-1)\frac{\Psi}{2}} \cdot \frac{\sin(\frac{N\Psi}{2})}{\sin(\frac{\Psi}{2})} \end{aligned} \quad (3.12)$$

The complex exponential term in the final expression above represents the phase shift of the array phase center, relative to the origin. If the center of the array is located at the origin, this phase term goes away.

$$AF = \frac{\sin(\frac{N\Psi}{2})}{\sin(\frac{\Psi}{2})} \quad (3.13)$$

Figure 3.3 shows various plots of the array factor AF versus the array phase function Ψ as the number of elements in the array is increased. **Note that these are NOT plots of AF versus the antenna elevation angle θ .**

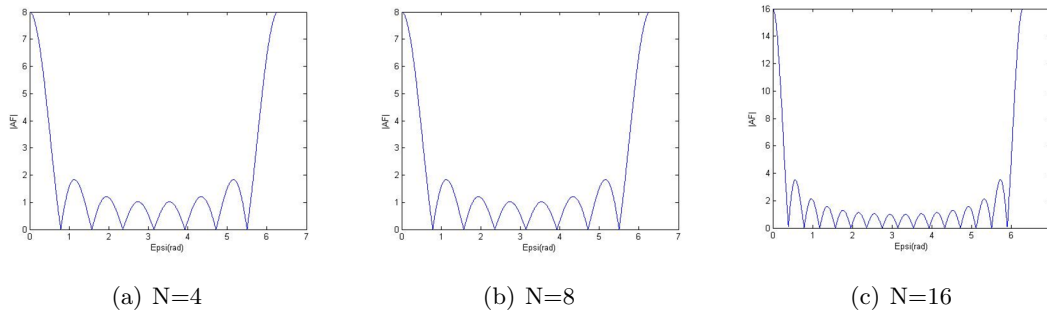


Figure 3.3: Array factor AF versus the array phase function Ψ

Some general characteristics of the array factor AF with respect to Ψ

$AF_{max} = N$ at $\Psi = 0$ (main lobe).

Total number of lobes = $N-1$ (one main lobe, $N-2$ side lobes).

Main lobe width = $4\pi/N$, minor lobe width = $2\pi/N$

The peaks of the array function are found by determining the zeros of the numerator term where the denominator is simultaneously zero.

- Numerator

$$\sin\left(\frac{N\Psi}{2}\right) = 0 \quad (3.14)$$

so,

$$\frac{N\Psi}{2} = \pm n\pi \quad (3.15)$$

$$\theta_n = \cos^{-1}\left[\frac{\lambda}{2\pi d}\left(-\alpha \pm \frac{2n\pi}{N}\right)\right] \quad n = 1, 2, 3 \dots \quad n \neq 0, N, 2N \dots \quad (3.16)$$

where α , is as before the linear phase difference between currents feeding individual antenna elements.

- Denominator

$$\theta_{mn} = \cos^{-1}\left[\frac{\lambda}{2\pi d}(-\alpha \pm 2m\pi)\right] \quad m = 1, 2, 3 \dots \quad (3.17)$$

The $m = 0$ term,

$$\theta_m = \cos^{-1}\left(\frac{\lambda\alpha}{2\pi d}\right) \quad (3.18)$$

represents the angle which makes $\Psi = 0$ (main lobe).

Finally we steer the lobe by changing the α (linearly progressive phase).

For example, when α is set to 31.3° , the main lobe will point 80° , as Figure 3.4 shows.

3.4 Grating lobes

A grating lobe is another unwanted peak value in the radiation pattern of the array. Grating lobes will occur whenever the size of individual array antenna elements is equal to or greater than the operating wavelength. There will be no grating lobes when the antenna element size is smaller than half a wavelength[33]. (For element sizes between one-half and one wavelength, the generation of grating lobes will depend on the steering angle.)

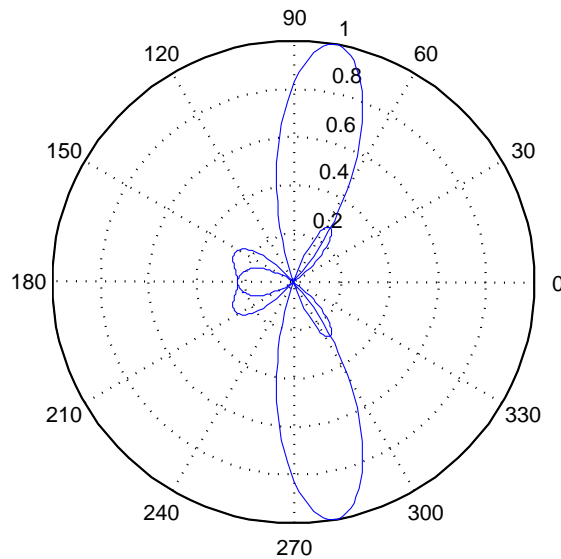


Figure 3.4: Matlab Simulation result with $\theta = 80^\circ$

Because $|\cos(\theta_m)| \leq 1$, from Equation 3.17 we get the term:

$$\left[\frac{\lambda}{2\pi d}(-\alpha \pm 2m\pi) \right] \leq 1 \quad (m = 0, 1, 2, 3 \dots) \quad (3.19)$$

where θ_m is the pointing direction.

We transform the term into:

$$-\frac{\alpha}{d_0} \pm \frac{m}{d_0} \quad (3.20)$$

where $d_0 = \frac{d}{\lambda}$.

If $d_0 \leq 0.5$, then only $m = 0$ produces a valid outcome. In other words, only the main lobe

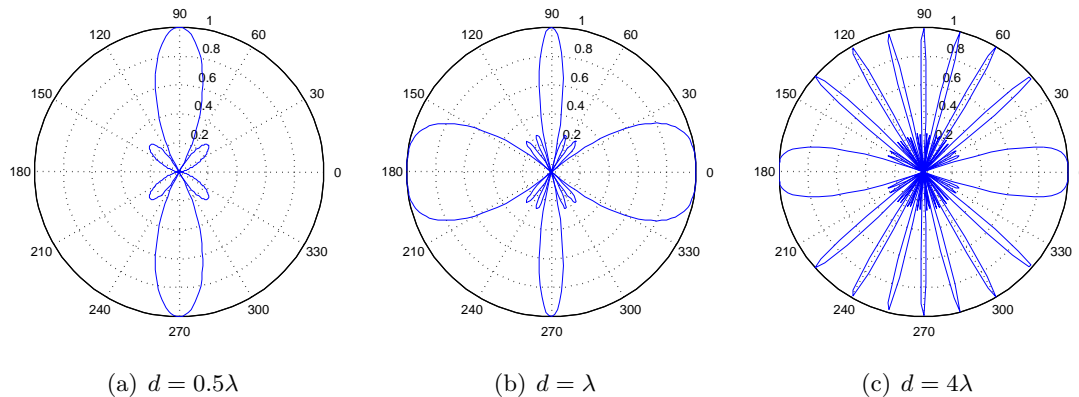


Figure 3.5: Grating lobes for various array element separation

is generated, as Figure 3.6(a) shows.

If $d_0 = 1$, not only $m = 0$, but also $m = 1$ produce valid outcomes. In this case, two symmetric grating lobes are introduced, whose amplitude is the same as the main lobe, as Figure 3.6(b) shows.

The bigger the spacing, d , between elements, the more values of m that can produce valid outcomes, ultimately the more grating lobes that are generated, as Figure 3.5(c) shows.

While $0.5\lambda < d < \lambda$, the grating lobes is decided by d_0 , in other words, by the linear current phase difference applied to each of the antenna elements, as Figure 3.6 shows.

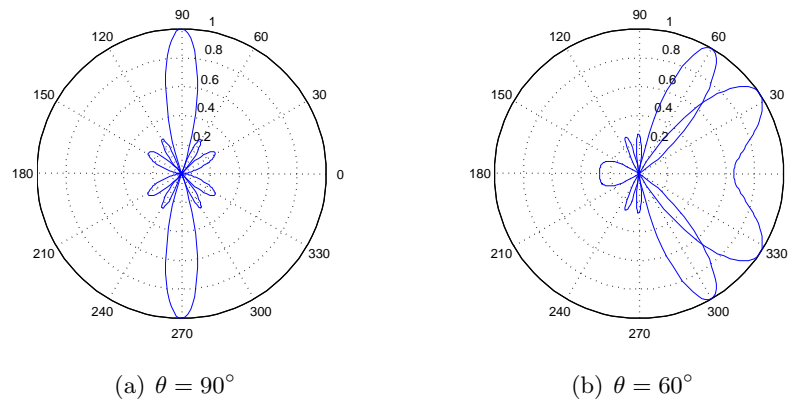


Figure 3.6: Grating lobes for array element separation $d = 0.75\lambda$

3.5 Conclusion

The larger the element the spacing, d , the narrower the main lobe, but then grating lobes will occur. So, in a practical antenna array systems, 0.5λ spacing is the optimum value, which minimizes the main lobe width, and also guarantees that no grating lobe is introduced.

Chapter 4

Test Platform Design

4.1 System Design Overview

The system is designed as a 4-element antenna array, but can be easily extended to n-elements. It mainly consists of five parts, as Figure 4.1 shows. The modulators, which are the core of the flexible continuous phase control, are responsible for changing the phase and adjusting the amplitude to form a certain beam. The source generates a constant sine wave divided into four identical paths to feed the modulators. The DACs (Digital to Analogue Converters) are for controlling the sine and cosine modulator inputs. The microcontroller is for calculating complex weights for each channel and to control the DACs through an Serial Peripheral Interface (SPI). Finally, the antenna array radiates the signal. Switched line phase shifters are commonly used to control the phase albeit discretely, however, quadrature modulator phase shifting is used in this work where flexible continuous phase control is now offered.

4.2 Phase Shifter

A phased array, which allows steering of the main lobe without mechanically rotating the antenna array or the formation of a certain radiation pattern, consists of a set of radiating elements fed by means of phase shifted sources.

4.2.1 Switched line phase shifter

This consists of a number of sections using two-way switching among different line lengths to achieve a phase shift, as Figure 4.2 shows.

PIN diodes and FETs are usually employed as switching elements. PIN diodes behave as resistors to RF signals, where a dc current can control the resistance. A forward-biased diode will have a resistance of few Ω and a reverse-biased produces a resistance of 10 - 100k ohm.

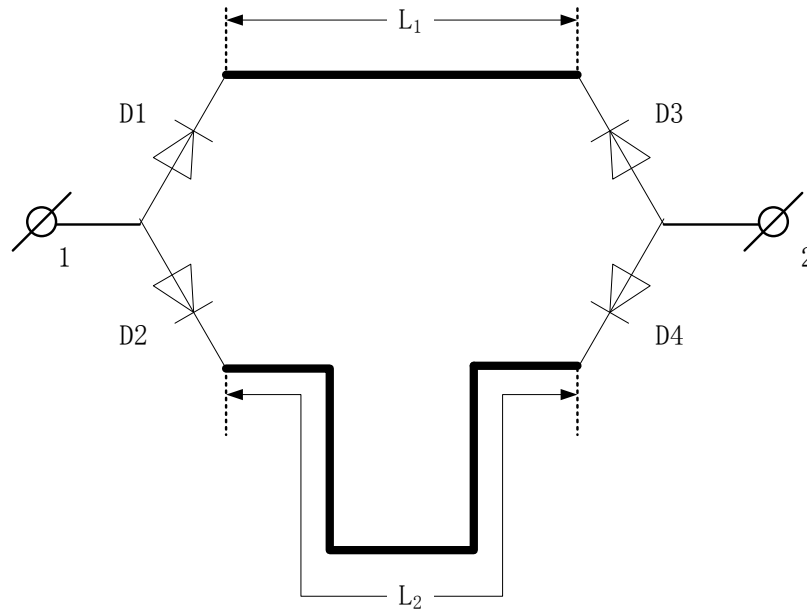


Figure 4.2: Diode switched line phase shifter

and the phase offset is $\arctan(4/3)=53.13$ degree. The wave is as shown in Figure 4.4. The theoretical insertion loss is 6dB, in practice it is slightly higher (nearer 8 dB or 9 dB). This may be a quite a severe disadvantage in many phased array applications, often restricting the use of vector modulators to IF stages rather than at the antenna elements themselves. The bandwidth, however, can be quite broad. Quadrature modulators are able to control the signal phase as well as the signal amplitude, which makes them particularly useful in smart antennas.

4.2.3 Quadrature Modulator AD 8346

The AD8346 is a silicon RFIC I/Q modulator for use from 0.8 GHz to 2.5 GHz, with excellent phase accuracy and amplitude balance, that allows high performance direct modulation to RF. A polyphase network phase splitter employs a differential LO input providing accurate phase quadrature from 0.8 GHz to 2.5 GHz. There is a buffer amplifier between two sections of the phase splitter to improve the signal-to-noise ratio. Two differential V-to-I converters are used to feed mixers with the baseband modulation signals. The outputs of the mixers are summed and matched to 50 ohm impedance.

The schematic for this project is shown in Figure 4.5. Port1 is connected to the AD5308 Digital to Analogue converter. The LO is fed by a Wilkinson power divider.

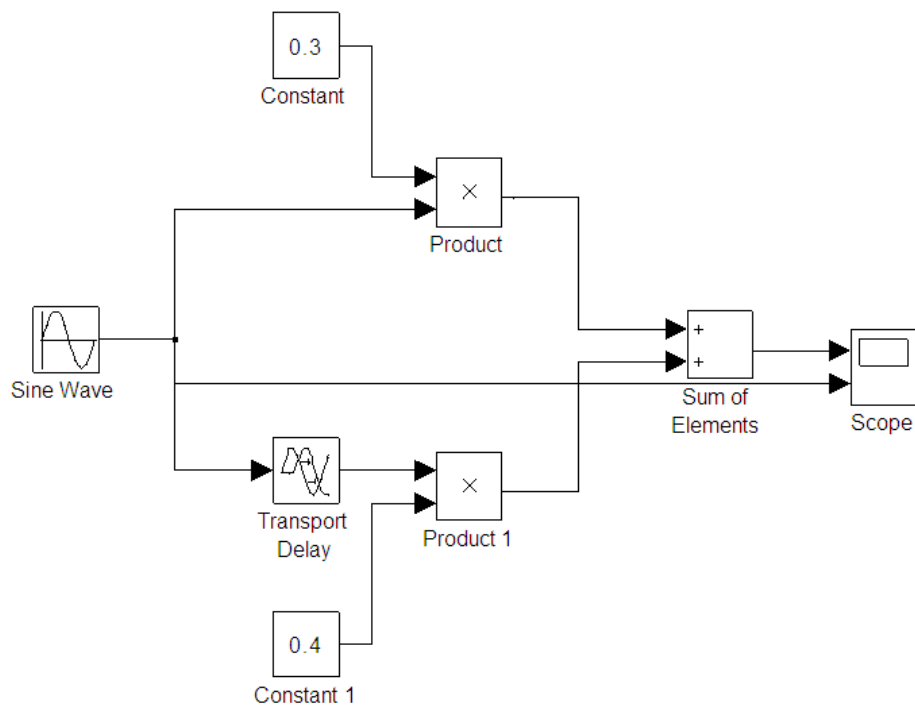


Figure 4.3: Quadrature modulator phase shifter Simulink model

LO Drive

The LO terminal can be driven single-ended (shown in Figure 4.6) at a cost of slightly higher LO feedthrough. LOIN must be ac coupled to ground with a capacitor and LOIP is driven through a coupling capacitor from a 50 ohm source.

Since the LO port is internally matched to a 50 ohm source, no additional matching circuit is required. A LO drive level of between -6dBm and -12dBm is required. A drive level of -10dBm is recommended for optimal performance. The insertion loss of the Wilkinson Power Divider designed for this project is -10dB, thus the output power level of the signal generator is set to 0dbm. Although a -6dBm level would improve the temperature stability performance, higher levels degrade linearity, while lower levels tend to increase the noise floor.

RF output

Figure 4.7 describes the RF output interface. The port is designed to drive a 50 ohm load and must be ac coupled (usually by a 100pF capacitor). When the I and Q inputs are driven in quadrature by 2 V p-p signals, it results in approximately -10 dBm output power.

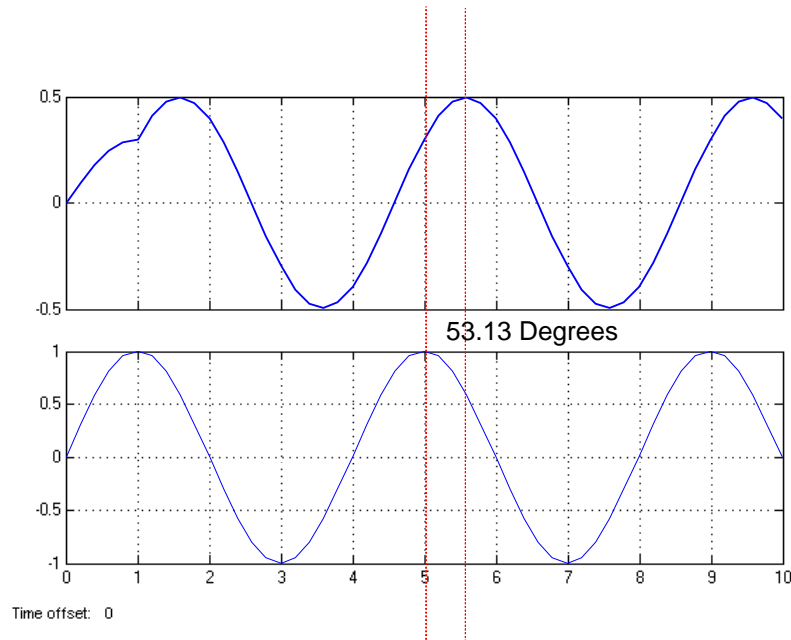


Figure 4.4: Quadrature Modulator Simulation Result

4.3 Local Oscillator Design

Many kinds of RF applications, such as antenna arrays, demand power to be distributed to several devices. One solution can be to use a power divider. Here, we need to split a 2.45GHz sine wave signal from a Vector Signal Generator (Agilent E8267D PSG) to feed four modulator (Linear Technology LT5572) local oscillators.

4.3.1 Power Divider Introduction

Some RF applications demand power to be divided between various paths. One of the solutions can be to utilize a power splitter/divider. Power dividers are reciprocal devices, which can also combine power from output ports into the input port. The two main types of power divider are, reactive and resistive, which each has its own specific advantages and applications. This section explains both power divider types and compares them to decide which suits this project more.

4.3.2 Resistive divider

Figure 4.8 shows the schematic of a simple 2-way resistive power divider. Z_0 denotes the characteristic impedance. An N-way divider can be easily designed by adding new

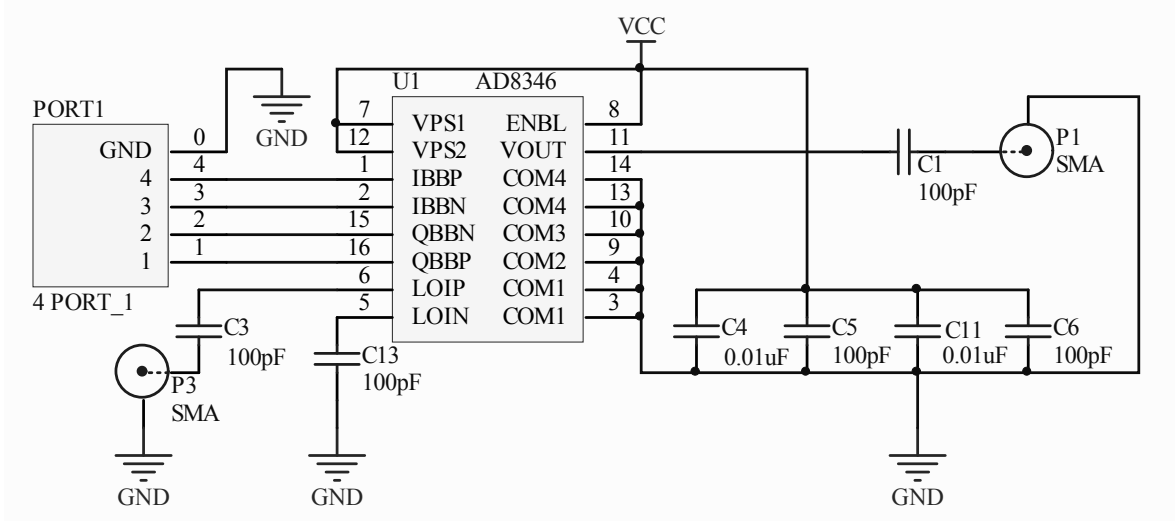


Figure 4.5: Quadrature Modulator AD8346 Circuit Schematic

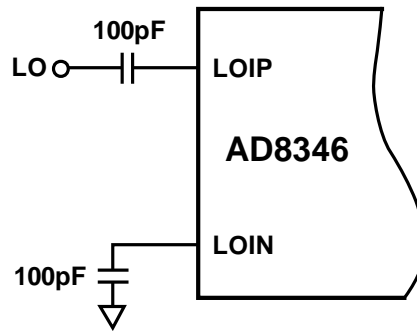


Figure 4.6: Single-Ended LO Drive

branches and replacing the resistors. Equation 4.1 calculates the resistance value. Resistive power dividers generally are more compact comparing to reactive dividers due to its lumped elements structure. They have an extremely broad operating frequency and they are also the only type that can handle DC. However, these units can be limited by the power tolerances of the resistors. High loss and poor isolation make them a bad choice for applications with low insertion loss and isolation requirements.

Resistor values for an N-way resistive divider:

$$R = Z_0 \cdot \left(\frac{N - 1}{N + 1} \right) \tag{4.1}$$

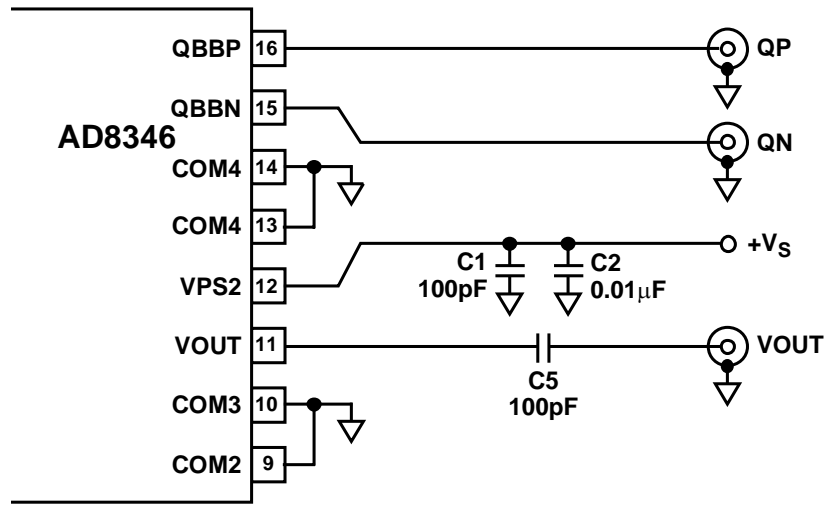


Figure 4.7: RF output interface

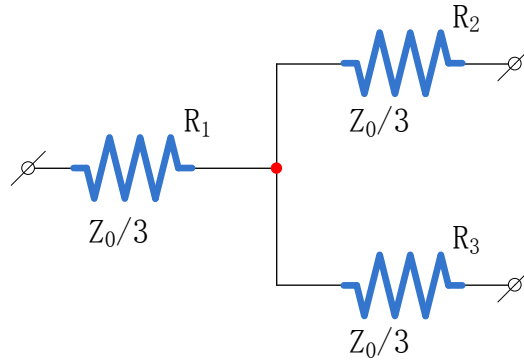


Figure 4.8: Resistive Divider

where Z_0 is the characteristic impedance of the system, here 50Ω . For 4-way divider, this means:

$$R = 50\Omega \cdot \left(\frac{4 - 1}{4 + 1} \right) = 30\Omega \quad (4.2)$$

Transferred power ratio = $(1/N)^2$

Transferred power ratio = $(1/2)^2 = -12.04 \text{ dB}$

Since ideal resistors are linear components, the S-parameters should stay constant no matter how high the frequency is. In reality, real resistors are non-ideal, for example here is the performance of a real SMT resistor model (shown in Figure 4.9), simulated using Agilent's ADS.

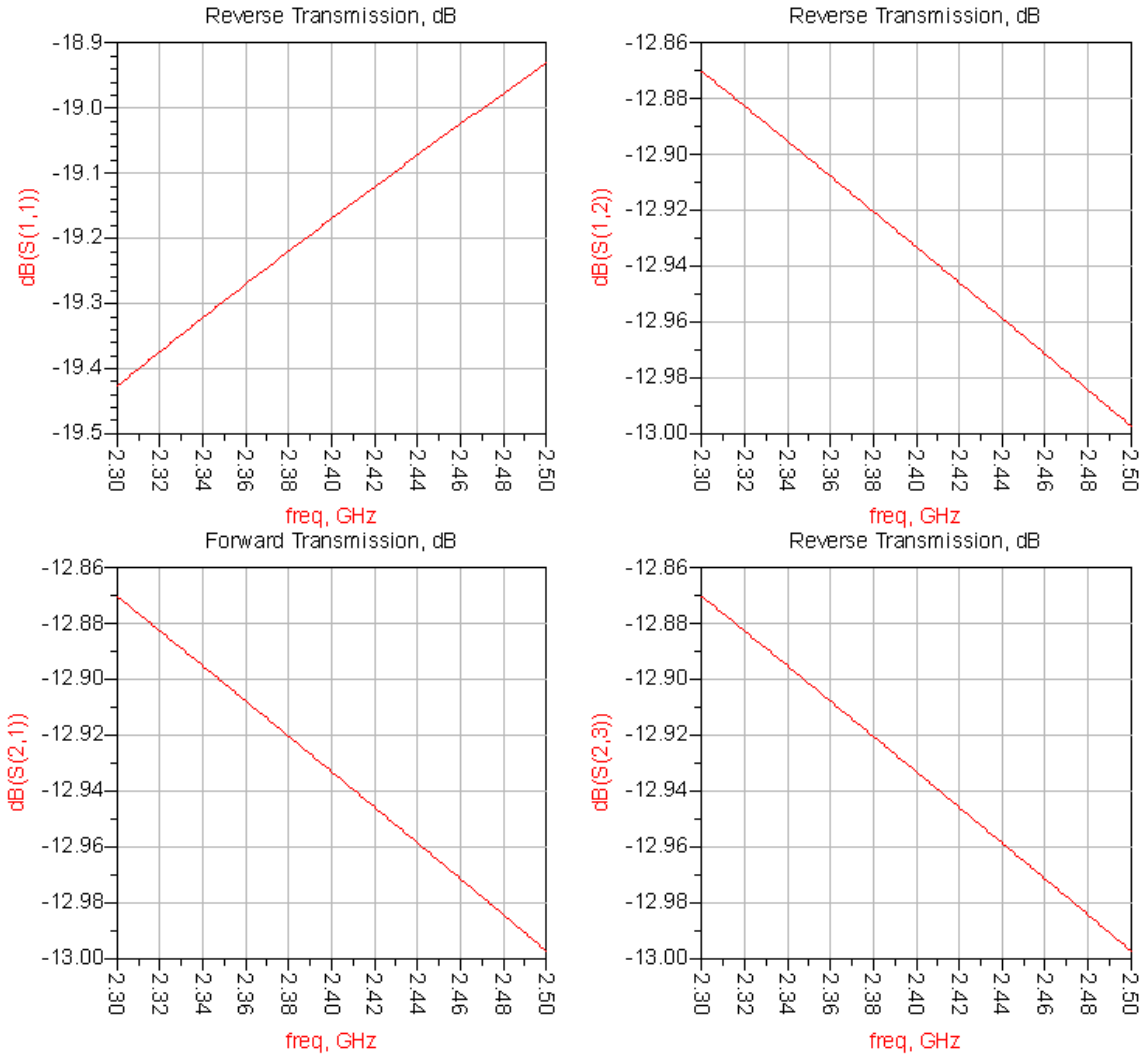


Figure 4.9: ADS S-parameter simulation for resistive divider

4.3.3 Reactive power divider

With the development of wireless communication technology, the carrier power requirements (in terms of losses) are increasing. Micro-strip technology plays an important role in low power consumption and compact high frequency circuits. For RF circuits such as mixers and power amplifiers, power splitting and coupling components are essential parts. This section describes the most frequently used type of reactive power divider based on a micro-strip line, the Wilkinson power divider.

Currently, dual working frequency dividers have been developed, introduced in [34]. This project needs a 4-way splitter (insertion loss -6.02dB) which consists of three 2-way dividers. This section begins with a theoretical description followed by simulations.

Finally, a practical board has been made and measured using a Rohde & Schwarz Vector Network Analyzer (VNA) and compared with the simulation result.

Figure 4.10 shows the structure of a transmitting line divider. The characteristic port

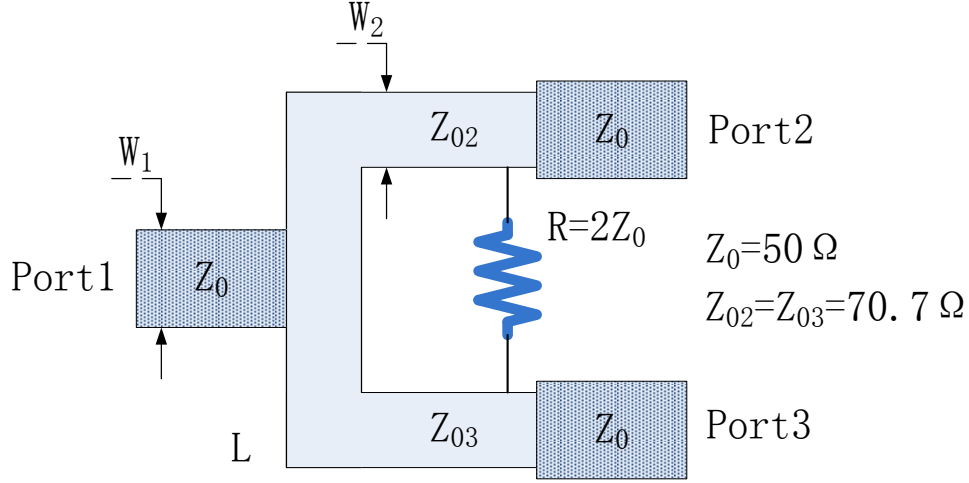


Figure 4.10: Structure of 2-way Reactive Power Divider

impedance is Z_0 . The electrical length of the two split paths is $\lambda/2$ for both, with characteristic impedance of Z_{02} , Z_{03} terminated by loads R_2 and R_3 .

Three assumptions are made at first:

1. No reflection at Port1
2. The output voltages at Ports 2 and 3 are identical.
3. The output power ratio of Ports 2 and 3 are $1/k^2$.

The following equations based on the three assumptions are obtained.

$$\left\{ \begin{array}{l} \frac{1}{Z_{in2}} + \frac{1}{Z_{in3}} = \frac{1}{Z_0} \\ \frac{\left(\frac{1}{2} \cdot \frac{U_2^2}{R_2}\right)}{\left(\frac{1}{2} \cdot \frac{U_3^2}{R_3}\right)} = \frac{1}{k^2} \\ U_2 = U_3 \end{array} \right. \quad (4.3)$$

Where U_2 and U_3 are the output voltage of port 2 and port 3. According to transmission line theory,

$$\begin{cases} Z_{in2} \cdot R_2 = Z_{o2}^2 \\ Z_{in3} \cdot R_3 = Z_{o3}^2 \end{cases} \quad (4.4)$$

If $R_2 = kZ_0$, then Z_{o2} , Z_{o3} , R_3 can be calculated:

$$\begin{cases} Z_{o2} = Z_0 \sqrt{k(1+k^2)} \\ Z_{o3} = Z_0 \sqrt{k(1+k^2)}/k^3 \\ R_3 = Z_0/k \end{cases} \quad (4.5)$$

An equal power divider is required, therefore, $k = 1$. At this point, the key parameters have been identified and their relationship established.

Calculations

- All resistors: $R = 2Z_0$
- Micro strip Line: $L = \lambda/4$ $Z = \sqrt{2}Z_0$
- Transferred power ratio = $1/N$
- Transferred power ratio = -6.02dB

Simulations

The ADS simulation result is shown in Figure 4.11, where the operating frequency is 2.45GHz. The optimization parameters and schematics are shown in the appendix.

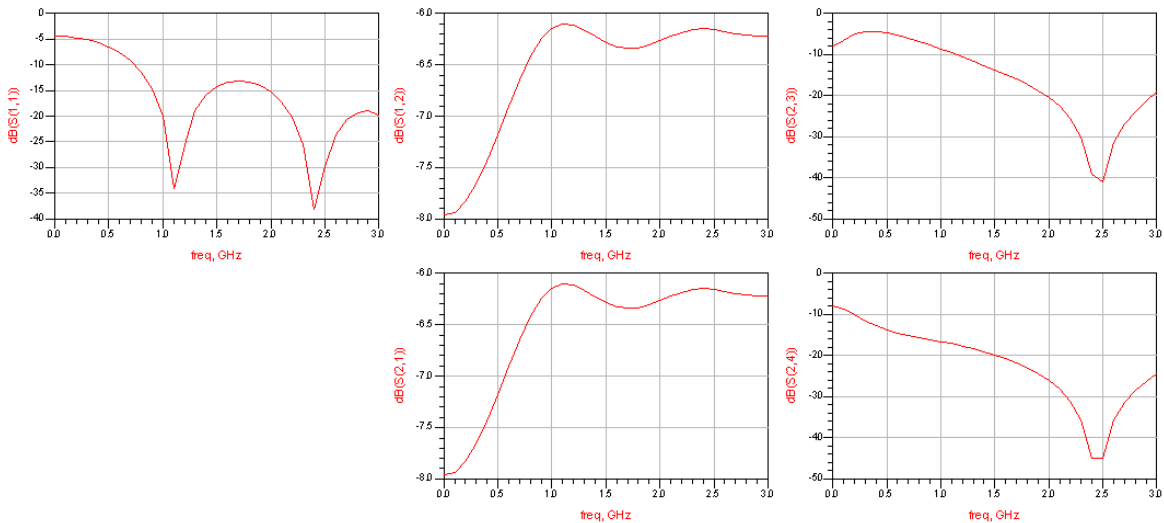


Figure 4.11: Reactive Power Divider Simulation Result



Figure 4.12: Wilkinson Power Divider VNA Measurements

4.3.4 Practical Wilkinson Power Divider

Figure 4.12 shows that the best operating point for this divider is at 3.18GHz with the lowest insertion loss at -6.19dB. This is quite different from the simulation result, possibly caused by the uncertainty of FR-4 substrate permittivity. The upper curve indicates the S_{11} of the Wilkinson power divider while the lower curve describes S_{21} . Other Wilkinson output ports have similar S_{21} curves which are shown in the appendix section.

Comparison

The Vector Signal Generator can generate up to 16dBm [35], but this system is noise sensitive. Resistive dividers require much more power input to reach the same power output as reactive ones. Although this system requires extreme amplitude and phase identities, where resistive dividers are superior, these can be compensated by the quadrature modulator. Also, for this system, a fixed 2.45GHz operating frequency is

needed. So the reactive power divider should be a better choice. Figure 4.13 shows key parameters of two manufactured and one self-made power splitter.

Conclusion

Model No.	151 – 262 - 004	50PD-293	DIY
Impedance(Ohms)	50	50	50
Insertion Loss(dB)	6.37dB	6.37dB	10.12dB
VSWR	1.30:1	1.50:1	9.96:1
Amplitude Tracing	0.3dB	0.7dB	0.5dB
Input Power	2W	2W	Unmeasured
Connectors	SMA Female	SMA Female	SMA Female
Operating Temp.(degree)	-40 85	0 70	Unmeasured

Figure 4.13: Comparison of two commercial and a self-made power splitters

Although the self-made Wilkinson power divider has a much higher insertion loss than the theoretical divider, this is a not insurmountable loss of -10dB. In the case of a 0dBm output Agilent E8267D PSG, the modulators are still fed with a -10dB source, which is the optimum power for the local oscillators[36]. Therefore, this self-made power divider can still be used to meet the research requirements, so costly commercially manufactured dividers are not necessary.

4.4 I,Q Input Control Circuits

4.4.1 DAC Selection

The proposed circuit includes two DACs to create a differential input for the modulator.

Three DACs were identified as potential candidates for the final electronic circuit, the AD5308, BH2221 and BU2501 (shown in Figure 4.14). The three components were compared under the following criteria; number of channels, bit resolution, complexity, control, non-linear error, reference voltage supply, lead time, price and sampling rate. The specification for the DAC includes a minimum 8-bit resolution, sampling can be as low as 1 kHz, control can be any serial interface standard, and supply voltage may range from 3-5V, with a minimum of 10 channels, package type to ideally accommodate

	AD5308	BH2221FV	BU2501
No. of channels	16	12	12
Bit resolution	8	8	8
Control	SPI I ² C	3-Line serial	3-Line serial
Non-linear error	1 LSB	1.5 LSB	N A
Sampling Rate	167 Hz	10 MHz	4 Hz
Speed of Development	Fast	Slow	Slow
Power supply	2.7V 5.5V	2.7V 5.5V	2.7V 3.6V
Package type	TSSOP16	SSOP-B20	SSOP-B20
Lead time	Immediate	Immediate	Immediate
Price	€2.8	€5.48	€4.80
Internal Reference	N A	N A	N A
Other relevant Features	<ol style="list-style-type: none"> 1. Channel Monitor 2. Simultaneous output 3. User-programmable offset 4. Thermal monitor 	<ol style="list-style-type: none"> 1. Built-in RESET Function 	

Figure 4.14: DAC chips comparison

hand soldering, no lead time and efficient use of the ATmega128 ports.

Taking the project specification into account, the three chips have equal resolution. An external reference chip Ref192 ensures the chips get the same voltage reference input, which reduces the I/Q inputs errors of the modulators. The SPI and I²C standard interface increase the compatibility with ATmega128 and allows the use of a more mature standard. The simultaneous output feature can minimize the transient error in trying to simultaneously control four (or more later) antennas.

Also, the high resolution and low non-linear error increase the output accuracy.

Moreover, other features are also present; such as low output noise and also the channel monitoring feature, both of which could prove critical in evaluating the performance of the antenna arrays. The thermal monitoring feature prevents the Ref192 chip being over-heated. Finally, more channels and higher sampling speeds can be used for extended experiments in the future.

The DAC schematic is shown in Figure 4.15. Port 5 is connected to the ATmega128 controller, for controlling purposes, and Port7 is connected with I/Q of quadrature modulator.

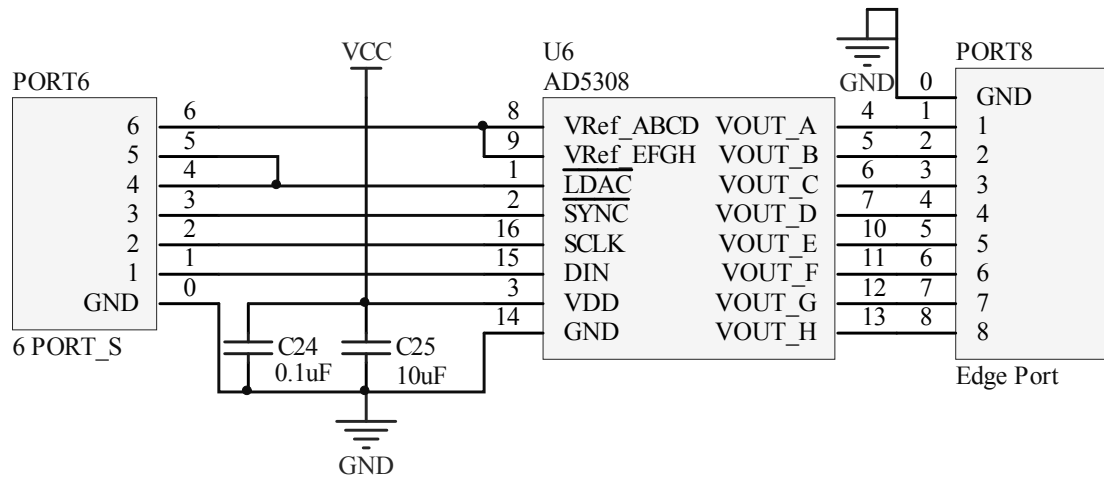


Figure 4.15: DACs Interface Circuit Schematic

4.4.2 REF19x Series Voltage Reference

The REF19x series precision band gap voltage references include a patented temperature drift curvature correction circuit. Laser trimming of highly stable thin-film resistors guarantee an ultra low temperature coefficient and high initial accuracy.

The REF19x is made up of low dropout voltage (LDV) devices providing stable output voltage from supplies as low as 100mV above the output voltage, consuming less than $45\mu A$ and less than $15\mu A$, when sleep mode is enabled, by applying a low TTL or CMOS level to SLEEP pin.

Figure 4.16 indicates the nominal output voltage of the 19x series. [36] states that the I & Q input should be DC-biased to approximately 1.2V, which is half of 2.5V. Figure 4.17 shows the accuracy of different grades.

Part Number	Nominal Output Voltage (V)
REF191	2.048
REF192	2.50
REF193	3.00
REF194	4.50
REF195	5.00
REF196	3.30
REF198	4.096

Figure 4.16: Nominal Output Voltage

Parameter	Symbol	Condition	Min	Typ	Max	Unit
INITIAL ACCURACY ¹	V_o	$I_{OUT} = 0 \text{ mA}$				
E Grade			2.498	2.500	2.502	V
F Grade			2.495		2.505	V
G Grade			2.490		2.510	V
LINE REGULATION ²	$\Delta V_o / \Delta V_{IN}$	$3.0 \text{ V} \leq V_s \leq 15 \text{ V}, I_{OUT} = 0 \text{ mA}$				
E Grade				2	4	ppm/V
F and G Grades				4	8	ppm/V

Figure 4.17: Electrical characteristics-REF192 @ $T_A = 25^\circ\text{C}$

Figure 4.18 shows the schematic. As [37] described, voltage input is decoupled by a $0.1\mu\text{F}$ and a $10\mu\text{F}$ capacitor in parallel, output is decoupled by a $0.1\mu\text{F}$ and a $1\mu\text{F}$ capacitor.

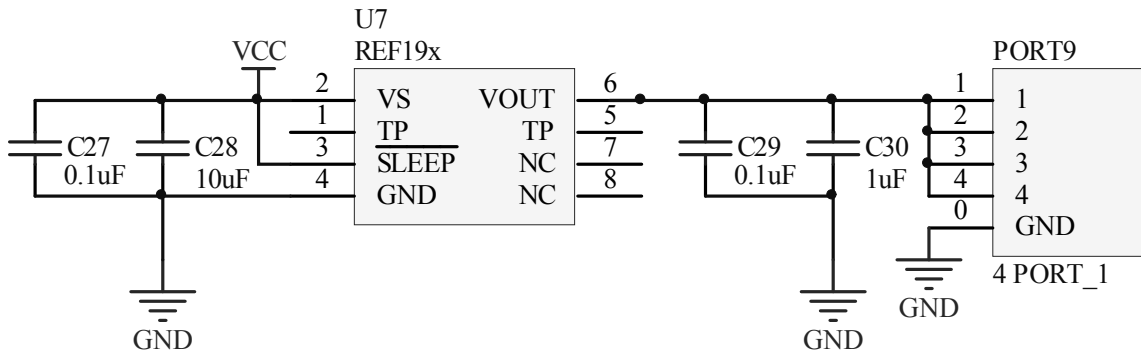


Figure 4.18: Circuit schematic for REF192

4.5 Radiation Units

Micro-strip antennas are a category of antenna developed at the end of the last century. They are light, simple, compact, low-cost, with a high radiation efficiency, where it is easy to achieve dual or multiple operating frequencies. These advantages make them widely used in new cell phones, PDAs, laptops, etc.

Much research on micro-strip antenna geometry developed new structures, such as the reverse “L” [38], the reverse “F” [39] and the Photonic-Band-Gap Micro-strip Antenna, each of which is useful for specific applications. The reverse “L” offer dual operating frequencies, which is able to meet requirements of both 2.4 to 2.5 GHz and 5.0 to 6.0 GHz for Bluetooth and Local Area Network communications. The most significant advantage of reverse “F” antenna is its compactness, which made it very useful on mobile devices. And its radiation range can reach 52m (Gain = 2.2dB) compared to

16m (G = -3dB) for common patch antennas.

In this section, a rectangular patch antenna is developed, performed a simulation and optimized the impedance matching by Advanced Design Software, specified with a center frequency of 2.4GHz and with a 200MHz bandwidth.

Rectangular patch antennas can be treated as a low resistance transmission line, with a width (W) and a length (L). Normally, $L \approx \lambda_e/2$ and $\lambda_e = \lambda_0/\sqrt{\epsilon_e}$, where λ_e is the wavelength in the micro-strip. The thickness of the substrate is t ($t \ll \lambda_0$). λ_0 is the wavelength in free space. The operating frequency is denoted by f .

Width Calculation:

$$W = \frac{c}{2f} \left(\frac{\epsilon_r + 1}{2} \right)^{-1/2} \quad (4.6)$$

where ϵ_r is relative permittivity.

Length Calculation:

$$L = \frac{c}{f\sqrt{\epsilon_e}} - 2\Delta l \quad (4.7)$$

$$\epsilon_e = \frac{\epsilon_r + 1}{2} + \frac{\epsilon_r - 1}{2} \left(1 + \frac{10h}{w} \right)^{-1/2} \quad (4.8)$$

where ϵ_e is effective permittivity.

$$\Delta l = 0.412h \frac{(\epsilon_e + 0.3) \left(\frac{w}{h} + 0.264 \right)}{(\epsilon_e - 0.258) \left(\frac{w}{h} + 0.8 \right)} \quad (4.9)$$

where h is the copper layer thickness.

Many kinds of substrates, with dielectric constants in the range of $2.2 \leq \epsilon_r \leq 12$ can achieve a good response. A substrate that would offer a good antenna performance is usually thick, while the dielectric constant is low. A lower dielectric constant provides a better performance compared to a thin substrate[40]. The most common FR-4 substrate is chosen for budgetary reasons, compared to the more expensive ceramic substrates with a higher dielectric constant.

The specifications of the rectangle patch antenna are listed in Figure 4.19.

According to Equations 4.7 and 4.8 and design specifications, the size is W=37.0mm and L=28.2mm. The next step is to calculate the micro-strip line width. Using the Advanced Design Software micro-strip line calculation function, yields the design specification shown in Figure 4.20.

The feed point is set in the middle of the antenna, where a further optimization will

Center Frequency f_0	2.4 GHz
Substrate	FR-4
Dielectric Constant	4.9
Substrate Height	1.6 mm
Loss Tangent	0.025
Copper Thickness	0.035 mm

Figure 4.19: Design specification for rectangular patch antenna

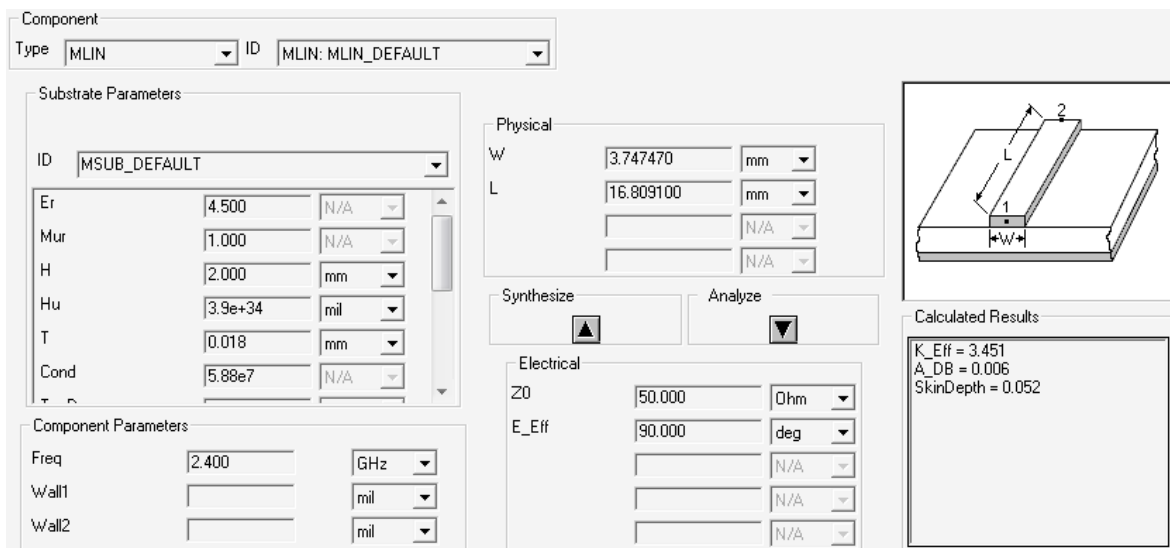


Figure 4.20: Micro-strip line calculation function in ADS

be performed later. The layout is as Figure 4.21 and the characteristics are showed in Figure 4.23.

From Figure 4.23 indicates the antenna is far from a perfect impedance match. ADS provides an optimization method, which is suitable for this task. Adjusting the length makes the real part of the impedance approaches 50 ohms. Also, adding a small part of 50 ohm transmission line in parallel eradicates the imaginary part.

Simulation results after optimization are shown in Figure 4.22. The radiation characteristics are shown in Figure 4.23, where the radiation efficiency is very high. The measured S_{11} is shown in Figure 4.24. The result appears to be acceptable, while the best operating frequency is slightly different from the frequency predicted by simulations.

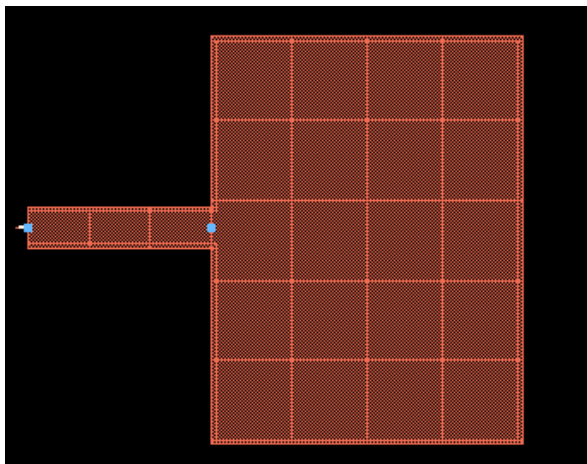


Figure 4.21: Rectangular patch antenna layout

4.6 Controlling Unit

4.6.1 Microcontroller ATmega128L

The ATmega128 is a low-power CMOS 8-bit microcontroller based on the AVR enhanced RISC architecture, with single cycle processing time, allows the ATmega128 reach 1MIPS per Mhz. This balances the power consumption and processing speed. This research requires a relatively simple beamforming algorithm, which means that a low-cost ATmega128L with an 8MHz oscillator is able to complete the task.

The AVR core has abundant instructions and 32 general purpose registers, all of which are directly connected to the Arithmetic Logic Unit (ALU). This feature allows access to two independent registers in a single clock cycle. This structure greatly improves code efficiency, while achieving throughputs up to ten times faster than common CISC microcontrollers.

128 Kbytes of in-system programmable flash memory, with Read-While-Write capabilities, can store the lookup table for I/Q inputs. A specific SPI serial port reduces the complexity of the program for driving AD5308 DACs. An I2C interface can be used for displaying the current parameters on a PCD8544 LCD module during the experiments.

4.6.2 PCD8544 LCD Display

The PCD8544 is a low power CMOS LCD driver for driving a graphic display of 48 rows and 84 columns. On-chip generation of LCD supply and bias voltages and other necessary functions are all integrated on a single chip, which minimizes the external

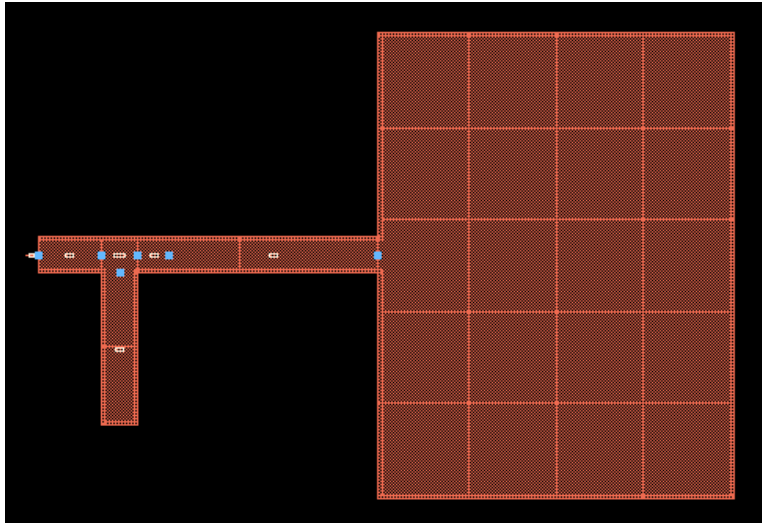


Figure 4.22: Optimized rectangular patch antenna layout

components and lowers power consumption. A serial bus interface is used to connect the PCD8544 to the main controller, with a full speed of up to 4Mbps.

4.6.3 Software

The program mainly consists of three parts, which are the I/Q look-up table, the LCD driver and the AD5308 driver. The look-up table is pre-calculated, using a Matlab program, according to Equation 3.18, which stores the excitation phase and amplitude values. The LCD Driver drives the PCD8544 LCD, displaying current working parameters, like the excitation phase, phase offsets or steering angle. The AD5308 driver controls the two AD5308 DACs to renew the voltage feeding the I/Q quadrature modulators' inputs.

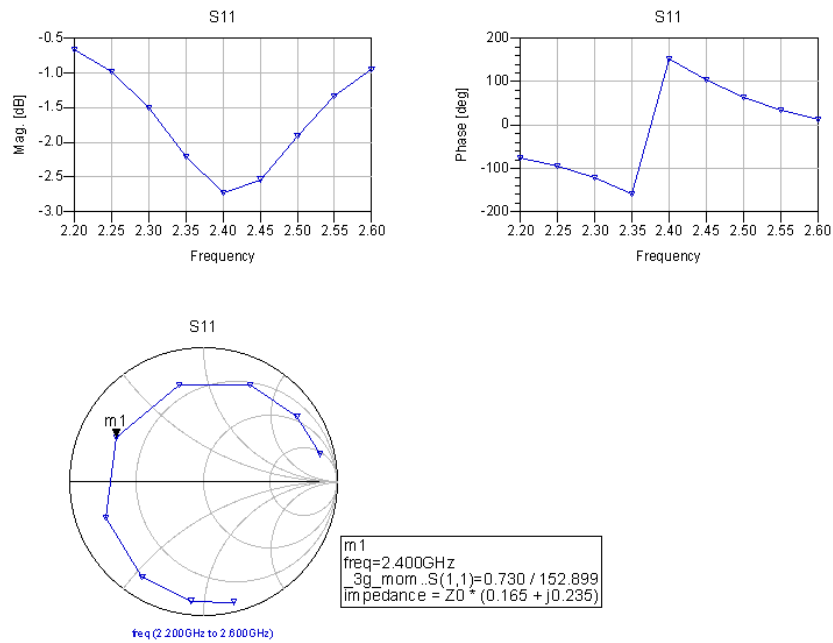


Figure 4.23: Rectangle Patch Antenna Simulation Result

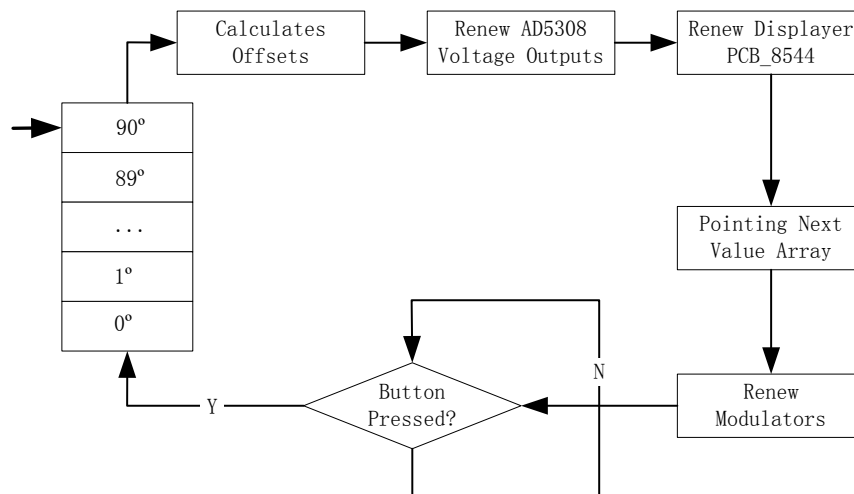


Figure 4.26: Software flow diagram

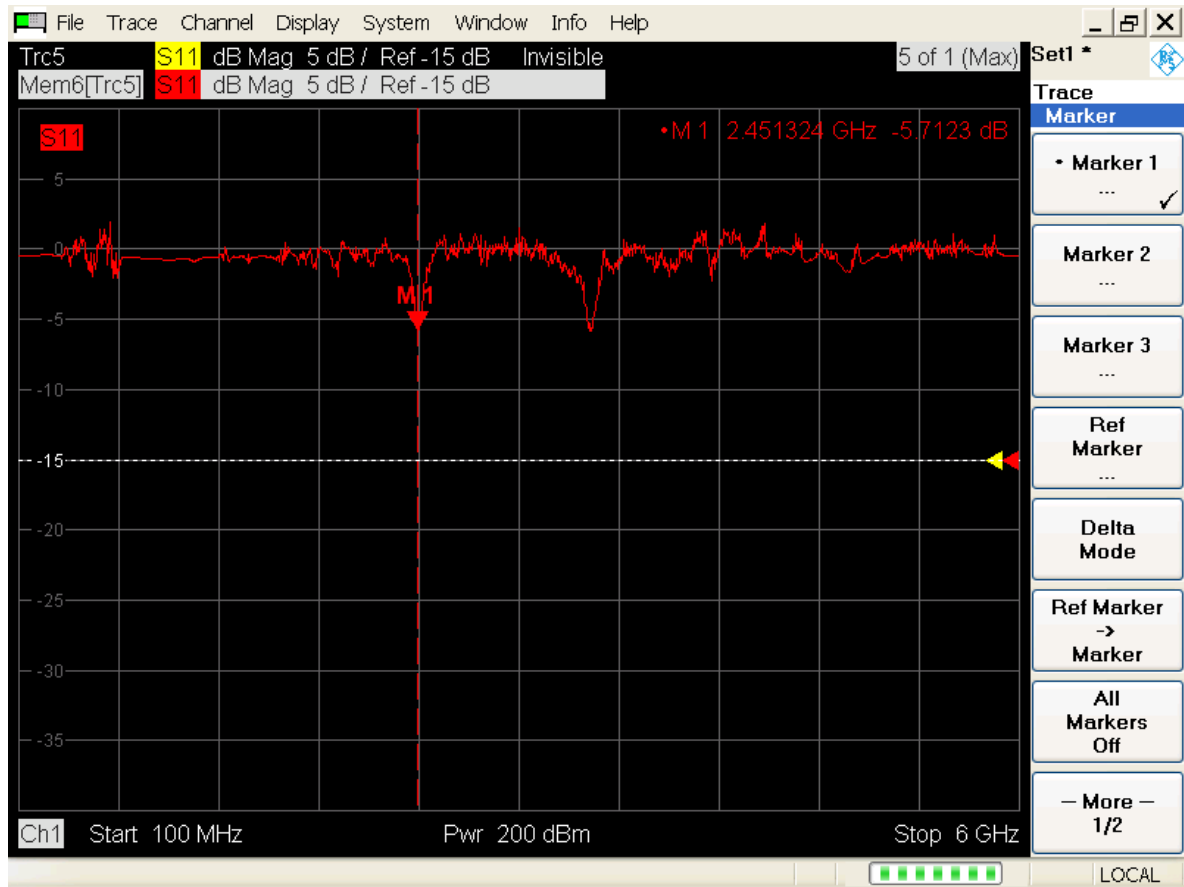


Figure 4.24: Rectangle Patch Antenna VNA Measurement Result

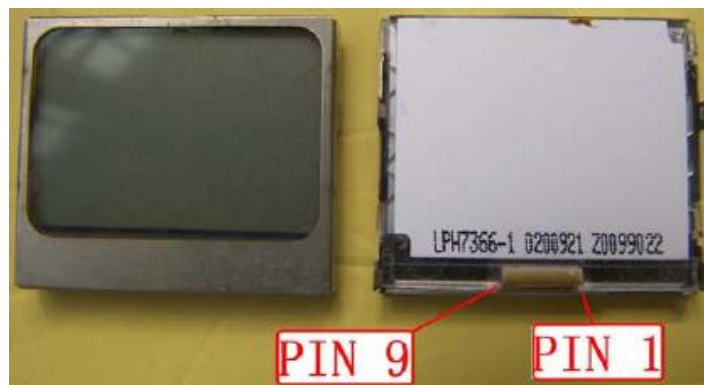


Figure 4.25: PCD8544 LCD

Chapter 5

Platform Tests

5.1 Calibration

A Look-Up Table (LUT) of theoretical I & Q voltage values versus steering angle has been pre-computed using Matlab and stored within the microcontroller memory map. When using the LUT values, the actual resultant phase output can be quite different from the desired waveform, with a typical example shown in Figure 5.1. This error is caused partly by a non-linear error from the quadrature modulator(s).

In order to compensate for this, a software program for manual calculation was written, which can individually adjust each I and Q input of the modulator. Although the manual method is crude, it is effective, as seen in Figure 5.2.

5.2 Gain measurement methods

Antenna measurements are important in both design and manufacture. Once a design is finished, a measurement must be made to check the performance of the whole system, to see if it can meet certain specifications. Antenna parameters are many and varied, although typically only a few key parameters are measured, such as gain, the radiation patterns and impedance (which is in turn related to the antenna bandwidth). The main purpose of this section is to describe the parameters measured and also the various measurement methods.

5.2.1 Standard-gain horn antenna comparison method

The signal obtained from the antenna under test is compared with that from an antenna of known gain (usually a standard-gain horn antenna).



Figure 5.1: Practical Quadrature Modulator Outputs

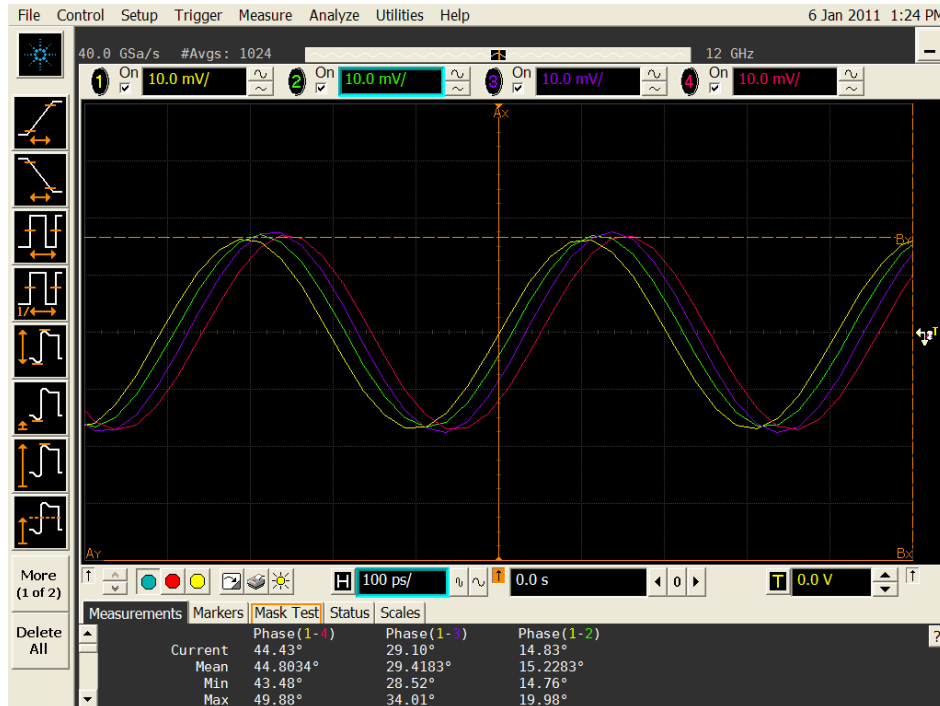


Figure 5.2: Calibrated Quadrature Modulator Outputs

The gain (G) of the target antenna is simply calculated using Equation 5.1.

$$G = P_R \cdot \frac{G_s}{P_s} \quad (5.1)$$

Where P_R is the power received by the antenna under test, G_s is the gain of the standard-gain horn and P_s is the power received by the known antenna. This method requires no knowledge of the path loss due to the distance between the source antenna and target antenna.

5.2.2 Two-antenna method

The two-antenna method shown in Equation 5.2 and derived from the Friis Transmission equations [41].

$$G = \frac{P_R(4\pi)^2 r^2}{G_s P_s \lambda^2} \quad (5.2)$$

In this case, a measurement of P_R determines the antenna gain (G) when P_s , G_s , λ and r are known. If G_s is not known, then identical antennas must be applied in both transmitter and receiver, so that G_s is replaced in the equation by another G, thereby simplifying the calculations.

5.2.3 Three-antenna method

Three unknown gain antennas G_1 , G_2 and G_3 are set as source and test them in three possible combination pairs. The received powers can be calculated from Equation 5.3, where P_s is source power.

$$\begin{aligned} P_{12} &= \frac{P_s G_1 G_2 \lambda^2}{(4\pi)^2 r^2} & G_1 &= \frac{4\pi r}{\lambda} \sqrt{\frac{P_{13} P_{12}}{P_s P_{23}}} \\ P_{23} &= \frac{P_s G_2 G_3 \lambda^2}{(4\pi)^2 r^2} & \Rightarrow G_2 &= \frac{4\pi r}{\lambda} \sqrt{\frac{P_{12} P_{23}}{P_s P_{13}}} \\ P_{13} &= \frac{P_s G_1 G_3 \lambda^2}{(4\pi)^2 r^2} & G_3 &= \frac{4\pi r}{\lambda} \sqrt{\frac{P_{23} P_{13}}{P_s P_{12}}} \end{aligned} \quad (5.3)$$

5.2.4 Comparison

The two-antenna and three antenna method rely on either there being a constant, uniform path loss or knowledge of the path loss, between each source and the antenna under test. In reality, therefore, as this uniformity is a challenge to guarantee, the

calculations are more complex.

By the same token, the standard antenna comparison method is also a simplification, in that it requires knowledge of the standard antenna gain only, thereby ignoring the impedance mismatch difference between the two antennas. For a standard horn antenna with known gain given by the manufacturer, and known impedance mismatch at all frequencies, then the comparison method is the optimum choice. For this reason the comparison method was used here.

5.3 Beam angle platform test

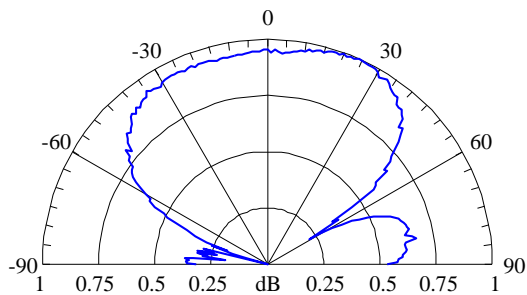


Figure 5.3: Measured Patch Antenna Radiation Pattern

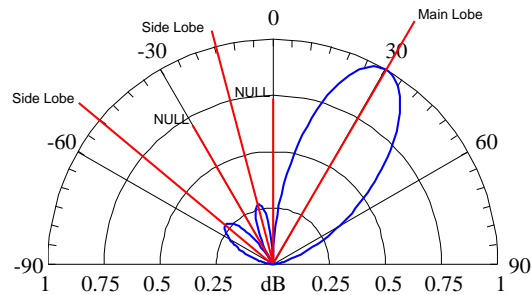


Figure 5.4: Array Factor 30°

According to Equation 3.1, the overall array radiation pattern can be determined by multiplying an individual patch antenna radiation pattern (Figure 5.3) with the array factor (Figure 5.4). It is shown as a theoretical pattern (red dashed lines) in Figure 5.5, 5.7, 5.9, 5.11 in order to compare it with the measured pattern (blue line).

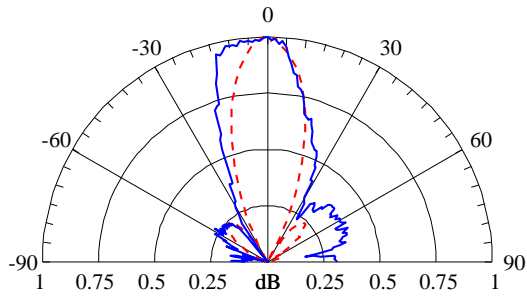


Figure 5.5: Measured Array Radiation Pattern Pointing 0°

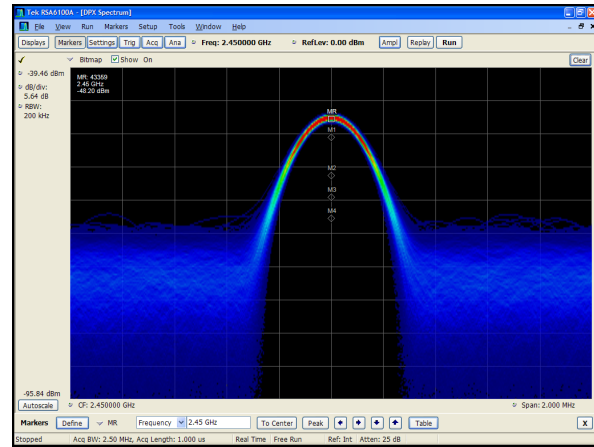


Figure 5.6: Spectrum Analyser Measurement on 0°

Looking at the graph in (Figure 5.5), the test platform generated an acceptable radiation pattern. The main lobe appears on the 0° axis, with two side lobes off this axis on 54° and -48°, while the nulls are on -33° and 35°. Moreover, most of the radiation power is clearly focused in the main lobe. Figure 5.6 shows the result from a Tektronix Real-Time Spectrum Analyzer (RTSA) using DPX technology. DPX displays a large amount of transient information. The persistent function provides a color bitmap showing power level, frequency and density simultaneously. The power level reaches -48.20dBm. **NOTE: The radiation pattern graphics have been normalized. In this case, therefore, they have no direct relation with spectrum analyser figures.**

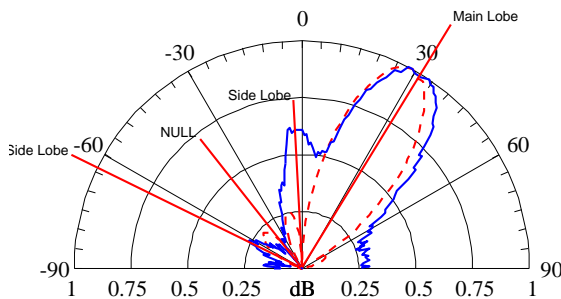


Figure 5.7: Measured Array Radiation Pattern Pointing 30°

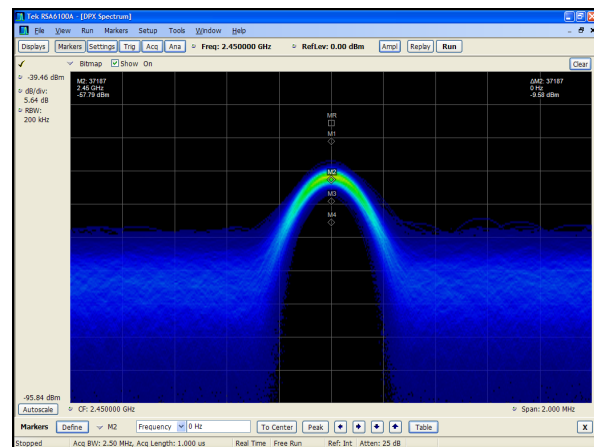


Figure 5.8: Spectrum Analyser Measurement on 30°

When the main lobe is steered from 0° to 30° (Figure 5.7), the lobe maintains its shape and stays focused. Side lobes position and nulls still maintain position after the transition. The main lobe power level reaches -57.79dBm as figure 5.8 shows.

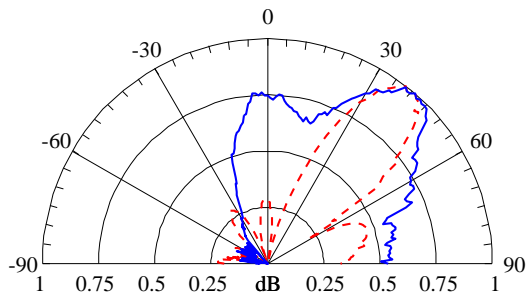


Figure 5.9: Measured Array Radiation Pattern Pointing 45°

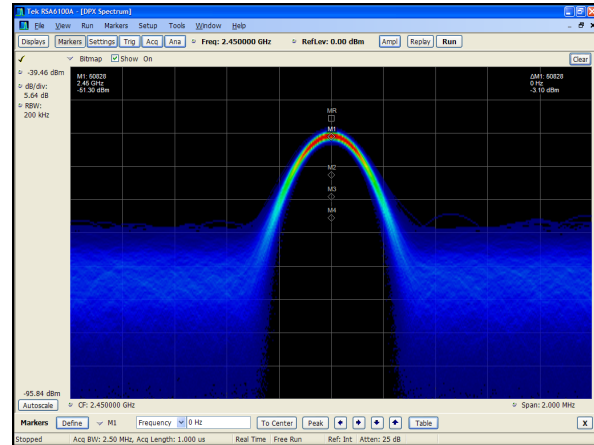


Figure 5.10: Spectrum Analyser Measurement on 45°

When the main lobe steering angle exceeded 30° distortion occurred, the more steering the more serious distortion, as Figure 5.9 shows. Figure 5.10 displays the power level at this angle as -51.30dBm .

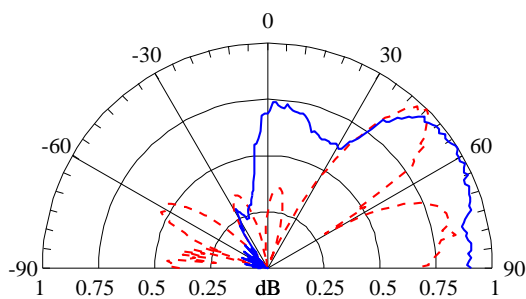


Figure 5.11: Measured Array Radiation Pattern Pointing 60°

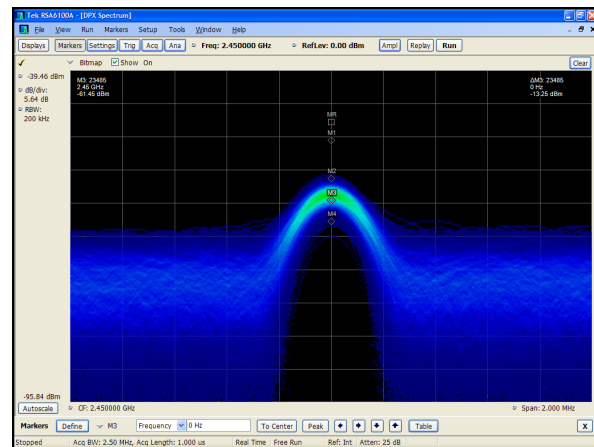


Figure 5.12: Spectrum Analyser Measurement on 60°

Finally, the main lobe was steered to 60° , but the distortion was quite severe. The boundary of null, main lobe or side lobes is very blurred. The only conclusion one can draw from Figure 5.11 is that the radiation power is mainly distributed on the right

hand side of the axis.

It can be concluded that for the crude antenna test platform employed, the underlying principles of phase flexibility and continuity are obtainable. This means that the effective range of this uniform linear antenna array (with identical amplitude) is -30° to 30° , which would require at least three arrays to cover all 360° . Also, Figure 5.12 demonstrates that as the steering angle increase, the power level falls.

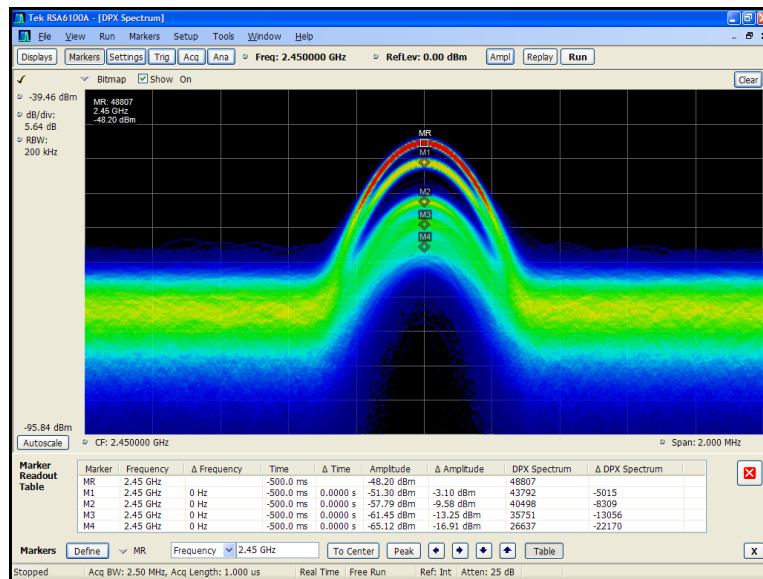


Figure 5.13: Sweeping Test

When the controller is set to sweep mode, the platform sweeps the beam angle continually. Figure 5.13 clearly shows the power levels in selected directions, with the received power measurements for each electronic steering angle further confirmation of the correct operation of the flexible steering angle selection. Detailed data from Figure 5.13 is shown in Figure 5.14.

Marker	Amplitude(dBm)	Delta Amplitude(dBm)	Pointing Direction (Degree)
MR	-48.20	N A	0
M1	-51.30	-3.10	45
M2	-57.79	-9.58	30
M3	-61.45	-13.25	60
M4	-65.12	-16.91	Background Noise

Figure 5.14: Detailed data in Sweeping Mode

Chapter 6

Summary & Future Work

6.1 Conclusion

This thesis details the current state of smart antenna development and its very promising future application. Several key concepts are explained such as beamforming, phase and steering angle, side lobes, as well as a method for radiation pattern measurement. The thesis contextualizes the research, in part by comparing smart antennas with traditional antennas. The key role of calibration in a successful outcome is examined and then pursued in the actual realization. Three popular calibration methods are described: Injection method, Blind Calibration method and Wireless Feedthrough method. The thesis also describes the design, theoretical analysis, calibration process and measurements. Finally, a set of measurement results are presented, which confirmed the suitability of the system for both further research and actual deployment. For a traditional experimental platform, only a single operating frequency and fixed antenna array elements can be used. However, the flexible design tested here allows one to vary the number of channels and also the operating frequency between values of 0.8GHz and 2.5GHz. This can be simply achieved by replacing the power divider (which is frequency dependent). The processing unit, the ATmega128, could also be changed to more powerful chips, such as an FPGA or DSP, to handle a more complex digital beamforming algorithm, coding or MIMO technologies.

The innovative aspect of this design incorporates quadrature modulators into the platform. Only a restricted number of phase steering angles can be set without any amplitude modification using the conventional switched strip line. A quadrature modulator is a non-linear analogue device providing the ability to vary both phase and amplitude which is a critical feature for smart antenna experiments.

6.2 Future work

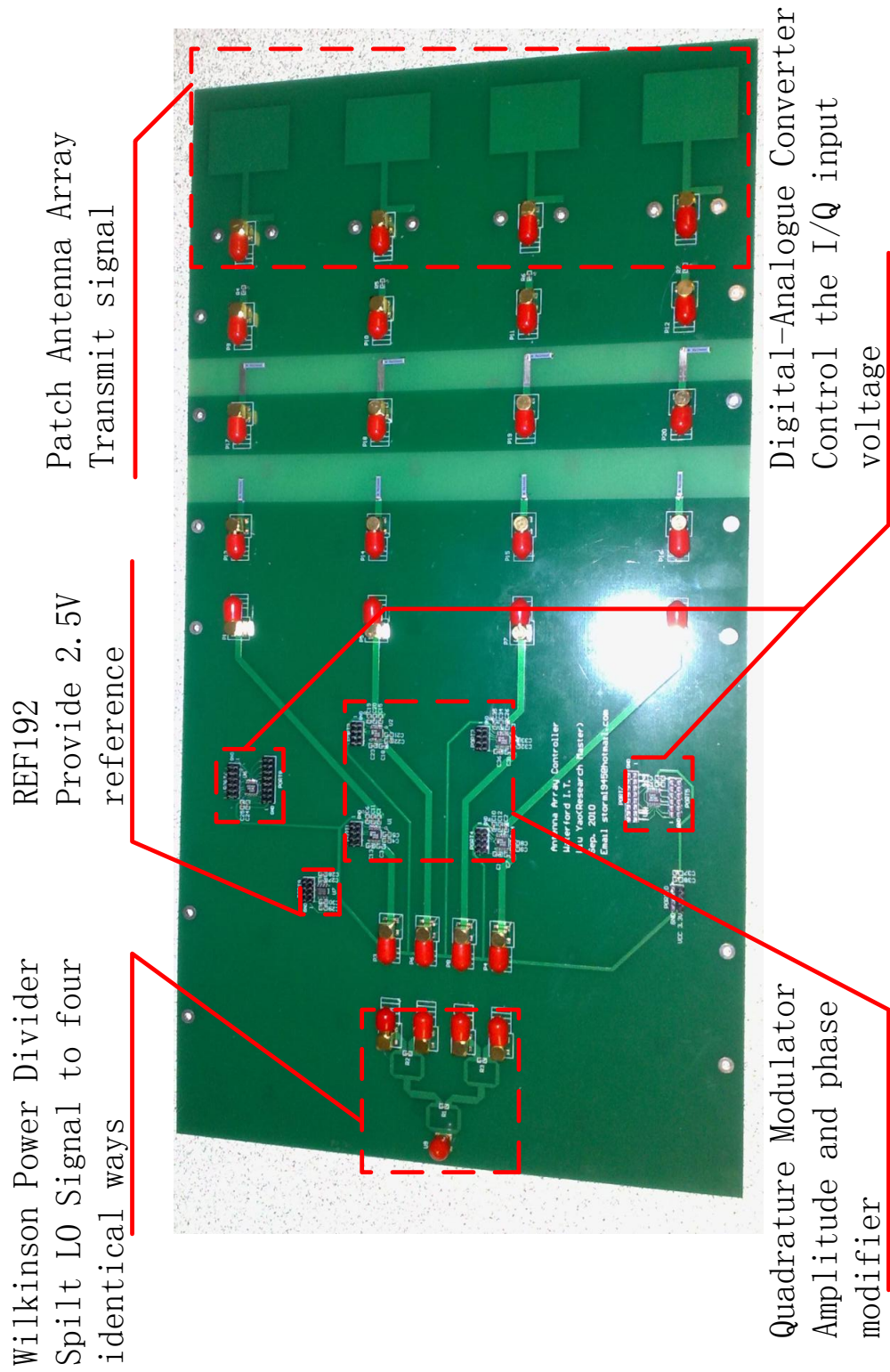
This platform could be used as a demonstration kit for educational purposes, as an example of a smart antenna transmitter. In the case of research or even product development, developers may put their algorithm to the test using this platform, thereby solving defects at an early stage. Furthermore, when combined with currently available products, an interesting possibility will arise. Take a wireless LAN router for example, if the LAN router antenna is replaced with the platform from this thesis, then the signal can be focussed on the user's direction. In this case, coverage could be enhanced without a signal power increase. Since the signal is focussed in selected directions, it is also less likely to be intercepted and captured, thereby enhancing security. More potential benefits could be confirmed through further research.

Appendix A

Graphics

A series of of platform related illustrations are given here, including practical PCB board photos, antenna testing set, controller circuit schematic & PCB layout, Wilkinson power divider schematic and optimization parameters in ADS.

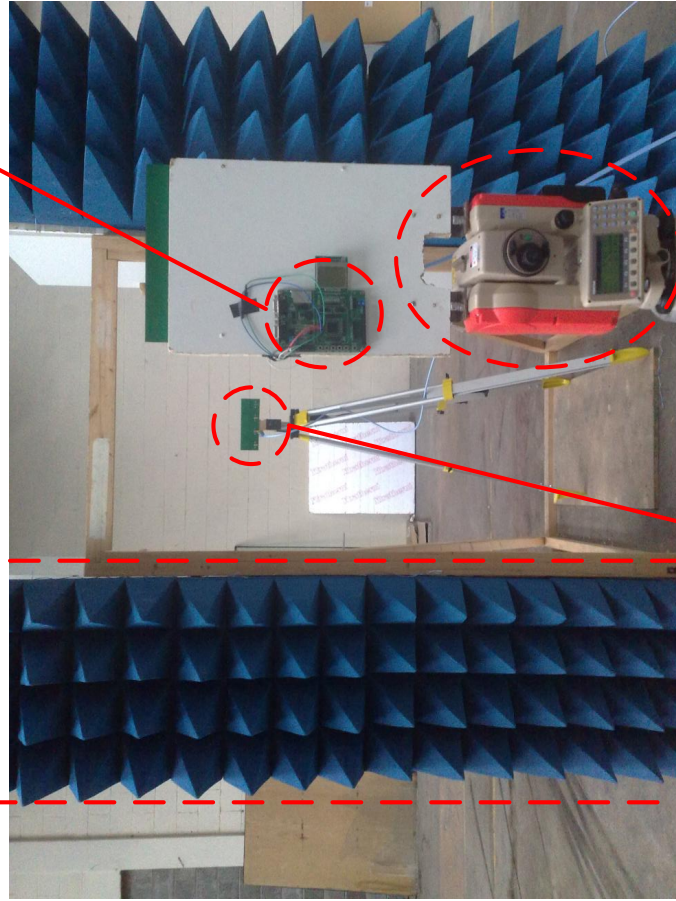
Smart Antenna Experiment Platform Photo



Radiation Pattern Characterization (Comparison Method)

Pyramidal Absorber
Absorb microwaves,
lower interferences

ATmega128 Controller
Control the beamforming,
display parameters

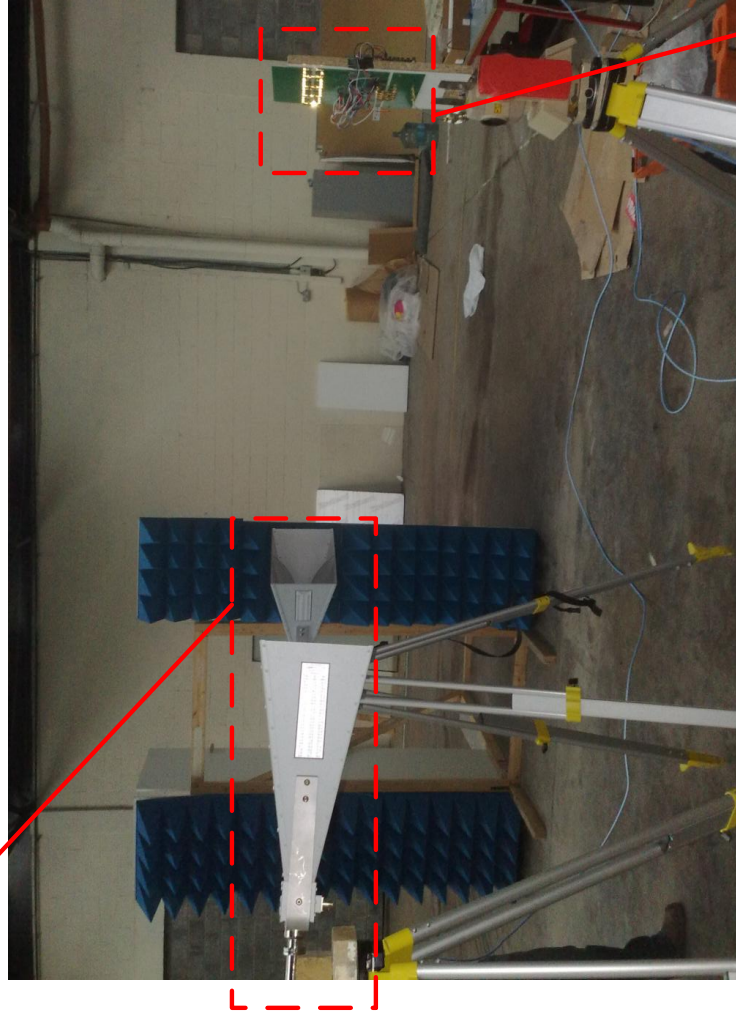


Patch Antenna Array
Receive signal from
smart antenna

Total Station
Rotate and Measure degree
with extreme accuracy

Radiation Pattern Characterization (Two antenna method)

Standard horn antennas
Receive signal from the
platform



Testing Platform

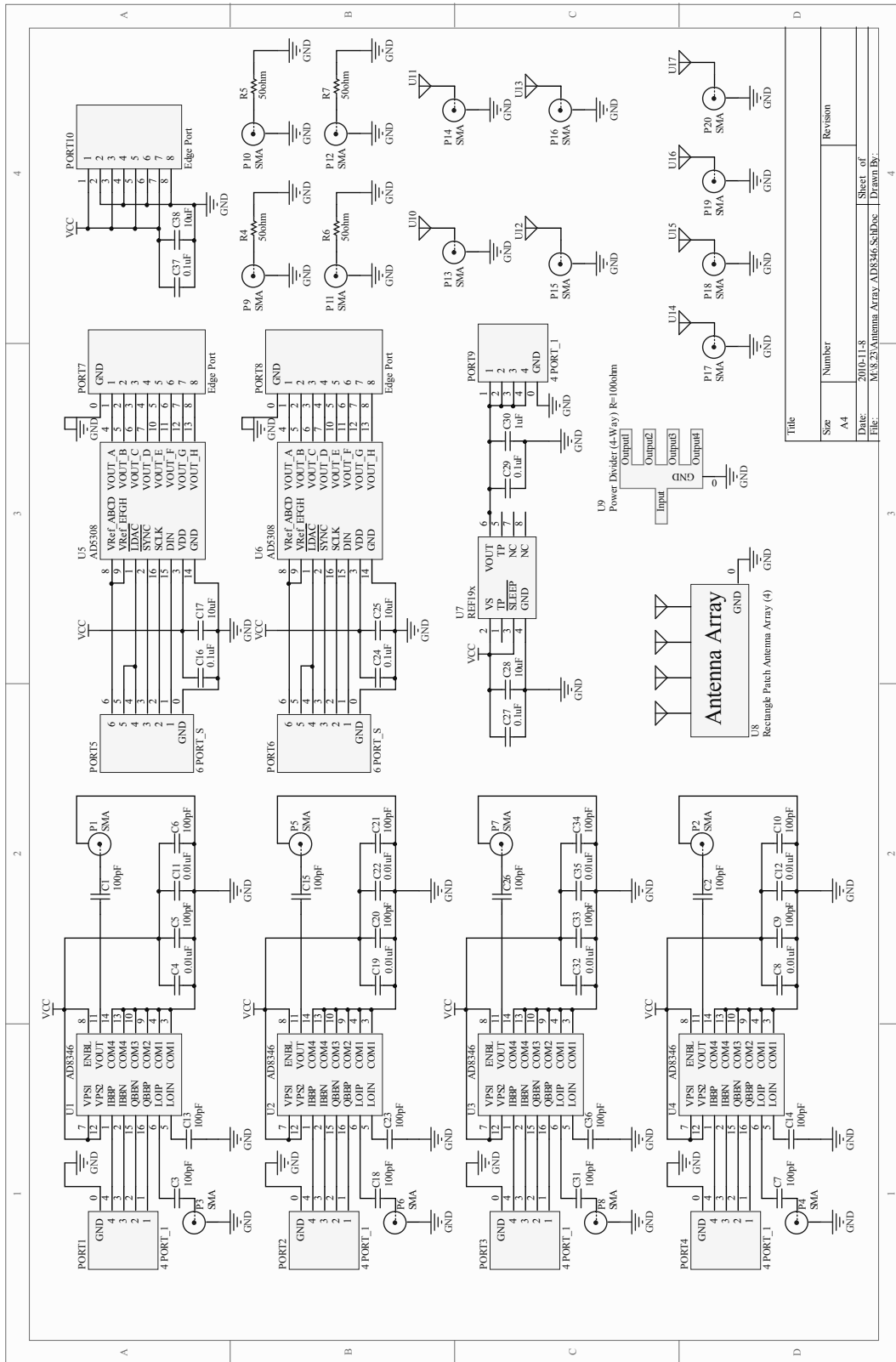
Radiation Pattern Characterization (In Anechoic Chamber)

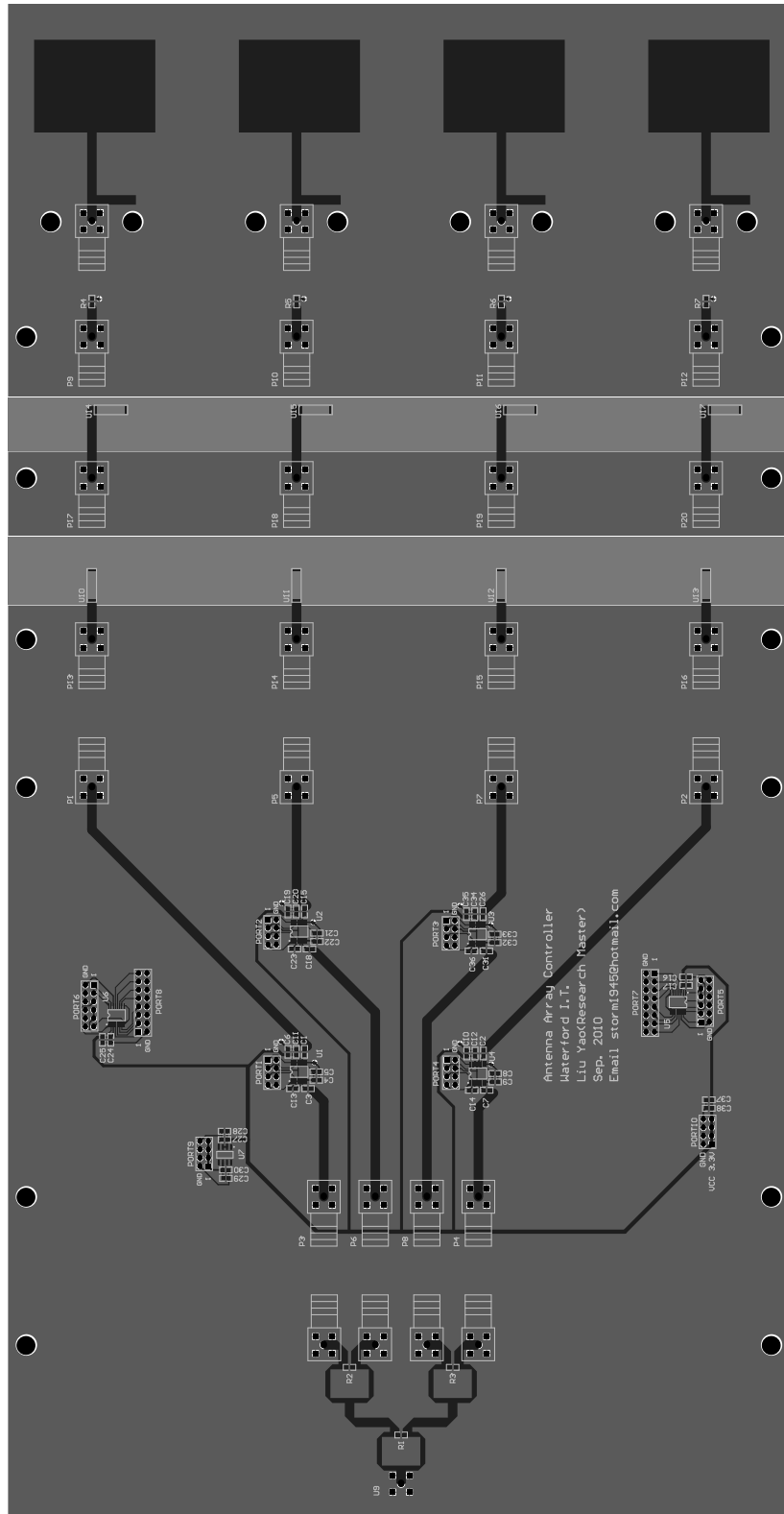
Metal Screen
Lower signal leakage

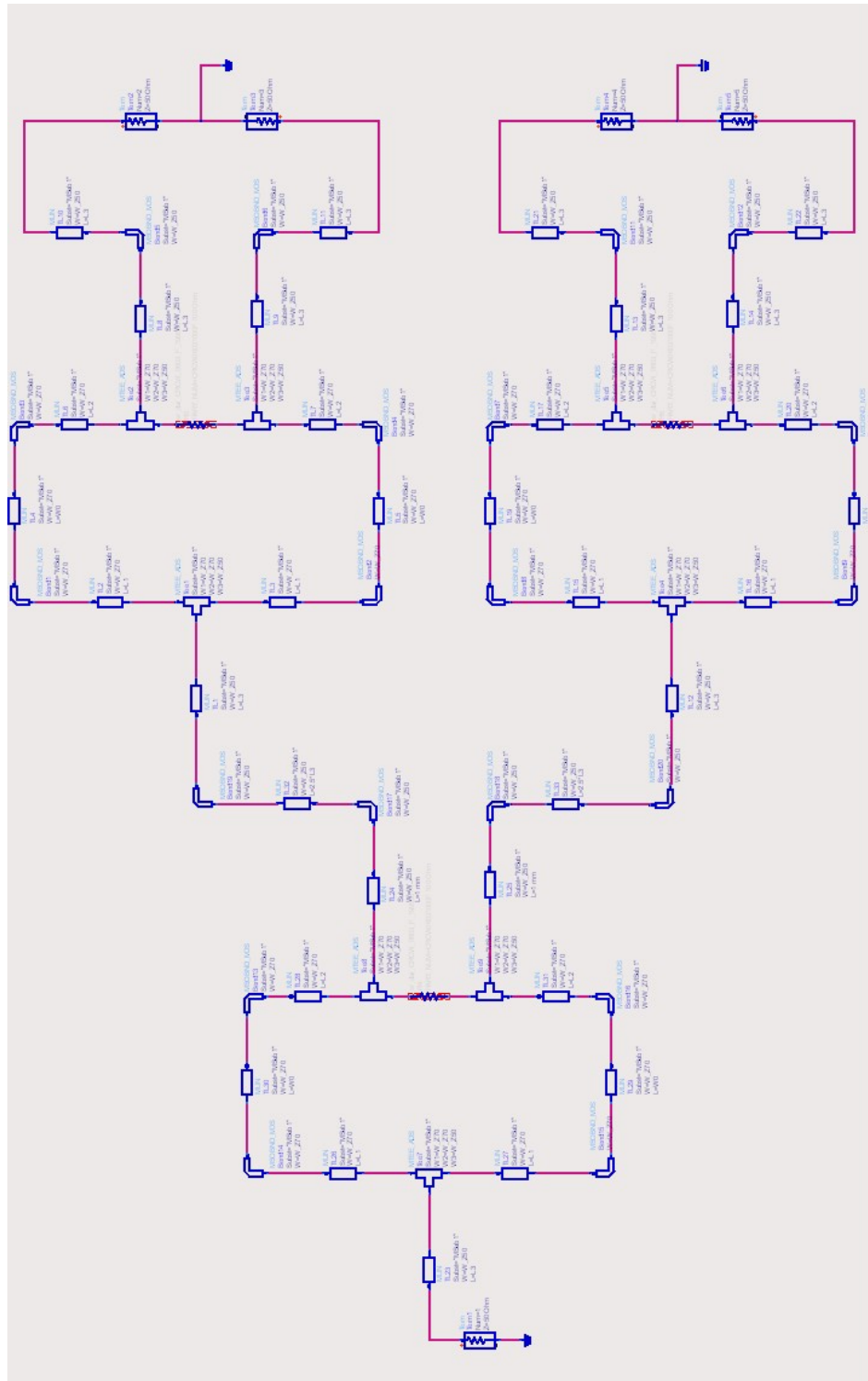
Anechoic Chamber
Lower interference greatly



Vector Network
Analyser (VNA)
Measuring S-parameters







VAR	GOAL	OPTIM
MSub		
MSUB		
MSub1		
H=1.6 mm		
E _r =4.7		
Mur=1		
Cond=5.88E+7		
Hu=3.9e+34 mil		
T=0.018 mm		
TanD=0.00		
Rough=0 mm		
VAR1		
W_Z50=2.90 mm		
W_Z70=1.52 mm		
Quar_L=17.02 mm		
Delta_L=0.5mm {o}		
L_R=1 mm		
L1=((2*Quar_L+L_R)*0.3-W_Z50)/2		
L3=4mm		
W0=(2*Quar_L+L_R)*0.2+Delta_L		
L2=((2*Quar_L+L_R)*0.3-2*W_Z50-L_R)/2		
Goal		
Optim Goal1		
Expr="dB(S(1,1))"		
SimInstanceName="SP1"		
Min=-		
Max=-44		
Weight=-		
RangVar[1]="freq"		
RangMin[1]=2.4 GHz		
RangMax[1]=2.4 GHz		
Optim		
Optim 1		
Optim Type=Random		
Maxiters=200		
DesiredError=0.0		
StatusLevel=4		
FinalAnalysis="None"		
NormalizeGoals=no		
SetBestValues=yes		
SaveSols=yes		
SaveGoals=yes		
SaveOptim Vars=no		
UpdatedDataset=yes		
SaveNominal=no		
SaveAllIterations=no		
UseAllOptVars=yes		
UseAllGoals=yes		

Appendix B

ATmega128 C code

B.1 5110cmd.h

```
1 #include <avr/io.h>
2 #include <util/delay.h>
3 vhgghg\section{5110cmd.h}
4 \markright{Appendix~\ref{appendix:design} - ATmega128 C
   code - 5110cmd.h}
5 \begin{lstlisting}[numbers=left,basicstyle=\ttfamily,
   breakindent=0pt,breaklines=true]
6 #define BACKLED_EN      1      //PA1
7
8 #define SCLK            1      //PB1
9 #define SDIN            2      //PB2
10 #define LCD_DC         3      //PA3
11 #define LCD_CE         2      //PA2
12 // #define LCD_RST
13
14 #define LCD_PORT        PORTB
15 #define LCD_DIR        DDRB
16 #define LCD_IN         PINB
17
18 #define LCD_PORT2       PORTA
19 #define LCD_DIR2       DDRA
20
```

```
21 void LCD_init(void);
22 void LCD_clear(void);
23 void LCD_set_XY(unsigned char x,unsigned char y);
24 void LCD_write_char(unsigned char c);
25 void LCD_write_english_string(unsigned char X,unsigned char
    Y,char *s);
26 void LCD_write_chinese_string(unsigned char X, unsigned
    char Y,unsigned char ch_with,unsigned char num,unsigned
    char line,unsigned char row);
27 void LCD_draw_bmp_pixel(unsigned char X,unsigned char Y,
    unsigned char *map,unsigned char Pix_x,unsigned char Pix_y)
    ;
28 void LCD_write_byte(unsigned char dat, unsigned char
    command);
```

B.2 5110cmd.c

```

1 #include "5110cmd.h"
2 // 6 x 8 font
3 // 1 pixel space at left and bottom
4 // index = ASCII - 32
5 const unsigned char font6x8[][6] =
6 {
7     { 0x00, 0x00, 0x00, 0x00, 0x00, 0x00 }, // sp
8     { 0x00, 0x00, 0x00, 0x2f, 0x00, 0x00 }, // !
9     { 0x00, 0x00, 0x07, 0x00, 0x07, 0x00 }, // "
10    { 0x00, 0x14, 0x7f, 0x14, 0x7f, 0x14 }, // #
11    { 0x00, 0x24, 0x2a, 0x7f, 0x2a, 0x12 }, // $
12    { 0x00, 0x62, 0x64, 0x08, 0x13, 0x23 }, // %
13    { 0x00, 0x36, 0x49, 0x55, 0x22, 0x50 }, // &
14    { 0x00, 0x00, 0x05, 0x03, 0x00, 0x00 }, // '
15    { 0x00, 0x00, 0x1c, 0x22, 0x41, 0x00 }, // (
16    { 0x00, 0x00, 0x41, 0x22, 0x1c, 0x00 }, // )
17    { 0x00, 0x14, 0x08, 0x3E, 0x08, 0x14 }, // *
18    { 0x00, 0x08, 0x08, 0x3E, 0x08, 0x08 }, // +
19    { 0x00, 0x00, 0x00, 0xA0, 0x60, 0x00 }, // ,
20    { 0x00, 0x08, 0x08, 0x08, 0x08, 0x08 }, // -
21    { 0x00, 0x00, 0x60, 0x60, 0x00, 0x00 }, // .
22    { 0x00, 0x20, 0x10, 0x08, 0x04, 0x02 }, // /
23    { 0x00, 0x3E, 0x51, 0x49, 0x45, 0x3E }, // 0
24    { 0x00, 0x00, 0x42, 0x7F, 0x40, 0x00 }, // 1
25    { 0x00, 0x42, 0x61, 0x51, 0x49, 0x46 }, // 2
26    { 0x00, 0x21, 0x41, 0x45, 0x4B, 0x31 }, // 3
27    { 0x00, 0x18, 0x14, 0x12, 0x7F, 0x10 }, // 4
28    { 0x00, 0x27, 0x45, 0x45, 0x45, 0x39 }, // 5
29    { 0x00, 0x3C, 0x4A, 0x49, 0x49, 0x30 }, // 6
30    { 0x00, 0x01, 0x71, 0x09, 0x05, 0x03 }, // 7
31    { 0x00, 0x36, 0x49, 0x49, 0x49, 0x36 }, // 8
32    { 0x00, 0x06, 0x49, 0x49, 0x29, 0x1E }, // 9
33    { 0x00, 0x00, 0x36, 0x36, 0x00, 0x00 }, // :

```

```
34     { 0x00, 0x00, 0x56, 0x36, 0x00, 0x00 }, // ;
35     { 0x00, 0x08, 0x14, 0x22, 0x41, 0x00 }, // <
36     { 0x00, 0x14, 0x14, 0x14, 0x14, 0x14 }, // =
37     { 0x00, 0x00, 0x41, 0x22, 0x14, 0x08 }, // >
38     { 0x00, 0x02, 0x01, 0x51, 0x09, 0x06 }, // ?
39     { 0x00, 0x32, 0x49, 0x59, 0x51, 0x3E }, // @
40     { 0x00, 0x7C, 0x12, 0x11, 0x12, 0x7C }, // A
41     { 0x00, 0x7F, 0x49, 0x49, 0x49, 0x36 }, // B
42     { 0x00, 0x3E, 0x41, 0x41, 0x41, 0x22 }, // C
43     { 0x00, 0x7F, 0x41, 0x41, 0x22, 0x1C }, // D
44     { 0x00, 0x7F, 0x49, 0x49, 0x49, 0x41 }, // E
45     { 0x00, 0x7F, 0x09, 0x09, 0x09, 0x01 }, // F
46     { 0x00, 0x3E, 0x41, 0x49, 0x49, 0x7A }, // G
47     { 0x00, 0x7F, 0x08, 0x08, 0x08, 0x7F }, // H
48     { 0x00, 0x00, 0x41, 0x7F, 0x41, 0x00 }, // I
49     { 0x00, 0x20, 0x40, 0x41, 0x3F, 0x01 }, // J
50     { 0x00, 0x7F, 0x08, 0x14, 0x22, 0x41 }, // K
51     { 0x00, 0x7F, 0x40, 0x40, 0x40, 0x40 }, // L
52     { 0x00, 0x7F, 0x02, 0x0C, 0x02, 0x7F }, // M
53     { 0x00, 0x7F, 0x04, 0x08, 0x10, 0x7F }, // N
54     { 0x00, 0x3E, 0x41, 0x41, 0x41, 0x3E }, // O
55     { 0x00, 0x7F, 0x09, 0x09, 0x09, 0x06 }, // P
56     { 0x00, 0x3E, 0x41, 0x51, 0x21, 0x5E }, // Q
57     { 0x00, 0x7F, 0x09, 0x19, 0x29, 0x46 }, // R
58     { 0x00, 0x46, 0x49, 0x49, 0x49, 0x31 }, // S
59     { 0x00, 0x01, 0x01, 0x7F, 0x01, 0x01 }, // T
60     { 0x00, 0x3F, 0x40, 0x40, 0x40, 0x3F }, // U
61     { 0x00, 0x1F, 0x20, 0x40, 0x20, 0x1F }, // V
62     { 0x00, 0x3F, 0x40, 0x38, 0x40, 0x3F }, // W
63     { 0x00, 0x63, 0x14, 0x08, 0x14, 0x63 }, // X
64     { 0x00, 0x07, 0x08, 0x70, 0x08, 0x07 }, // Y
65     { 0x00, 0x61, 0x51, 0x49, 0x45, 0x43 }, // Z
66     { 0x00, 0x00, 0x7F, 0x41, 0x41, 0x00 }, // [
67     { 0x00, 0x00, 0x41, 0x41, 0x7F, 0x00 }, // ]
68     { 0x00, 0x04, 0x02, 0x01, 0x02, 0x04 }, // ^
```

```

69     { 0x00, 0x40, 0x40, 0x40, 0x40, 0x40 }, // _
70     { 0x00, 0x00, 0x01, 0x02, 0x04, 0x00 }, // '
71     { 0x00, 0x20, 0x54, 0x54, 0x54, 0x78 }, // a
72     { 0x00, 0x7F, 0x48, 0x44, 0x44, 0x38 }, // b
73     { 0x00, 0x38, 0x44, 0x44, 0x44, 0x20 }, // c
74     { 0x00, 0x38, 0x44, 0x44, 0x48, 0x7F }, // d
75     { 0x00, 0x38, 0x54, 0x54, 0x54, 0x18 }, // e
76     { 0x00, 0x08, 0x7E, 0x09, 0x01, 0x02 }, // f
77     { 0x00, 0x18, 0xA4, 0xA4, 0xA4, 0x7C }, // g
78     { 0x00, 0x7F, 0x08, 0x04, 0x04, 0x78 }, // h
79     { 0x00, 0x00, 0x44, 0x7D, 0x40, 0x00 }, // i
80     { 0x00, 0x40, 0x80, 0x84, 0x7D, 0x00 }, // j
81     { 0x00, 0x7F, 0x10, 0x28, 0x44, 0x00 }, // k
82     { 0x00, 0x00, 0x41, 0x7F, 0x40, 0x00 }, // l
83     { 0x00, 0x7C, 0x04, 0x18, 0x04, 0x78 }, // m
84     { 0x00, 0x7C, 0x08, 0x04, 0x04, 0x78 }, // n
85     { 0x00, 0x38, 0x44, 0x44, 0x44, 0x38 }, // o
86     { 0x00, 0xFC, 0x24, 0x24, 0x24, 0x18 }, // p
87     { 0x00, 0x18, 0x24, 0x24, 0x18, 0xFC }, // q
88     { 0x00, 0x7C, 0x08, 0x04, 0x04, 0x08 }, // r
89     { 0x00, 0x48, 0x54, 0x54, 0x54, 0x20 }, // s
90     { 0x00, 0x04, 0x3F, 0x44, 0x40, 0x20 }, // t
91     { 0x00, 0x3C, 0x40, 0x40, 0x20, 0x7C }, // u
92     { 0x00, 0x1C, 0x20, 0x40, 0x20, 0x1C }, // v
93     { 0x00, 0x3C, 0x40, 0x30, 0x40, 0x3C }, // w
94     { 0x00, 0x44, 0x28, 0x10, 0x28, 0x44 }, // x
95     { 0x00, 0x1C, 0xA0, 0xA0, 0xA0, 0x7C }, // y
96     { 0x00, 0x44, 0x64, 0x54, 0x4C, 0x44 }, // z
97     { 0x14, 0x14, 0x14, 0x14, 0x14, 0x14 } // horiz
    lines
98 };
99 /*****
100 /*****
101 Array Name      :      PIXEL_BMP
102 Function        :      48X24 bitmap

```

```

103 editor          :          Notepad 2
104 *****/
105 unsigned char AVR_bmp []=  {
106          0x00,0x00,0x00,0x00,0x80,0xE0,0xFC,0xFF,0
          xFF,0xFF,0x7F,0xFF,0xFE,0xFC,0xF0,0xC1,
107          0x0F,0x7F,0xFF,0xFF,0xFE,0xF0,0xC0,0x00,0
          x00,0x00,0xC0,0xF8,0xFE,0xFF,0xFF,0x3F,
108          0x07,0xC1,0xF0,0xFE,0xFF,0xFF,0xFF,0x1F,0
          x07,0x8F,0xCF,0xFF,0xFF,0xFF,0xFE,0xFC,
109          0x00,0x80,0xF0,0xFC,0xFF,0xFF,0xFF,0x7F,0
          x7F,0x78,0x78,0x79,0x7F,0x7F,0xFF,0xFF,
110          0xFC,0xF0,0xC1,0x07,0x1F,0xFF,0xFF,0xFE,0
          xFC,0xFF,0xFF,0xFF,0x1F,0x07,0xC1,0xF0,
111          0xFE,0xFF,0xFF,0x3F,0x0F,0x0F,0x7F,0xFF,0
          xFF,0xFF,0xFF,0xE7,0x07,0x03,0x01,0x00,
112          0x02,0x03,0x03,0x03,0x03,0x03,0x00,0x00,0
          x00,0x00,0x00,0x00,0x00,0x03,
113          0x03,0x03,0x03,0x03,0x00,0x00,0x03,0x1F,0
          x3F,0x1F,0x07,0x00,0x00,0x02,0x03,0x03,
114          0x03,0x03,0x01,0x00,0x00,0x00,0x00,0x03,0
          x03,0x03,0x03,0x03,0x03,0x00,0x00,0x00
115 };
116 *****/
117 void LCD_init(void)
118 {
119 //set to output
120     LCD_DIR |= (1<<SCLK);
121     LCD_DIR |= (1<<SDIN);
122     LCD_DIR2 |= (1<<LCD_DC);
123     LCD_DIR2 |= (1<<LCD_CE);
124     LCD_DIR2 |= (1<<BACKLED_EN);
125
126
127     LCD_PORT2 &=~ (1<<LCD_CE); // disable lcd
128     _delay_us(1);

```

```
129     LCD_PORT2 |= (1<<LCD_CE); // Enable lcd
130         _delay_us(1);
131
132     LCD_write_byte(0x21, 0); // set lcd mode
133     LCD_write_byte(0xc8, 0); // set bias voltage
134     LCD_write_byte(0x06, 0); // temperature calibration
135     LCD_write_byte(0x13, 0); // 1:48
136     LCD_write_byte(0x20, 0); // use basic command
137     LCD_clear(); // clear screen
138     LCD_write_byte(0x0c, 0); // set mode to normal
139
140     LCD_PORT2 &=~ (1<<LCD_CE); // disable lcd
141 }
142 /*****/
143 void LCD_clear(void)
144 {
145     unsigned int i;
146
147     LCD_write_byte(0x0c, 0);
148     LCD_write_byte(0x80, 0);
149
150     for (i=0; i<504; i++)
151     {
152         LCD_write_byte(0, 1);
153     }
154 }
155 /*****/
156 void LCD_set_XY(unsigned char X, unsigned char Y)
157 {
158     LCD_write_byte(0x40 | Y, 0); // column
159     LCD_write_byte(0x80 | X, 0); // row
160 }
161 /*****/
162 void LCD_write_char(unsigned char c)
163 {
```

```

164     unsigned char line;
165
166     c -= 32;
167     for (line=0; line<6; line++)
168         {
169             LCD_write_byte(font6x8[c][line], 1);
170         }
171 }
172 /*****
173 /*-----
174 LCD_write_english_String : english letter display function
175
176 input parameters:*s      :english char pointer
177                 X,Y     : typing position,x 0-83 ,y 0-5
178 -----*/
179 void LCD_write_english_string(unsigned char X,unsigned char
180     Y,char *s)
181 {
182     LCD_set_XY(X,Y);
183     while (*s)
184     {
185         LCD_write_char(*s);
186         s++;
187     }
188 /*****
189 /*-----
190 LCD_write_chinese_string: display chinese on LCD
191
192 input parameters :X,Y position
193                 ch_with :chinese charater dot matrix width
194                 num     :how many char to display
195                 line    :dot matrix start line
196                 row     :space between lines
197 -----*/

```

```

198 void LCD_write_chinese_string(unsigned char X, unsigned
    char Y,unsigned char ch_with,unsigned char num,unsigned
    char line,unsigned char row)
199 {
200     unsigned char i,n;
201
202     LCD_set_XY(X,Y); //set start position
203
204     for (i=0;i<num;)
205     {
206         for (n=0; n<ch_with*2; n++) //type a char
207         {
208             if (n==ch_with) //the lower part of char
209             {
210                 if (i==0) LCD_set_XY(X,Y+1);
211                 else
212                     {
213                         LCD_set_XY((X+(ch_with+row)*i),Y+1);
214                     }
215             }
216             LCD_write_byte(HZK[line+i][n],1);
217         }
218         i++;
219         LCD_set_XY((X+(ch_with+row)*i),Y);
220     }
221 }
222 /*****
223 /*-----
224 LCD_draw_map      : drawing function
225
226 inputs:    X Y      :bitmap start position
227           *map     :bitmap dot matrix
228           Pix_x    :bitmap pixel length
229           Pix_y    :bitmap pixel width
230 -----*/

```

```

231 void LCD_draw_bmp_pixel(unsigned char X,unsigned char Y,
    unsigned char *map,unsigned char Pix_x,unsigned char Pix_y)
232 {
233     unsigned int i,n;
234     unsigned char row;
235
236     if (Pix_y%8==0)
237     {
238         row=Pix_y/8;        //calculating bitmap lines
239     }
240     else
241     {
242         row=Pix_y/8+1;
243     }
244     for (n=0;n<row;n++)
245     {
246         LCD_set_XY(X,Y);
247         for(i=0; i<Pix_x; i++)
248         {
249             LCD_write_byte(map[i+n*Pix_x], 1);
250         }
251         Y++;                //line breaking
252     }
253 }
254 /*****
255 /*-----
256 LCD_write_byte      : Writing data to LCD
257
258 Inputs          data :data inputs
259                 command :data/cmd writing selection
260 -----*/
261 void LCD_write_byte(unsigned char dat, unsigned char
    command)
262 {
263     int tmp_SPCR;

```

```
264     //because this function treats SPI interface as a
      general use interface which need disable spi
      controlling feature and backup SPCR contents.
265     tmp_SPCR = SPCR;
266     SPCR &=~ 0x40;
267     unsigned char i;
268     LCD_PORT2 &=~ (1<<LCD_CE); // Enable LCD_CE = 0
269
270     if (command == 0)
271     {
272         LCD_PORT2 &=~ (1<<LCD_DC); // Transmitting cmd
          LCD_DC = 0;
273     }
274     else
275     {
276         LCD_PORT2 |= (1<<LCD_DC); // Transmitting data
          LCD_DC = 1;
277     }
278
279     for(i=0; i<8; i++)
280     {
281         if(dat&0x80)
282         {
283             LCD_PORT |= (1<<SDIN);
284         }
285         else
286         {
287             LCD_PORT &=~ (1<<SDIN);
288         }
289         LCD_PORT &=~ (1<<SCLK);
290         dat = dat << 1;
291         LCD_PORT |= (1<<SCLK);
292     }
293     LCD_PORT |= (1<<LCD_CE);
294     SPCR = tmp_SPCR;
```

295 }

B.3 AD5308.h

```
1 #include <avr/io.h>
2 #include <util/delay.h>
3
4 //SPI Defination ,PB
5 #define SYNC2    5
6 #define SYNC1    4
7 #define MISO     3
8 #define MOSI     2
9 #define SCK      1
10 #define LDAC     0
11
12 void AD5308_SPI_SlaveInit(void);
13 void AD5308_SPI_DataTransmit(int dh,int dl,int cs);
14 void AD5308_Input_Register_Write(int address,int volt,int
    cs);
15 void AD5308_LDAC(void);
16 void AD5308_ALL_16CH(int value[4][4]);
```

B.4 AD5308.c

```

1 #include "AD5308.h"
2 //*****
3 //Define AD5308 as a SPI slave with LDAC disabled.
4 void AD5308_SPI_SlaveInit(void)
5 {
6   DDRB = 0X37;
7   PORTB = 0xFF;
8   //SPI Control, Mode 2, CLK F_CPU/16, MSB send first
9   SPCR = 0x59;
10  PORTB |= (1<<LDAC);
11  PORTB |= (1<<SYNC1);
12  PORTB |= (1<<SYNC2);
13  _delay_us(1);
14 }
15 //*****
16 //Write AD5308 with 16bit data.
17 void AD5308_SPI_DataTransmit(int dh,int dl,int cs)
18 {
19  PORTB &= ~(1<<cs);
20  _delay_us(1);
21  SPDR = dh;
22  while (!(SPSR & 0x80));
23  SPDR = dl;
24  while (!(SPSR & 0x80));
25  PORTB |= (1<<cs);
26  _delay_us(1);
27 }
28 //*****
29 //Write AD5308 reigster, address 0 - 7, volt 0-255
30 void AD5308_Input_Register_Write(int address,int volt,int
   cs)
31 {
32  int dh=0x00;int dl=0x00;int tmp=0x00;

```

```
33
34 //data high 8 bits DH: MSB is 0 for data transmission.
35 //Bit 6,5,4 is address.
36 //Bit 3,2,1,0 is high 4 bits of voltage.
37 dh = address;
38 dh = (dh<<4);
39 tmp = volt;
40 tmp =(tmp>>4);
41 tmp &= 0x0F;
42 dh |= tmp;
43
44 //data low 8 bits DL: low 4 bits is ignored for AD5038(8-
    bit).
45 //low 2 bits is ignored for AD5318(10-bit).
46 //AD5318(12-bit) use all bits.
47 tmp = volt;
48 tmp &= 0x0F;
49 tmp = (tmp<<4);
50 dl  = tmp;
51 AD5308_SPI_DataTransmit(dh,dl,cs);
52 }
53 //*****
54 //Updata Input registers to DAC registers.
55 //LDAC Mode should be properly set.
56 void AD5308_LDAC(void)
57 {
58 PORTB &=~ (1<<LDAC);
59 _delay_us(1);
60 PORTB |= (1<<LDAC);
61 }
62 //*****
63 //Updata 2 AD5308 all 16 channels simultaneously.
64 void AD5308_ALL_16CH(int value[4][4])
65 {
66 int i;
```

```
67     for(i=0;i<4;i++)
68     {
69     AD5308_Input_Register_Write(i,value[0][i],SYNC1);
70     }
71
72     for(i=0;i<4;i++)
73     {
74     AD5308_Input_Register_Write(i+4,value[1][i],SYNC1);
75     }
76
77     for(i=0;i<4;i++)
78     {
79     AD5308_Input_Register_Write(i,value[2][i],SYNC2);
80     }
81
82     for(i=0;i<4;i++)
83     {
84     AD5308_Input_Register_Write(i+4,value[3][i],SYNC2);
85     }
86 AD5308_LDAC();
87 }
```

B.5 global.h

```
1 char dirc_angle [4]={"CA"};
2 int eep_addr=0;
3 int eep_agl_addr=0;
4 int item=1;
5 //*****
6 //Voltage Value Matrix
7 int Voltage_Value [4] [4]=
8 {
9     {181,120,120,202},
10    {86,120,120,122},
11    {75,120,120,167},
12    {171,120,120,195},
13 };
14
15 const int para_data []=
16 {
17 181,202,86,122,75,167,171,195
18 };
19
20
21 const char dirc_matrix [] [4]=
22 {
23 "90"
24 };
```

B.6 main.c

```
1 #include <avr/io.h>
2 #include <util/delay.h>
3 #include <string.h>
4 #include <avr/eeprom.h>
5 #include <stdlib.h>
6
7 #include "AD5308.h"
8 #include "5110cmd.h"
9 #include "global.h"
10
11 #define K1 6 //PE6
12
13 #define N_VOLT 120 //negative input voltage
14 //*****

15 // Welcome Display
16 void Disp_Welcome(void)
17 {
18 LCD_init();
19 LCD_clear();
20 LCD_write_english_string(0,0,"-----");
21 LCD_write_english_string(0,1," Phased Array ");
22 LCD_write_english_string(0,2," Controller ");
23 LCD_write_english_string(0,3," Made By ");
24 LCD_write_english_string(0,4," Liu Yao ");
25 LCD_write_english_string(0,5,"-----");
26 }
27 //*****

28 // Parameter Display
29 void Disp_Para()
30 {
31 LCD_init();
```

```
32 LCD_clear();
33 int i;
34 char str[4];
35 for (i=0;i<=3;i++)
36 {
37 LCD_write_english_string(0,i,itoa(Voltage_Value[i][0],str
    ,10));
38 }
39
40 for (i=0;i<=3;i++)
41 {
42 LCD_write_english_string(51,i,itoa(Voltage_Value[i][3],str
    ,10));
43 }
44
45 LCD_write_english_string(0,4,itoa(item,dirc_angle,10));
46 LCD_write_english_string(0,5,"-----");
47 }
48 //*****

49 void Renew_Para()
50 {
51 Voltage_Value[0][0]=para_data[eeep_addr]; eeep_addr++;
52 Voltage_Value[0][1]=N_VOLT;
53 Voltage_Value[0][2]=N_VOLT;
54 Voltage_Value[0][3]=para_data[eeep_addr]; eeep_addr++;
55
56 Voltage_Value[1][0]=para_data[eeep_addr]; eeep_addr++;
57 Voltage_Value[1][1]=N_VOLT;
58 Voltage_Value[1][2]=N_VOLT;
59 Voltage_Value[1][3]=para_data[eeep_addr]; eeep_addr++;
60
61 Voltage_Value[2][0]=para_data[eeep_addr]; eeep_addr++;
62 Voltage_Value[2][1]=N_VOLT;
63 Voltage_Value[2][2]=N_VOLT;
```

```
64 Voltage_Value [2] [3]=para_data [eep_addr]; eep_addr++;
65
66 Voltage_Value [3] [0]=para_data [eep_addr]; eep_addr++;
67 Voltage_Value [3] [1]=N_VOLT;
68 Voltage_Value [3] [2]=N_VOLT;
69 Voltage_Value [3] [3]=para_data [eep_addr]; eep_addr++;
70
71 }
72 //-----
73 /*
74 int main(void)
75 {
76 AD5308_SPI_SlaveInit ();
77 AD5308_ALL_16CH (Voltage_Value [3]);
78 Disp_Welcome ();
79     _delay_ms (5000);
80 AD5308_SPI_SlaveInit ();
81 AD5308_ALL_16CH (Voltage_Value [3]);
82 Disp_Offset ();
83     _delay_ms (5000);
84 }
85 */
86 //-----
87
88 int main(void)
89 {
90 //Define PE6 K1 as a control switch.
91 PORTE &=~ (1<<K1);
92 DDRE &=~ (1<<K1);
93 PORTE |= (1<<K1);
94
95 PORTD |= ((1<<2) | (1<<3) | (1<<4) | (1<<5));
96 DDRD &= ~( (1<<2) | (1<<3) | (1<<4) | (1<<5));
97 loop:
98 AD5308_SPI_SlaveInit ();
```

```
99 AD5308_ALL_16CH(Voltage_Value);
100 Disp_Para();
101 _delay_ms(200);
102 for(;;)
103     {
104         if((PINE&0X40)==0X00)
105             {
106                 if(item==3){item=1;}
107                 else{item++;}
108                 break;
109             }
110
111         if((PIND&(1<<2))==0X00)
112             {
113                 if(Voltage_Value[item][0]<=255){
114                     Voltage_Value[item][0]++;}
115                 break;
116             }
117
118         if((PIND&(1<<3))==0X00)
119             {
120                 if(Voltage_Value[item][0]>=0){
121                     Voltage_Value[item][0]--;}
122                 break;
123             }
124
125         if((PIND&(1<<4))==0X00)
126             {
127                 if(Voltage_Value[item][3]<=255){
128                     Voltage_Value[item][3]++;}
129                 break;
130             }
131
132         if((PIND&(1<<5))==0X00)
133             {
```

```
131             if(Voltage_Value[item][3]>=0){
132                 Voltage_Value[item][3]--;}
133             }
134         }
135     goto loop;
136 }
```

Appendix C

Matlab Scripts

C.1 main.m

```
1 % for theta=90:-1:0
2 %     ii=theta;
3 theta = input('desire pointing direction(degree) = ');
4 theta_deg = theta;
5 theta = DEG2RAD(theta);
6 alpha = cos(theta)/pi;
7
8 a=zeros(1,4);
9 b=zeros(1,4);
10 phs_offset=[0,236,279.3,-2.5]; %90
11 amp_offset=[0,0.67,0.36,0.11];
12 phs_offset_rad=DEG2RAD(phs_offset);
13 phs=zeros(1,4);
14
15 a(1)=0.6;
16 b(1)=0.8;
17 amp(1)=get_amplitude(a(1),b(1));
18 phs(1)=get_phase(a(1),b(1));
19
20 for(i=2:1:4)
21     amp(i)=amp(1)*(1-amp_offset(i));
22     phs(i)=phs(1)+(i-1)*alpha-(phs_offset_rad(i));
```

```
23         %---nonlinear calibration
24
25         [a(i),b(i)]=movephase(phis(i),amp(i));
26     end
27     phs_deg=RAD2DEG(phis);
28
29     a_bit=a;
30     b_bit=b;
31     %-----Nagitive Voltage
32     a_bit=a_bit+(2.5/256)*120;
33     b_bit=b_bit+(2.5/256)*120;
34
35     a_bit=round(a_bit./(2.5/256));
36     b_bit=round(b_bit./(2.5/256));
37
38
39     fid=fopen('Data.txt','a+');
40     for i=1:1:4
41         fprintf(fid,'%d',a_bit(i));
42         fprintf(fid,',');
43         fprintf(fid,'%d',b_bit(i));
44         fprintf(fid,',');
45     end
46     fprintf(fid,'%s\r','');
47     fid2=fopen('Data_deg.txt','a+');
48     fprintf(fid2,'');
49     fprintf(fid2,'%d',theta_deg);
50     fprintf(fid2,'');
51     fprintf(fid2,'%s',',');
52     fclose('all');
```

C.2 get_amplitude.m

```
1 function amplitude = get_amplitude(a,b)
2 amplitude = (a^2+b^2)^(1/2);
3 return
4 end
```

C.3 get_phase.m

```
1 function phase=get_phase(a,b)
2 phase=atan(b/a);
3 return
4 end
```

C.4 movephase.m

```
1 function [ a,b ] = movephase( ag,amp )
2   x = mod(ag,2*pi);
3   if x == pi/2
4       a=0;b=amp;return;
5   elseif x == pi*3/2
6       a=0;b=-amp;return;
7   end
8   a = abs(sqrt( amp^2/(1+(tan(x)^2)) ));
9   b = abs(sqrt( amp^2-a^2 ));
10  if x > pi/2 && x <= pi
11      a = -a;
12  elseif x>pi && x < pi*3/2
13      a = -a;b = -b;
14  elseif x>pi*3/2
15      b = -b;
16  end
17  return
18  end
```

C.5 readcsvfile.m

```
1 function [amp,phase]=readcsvfile(a,b,c,d)
2 aa=csvread(a);
3 bb=csvread(b);
4 cc=csvread(c);
5 dd=csvread(d);
6
7 num(:,1)=size(aa);
8 num(:,2)=size(bb);
9 num(:,3)=size(cc);
10 num(:,4)=size(dd);
11
12 minnum=min([num(1,1),num(1,2),num(1,3),num(1,4)]);
13
14 j=num(1,1)-minnum;
15 while(j>0)
16     aa(minnum+j,:)=[];
17     j=j-1;
18 end
19 j=num(1,2)-minnum;
20 while(j>0)
21     bb(minnum+j,:)=[];
22     j=j-1;
23 end
24 j=num(1,3)-minnum;
25 while(j>0)
26     cc(minnum+j,:)=[];
27     j=j-1;
28 end
29 j=num(1,4)-minnum;
30 while(j>0)
31     dd(minnum+j,:)=[];
32     j=j-1;
33 end
```

```
34
35 amp (: ,1)=aa (: ,2);
36 amp (: ,2)=bb (: ,2);
37 amp (: ,3)=cc (: ,2);
38 amp (: ,4)=dd (: ,2);
39
40 phase (: ,1)=aa (: ,1);
41 phase (: ,2)=bb (: ,1);
42 phase (: ,3)=cc (: ,1);
43 phase (: ,4)=dd (: ,1);
44
45 return;
46 end
```

C.6 calibration.m

```
1 function [amp_offset,phase_offset] = calibration( amp,phase
   ,k )
2 phase = phase.*k;
3 %four chanel,so i = 4
4 for i=1:1:4
5 %find the absolute max value,tmp is the index of the max
   value elements
6 tmp = find(diff(sign(diff(-abs(amp(:,i))))))==2)+1;
7
8 j=1;
9     while( j <= (length(tmp)) )
10         tmp_v(j) = abs(amp(tmp(j),i));
11         j=j+1;
12     end
13 %solve the average value of the max values
14 amp_offset(i)=mean(tmp_v);
15
16 %find the phase of the max values
17 %find the negative peak
18 tmp_n = find(diff(sign(diff(amp(:,i))))==2)+1;
19 %find the positive peak
20 tmp_p = find(diff(sign(diff(amp(:,i))))==-2)+1;
21
22 j=1;
23     while( j <= (length(tmp_n)) )
24         tmp_ph(j) = mod(tmp_n(j),2*pi)-1.5*pi;
25         j=j+1;
26     end
27
28 j=1;
29     while( j <= (length(tmp_n)) )
30         tmp_ph( (length(tmp_n))+j ) = mod(tmp_p(j),2*pi)
           -0.5*pi;
```

```
31         j=j+1;
32     end
33 %solve the average value of the max values phase
34 phase_offset(i)=mean(tmp_ph);
35
36 end
37
38 %calculate amp,phase offset
39 for(i=2:1:4)
40     amp_offset(i)=amp_offset(i)-amp_offset(1);
41     phase_offset(i)=phase_offset(i)-phase_offset(1);
42 end
43 amp_offset(1)=0;
44 phase_offset(1)=0;
45
46 return;
47 end
```

C.7 nonlinear_main.m

```

1 %for theta=50:-1:50
2 theta = input('desire pointing direction(degree) = ');
3 theta_deg = theta;
4 theta = DEG2RAD(theta);
5 %dn=0.5
6 alpha = cos(theta)/pi;
7 alpha_deg = RAD2DEG(alpha);
8
9 a=zeros(1,4);
10 b=zeros(1,4);
11 % amp_offset=[0,0.67,0.36,0.11];
12 % phs_offset=[0,236,279.3,-2.5]; %90
13 amp_offset=[0,0.67,0.36,0.11];
14 %phs_offset=[0,236,279.3,-2.5];
15 phs_offset_rad=DEG2RAD(phs_offset);
16 phs_offset=zeros(1,4);
17 phs=zeros(1,4);
18
19 a(1)=0.6;
20 b(1)=0.8;
21 amp(1)=get_amplitude(a(1),b(1));
22 phs(1)=get_phase(a(1),b(1));
23
24 for(i=2:1:4)
25     amp(i)=amp(1)*(1-amp_offset(i));
26     phs(i)=phs(1)+(i-1)*alpha-(phs_offset_rad(i));
27     [a(i),b(i)]=movephase(phs(i),amp(i));
28 end
29 phs_deg=RAD2DEG(phs);
30
31 a_bit=a;
32 b_bit=b;
33 %-----Nagtive Voltage

```

```
34 a_bit=a_bit+(2.5/256)*120;
35 b_bit=b_bit+(2.5/256)*120;
36
37 a_bit=round(a_bit./(2.5/256));
38 b_bit=round(b_bit./(2.5/256));
39
40
41 fid=fopen('Data.txt','a+');
42 for i=1:1:4
43 fprintf(fid,'%d',a_bit(i));
44 fprintf(fid,',');
45 fprintf(fid,'%d',b_bit(i));
46 fprintf(fid,',');
47 end
48 fprintf(fid,'%s\r','');
49 fid2=fopen('Data_deg.txt','a+');
50 fprintf(fid2,'');
51 fprintf(fid2,'%d',theta_deg);
52 fprintf(fid2,'');
53 fprintf(fid2,'%s',',');
54 fclose('all');
55
56 %verify
57 % for i=1:1:4
58 %     amp_v(i)=sqrt(a(i)^2+b(i)^2);
59 %     phase_v(i)=RAD2DEG(atan(b(i)/a(i)));
60 % end
61
62 %end
```

C.8 arrayfactor.m

```
1 N=input('Num. of elements = ')
2 epsi=pi/500:pi/500:2*pi;
3 AF=sin(N*epsi./2)./(sin(epsi./2));
4 plot(epsi,abs(AF))
5 xlabel('Epsi(rad)');
6 ylabel('|AF|');
```

C.9 pointingdirection.m

```
1 N=4;
2 dn=2;
3 theta_m=input('pointing direction(degree) = ');
4 theta=360:-1:1;
5 alfa=-2*pi*dn*cos(deg2rad(theta_m));
6 epsi=2*pi*dn*cos(deg2rad(theta))+alfa;
7 AF=abs(sin(N*epsi./2)./(N*sin(epsi./2)));
8
9 % obtain for drawing
10 for i=1:1:181
11 AF_0(182-i)=AF(i);
12 end
13 figure;
14 plot(theta,AF)
15 % figure;
16 % polar(theta,abs(AF.*def))
17 % figure;
18 % polar(theta,def)
```

C.10 drawing.m

```
1 % Calculated AF
2 semipolar_dB([-90:1:0,1:1:90],AF60,0,1,4,'-')
3
4 % Experiments data
5 semipolar_dB([-90:1:0,1:1:90],((mapminmax(patch)+1)./2)
6     ,-1,1,4,'-')
7
8 % Compare experimental data and theoretical data
9 % com = AF60 .* ((mapminmax(patch)+1)./2);
10 % semipolar_dB([-90:1:0,1:1:90],((mapminmax(com)+1)./2)
11     ,0,1,4,'r--')
12 % hold on
13 % semipolar_dB([-90:1:0,1:1:90],((mapminmax(patch60)+1)./2)
14     ,0,1,4,'-')
15 % hold off
```

C.11 semipolar_dB.m

```

1 %*****
2 %       semipolar_dB(theta,rho,rmin,rmax,rticks,line_style)
3 %*****

4 %       SEMIPOLAR_DB is a MATLAB function that plots 2-D
      patterns in
5 %       polar coordinates where:
6 %           -90          <= THETA (in degrees) <= 90
7 %           -infinity <  RHO   (in dB)       <  +
      infinity
8 %
9 %       Input Parameters Description
10 %       -----
11 %       - theta (in degrees) must be a row vector from -90
      to 90 degrees
12 %       - rho (in dB) must be a row vector
13 %       - rmin (in dB) sets the minimum limit of the plot (
      e.g., -60 dB)
14 %       - rmax (in dB) sets the maximum limit of the plot (
      e.g.,  0 dB)
15 %       - rticks is the # of radial ticks (or circles)
      desired. (e.g., 4)
16 %       - linestyle is solid (e.g., '-') or dashed (e.g.,
      '--')
17 %
18 %       Credits:
19 %           S. Bellofiore
20 %           S. Georgakopoulos
21 %           A. C. Polycarpou
22 %           C. Wangsvick
23 %           C. Bishop
24 %

```

```
25 %           Tabulate your data accordingly, and call
    semipolar_dB to provide the
26 %           2-D polar plot
27 %-----

28
29 function hpol = semipolar_dB(theta,rho,rmin,rmax,rticks,
    line_style)
30
31 % Convert degrees into radians
32 theta = theta * pi/180;
33
34 % Font size, font style and line width parameters
35 font_size = 16;
36 font_name = 'Times';
37 line_width = 1.5;
38
39 % Parameters initialization
40 count = 0;
41
42 for i=1:length(theta),
43     temp(i)=theta(length(theta)+1-i);
44 end;
45 theta=temp;
46
47 if nargin < 5
48     error('Requires 5 or 6 input arguments.')
49 elseif nargin == 5
50     if isstr(rho)
51         line_style = rho;
52         rho = theta;
53         [mr,nr] = size(rho);
54         if mr == 1
55             theta = 1:nr;
56         else
```

```
57             th = (1:mr)';
58             theta = th(:,ones(1,nr));
59         end
60     else
61         line_style = 'auto';
62     end
63 elseif nargin == 1
64     line_style = 'auto';
65     rho = theta;
66     [mr,nr] = size(rho);
67     if mr == 1
68         theta = 1:nr;
69     else
70         th = (1:mr)';
71         theta = th(:,ones(1,nr));
72     end
73 end
74 if isstr(theta) | isstr(rho)
75     error('Input arguments must be numeric.');
```

```
76 end
77 if any(size(theta) ~= size(rho))
78     error('THETA and RHO must be the same size.');
```

```
79 end
80
81 % get hold state
82 cax = newplot;
83 next = lower(get(cax,'NextPlot'));
84 hold_state = ishold;
85
86 % get x-axis text color so grid is in same color
87 tc = get(cax,'xcolor');
```

```
88
89 % Hold on to current Text defaults, reset them to the
90 % Axes' font attributes so tick marks use them.
91 fAngle = get(cax, 'DefaultTextFontAngle');
```

```
92 fName    = get(cax, 'DefaultTextFontName');
93 fSize    = get(cax, 'DefaultTextFontSize');
94 fWeight  = get(cax, 'DefaultTextFontWeight');
95 set(cax, 'DefaultTextFontAngle', get(cax, 'FontAngle'), ...
96     'DefaultTextFontName',    font_name, ...
97     'DefaultTextFontSize',    font_size, ...
98     'DefaultTextFontWeight',  get(cax, 'FontWeight') )
99
100 % only do grids if hold is off
101 if ~hold_state
102
103 % make a radial grid
104     hold on;
105 % v returns the axis limits
106 % changed the following line to let the y limits become
    negative
107     hhh=plot([0 max(theta(:))],[min(rho(:)) max(rho(:))
108             ]);
109     v = [get(cax,'xlim') get(cax,'ylim')];
110     ticks = length(get(cax,'ytick'));
111     delete(hhh);
112 % check radial limits (rticks)
113
114     if rticks > 10 % see if we can reduce the number
115         if rem(rticks,2) == 0
116             rticks = rticks/2;
117         elseif rem(rticks,3) == 0
118             rticks = rticks/3;
119         end
120     end
121
122 % define a circle
123     th = 0:pi/50:pi;
124     xunit = cos(th);
```

```
125         yunit = sin(th);
126 % now really force points on x/y axes to lie on them
    exactly
127     inds = [1:floor((length(th)-1)/4):length(th)];
128     xunits(inds(2:2:4)) = zeros(2,1);
129     yunits(inds(1:2:5)) = zeros(3,1);
130
131     rinc = (rmax-rmin)/rticks;
132
133 % label r
134 % change the following line so that the unit circle is
    not multiplied
135 % by a negative number. Ditto for the text locations.
136     for i=(rmin+rinc):rinc:rmax
137         is = i - rmin;
138         plot(xunit*is,yunit*is,'-','color',tc,'
            linewidth',0.15); % 0.5
139         text(is+rinc/20,-0.085*(rmax-rmin),[num2str
            (i)],'horizontalalignment','center' );
140         text(-(is+rinc/20),-0.085*(rmax-rmin),[
            num2str(i)],'horizontalalignment','center'
            );
141     end
142
143 % plot spokes
144     th = (0:6)*2*pi/12;
145     cst = cos(th); snt = sin(th);
146     cs = [-cst*0; cst];
147     sn = [-snt*0; snt];
148     plot((rmax-rmin)*cs,(rmax-rmin)*sn,'-','color',tc,'
            linewidth',0.15); % 0.5
149
150 % plot the ticks
151     tmp_sb = (rmax-rmin)/30; % Length of the ticks
152     th2 = (0:36)*2*pi/72;
```

```
153         cst2 = cos(th2); snt2 = sin(th2);
154         cs2 = [(rmax-rmin-tmp_sb)*cst2; (rmax-rmin)*cst2];
155         sn2 = [(rmax-rmin-tmp_sb)*snt2; (rmax-rmin)*snt2];
156         plot(cs2,sn2,'-','color',tc,'linewidth',0.15); %
           0.5
157
158 % annotate spokes in degrees
159 % Changed the next line to make the spokes long enough
160         rt = 1.1*(rmax-rmin);
161         for i = 1:max(size(th))
162             text(rt*cst(i),rt*snt(i),int2str(abs(i
               *30-120)), 'horizontalalignment', 'center' );
163             if i == max(size(th))
164                 loc = int2str(0);
165             else
166                 loc = int2str(180+i*30);
167             end
168         end
169 % set viewto 2-D
170         view(0,90);
171
172 end
173
174 % Reset defaults.
175 set(cax, 'DefaultTextFontAngle', fAngle, ...
176         'DefaultTextFontName', font_name, ...
177         'DefaultTextFontSize', fSize, ...
178         'DefaultTextFontWeight', fWeight );
179
180 % transform data to Cartesian coordinates.
181 % changed the next line so negative rho are not plotted
           on the other side
182
183 for i = 1:length(rho)
184     if (rho(i) > rmin)
```

```
185     count = count + 1;
186     xx(i) = (rho(i)-rmin)*cos(theta(i)+pi/2);
187     yy(i) = (rho(i)-rmin)*sin(theta(i)+pi/2);
188     else
189         xx(i) = 0;
190         yy(i) = 0;
191     end
192 end
193
194 % Text 'dB' at the center of the plot
195 % =====
196 htext = text(0,-0.085*(rmax-rmin),'dB','horizontalalignment
    ','center');
197 set(htext,'FontSize',font_size);
198
199 % plot data on top of grid
200 if strcmp(line_style,'auto')
201     q = plot(xx,yy);
202 else
203     q = plot(xx,yy,line_style,'linewidth',line_width);
204 end
205
206 if nargout > 0
207     hpol = q;
208 end
209 if ~hold_state
210     axis('equal');axis('off');
211 end
212
213 % reset hold state
214 if ~hold_state, set(cax,'NextPlot',next); end
```

C.12 patchparacalutor.m

```
1 c=3e8;
2 ep_r=input('relative permittive=');
3 f=input('frequency=');
4 h=input('height=')
5 w=((ep_r+1)/2)^(-0.5)*c/(2*f);
6 ep_e=((ep_r+1)/2)+((ep_r-1)/2)*((1+(10*h/w))^-0.5));
7 delta_l=0.412*h*(ep_e+0.3)*(w/h+0.264)/((ep_e-0.258)*(w/h
+0.8));
8 l=c/(2*f*(ep_e^0.5))-2*delta_l
```

Reference

- [1] G. Tsoulos, “Smart antennas for mobile communication systems: benefits and challenges,” *Electronics Communication Engineering Journal*, vol. 11, pp. 84 – 94, Apr. 1999.
- [2] J. S. Thompson, P. M. Grant, and B. Mulgrew, “Performance of antenna array receiver algorithms for CDMA,” *Signal Processing*, vol. 68, no. 1, pp. 23 – 41, 1998.
- [3] J. Choi, “Beamforming for the multiuser detection with decorrelator in synchronous CDMA systems: approaches and performance analysis,” *Signal Processing*, vol. 60, no. 2, pp. 195 – 211, 1997.
- [4] P. O. C. Richard B. Ertel, “Overview of spatial channel models for antenna array communication systems,” *Personal Communications, IEEE*, vol. 5, no. 1, pp. 10 – 22, 1998.
- [5] Y. W. Horiki, “A study of automatic steering for suppression of ghosts in TV reception,” *Antennas and Propagation Society International Symposium, 2002. IEEE*, vol. 2, p. 110, 2002.
- [6] Y.-S. Kim and S.-H. Hwang, “Impact analysis of array weight error on the antenna array aided multicarrier DS-CDMA with synchronous uplink transmissions,” *AEU - International Journal of Electronics and Communications*, vol. 64, no. 4, pp. 372 – 376, 2010.
- [7] A. Quintero, D. Y. Li, and H. Castro, “A location routing protocol based on smart antennas for ad hoc networks,” *Journal of Network and Computer Applications*, vol. 30, no. 2, pp. 614 – 636, 2007.
- [8] N. T.-T. Tin, “An experimental system for characterizing wideband CDMA vector channels and smart antennas,” Master’s thesis, Queen’s University Kingston, Ontario, Canada, 2000.

- [9] A. Alexiou and M. Haardt, "Smart antenna technologies for future wireless systems: trends and challenges," *Communications Magazine, IEEE*, vol. 42, pp. 90 – 97, Sep. 2004.
- [10] R. Kohno, "Spatial and temporal communication theory using adaptive antenna array," *Personal Communications, IEEE*, vol. 5, pp. 28 – 35, Feb. 1998.
- [11] J.-W. Zhang, "The adaptive algorithms of the smart antenna system in future mobile telecommunication systems," in *Antenna Technology: Small Antennas and Novel Metamaterials, 2005. IWAT 2005. IEEE International Workshop on*, pp. 347 – 350, Mar. 2005.
- [12] M. Chryssomallis, "Smart antennas," *Antennas and Propagation Magazine, IEEE*, vol. 42, pp. 129 – 136, Jun. 2000.
- [13] S. Hossain, M. Islam, and S. Serikawa, "Adaptive beamforming algorithms for smart antenna systems," in *Control, Automation and Systems, 2008. ICCAS 2008. International Conference on*, pp. 412 – 416, Oct. 2008.
- [14] C. M. R. L. Cupo, G. Golden, "A four-element adaptive antenna array for IS-136 PCS base stations," in *IEEE VTC'97*, pp. 1577 – 1581, 1997.
- [15] J. H. Winters, "Forward link smart antennas and power control for IS-136," in *5th Stanford Smart Antennas Mobile Wireless Commun. Workshop*, 1998.
- [16] P. Lehne, O. Rostbakken, and M. Pettersen, "Estimating smart antenna performance from directional radio channel measurements," in *Vehicular Technology Conference, 1999. VTC 1999 - Fall. IEEE VTS 50th*, vol. 1, pp. 57 – 61, 1999.
- [17] S. K. and P. J., "Final report on ACTS," tech. rep., European Commission, 2000. <http://www.esma.europa.eu/system/files/2012-137.pdf>.
- [18] T. O. Chen Sun, Jun Cheng, *Handbook on Advancements in Smart Antenna Technologies for Wireless Networks*, ch. 19, pp. 398 – 402. United States of America by Information Science Reference, 2008.
- [19] T. S. Yoshio K. and T. I., "The software antenna: A new concept of kaleidoscopic antenna in multimedia radio and mobile computing era," *IEICE Trans. Commun.*, vol. E80-B, no. 8, pp. 1214 – 1217, 1997.

- [20] J. Pioch, "Arraycomm and sumitomo electric collaborate to supply advanced radio head technology to the WIMAX market," tech. rep., ArrayComm, Mar. 2010.
- [21] ArrayComm, "IntelliCell[®]: A fully adaptive approach to smart antennas," tech. rep., ArrayComm, Incorporated, 2480 North First Street San Jose, CA 95131 USA, 2002.
- [22] S. Ellingson, "Antenna design and site planning considerations for MIMO," in *Vehicular Technology Conference, 2005. VTC-2005-Fall. 2005 IEEE 62nd*, vol. 3, pp. 1718 – 1722, Sep. 2005.
- [23] A. Petosa, P. Strickland, and J. Wight, "Microstrip antenna array for mobile satellite communications," in *Antennas and Propagation Society International Symposium, 1992. AP-S. 1992 Digest. Held in Conjunction with: URSI Radio Science Meeting and Nuclear EMP Meeting., IEEE*, vol. 1, pp. 503 – 506, Jun. 1992.
- [24] S. R., "Smart antennas in packet switched indoor SDMA networks," Master's thesis, McMaster University, Sep. 1997.
- [25] M. Peng, G. Xu, W. Wang, and H.-H. Chen, "McWiLL: A new mobile broadband access technology for supporting both voice and packet services," *Systems Journal, IEEE*, vol. 4, pp. 495 – 504, Dec. 2010.
- [26] H. Fu, P. Gao, and H. Ding, "The reform schema of TD-SCDMA standard by CDMA/TDMA," in *Wireless Communications, Networking and Mobile Computing, 2008. WiCOM '08. 4th International Conference on*, pp. 1 – 6, Oct. 2008.
- [27] K. Kammerlander, "Benefits and implementation of TD-SCDMA," in *Communication Technology Proceedings, 2000. WCC - ICCT 2000. International Conference on*, vol. 2, pp. 1013 – 1016 vol.2, 2000.
- [28] D. Rabideau and P. Parker, "Ubiquitous mimo multifunction digital array radar," in *Signals, Systems and Computers, 2003. Conference Record of the Thirty-Seventh Asilomar Conference on*, vol. 1, pp. 1057 – 1064, Nov. 2003.
- [29] T. Y. Kukino K., "The auto calibration of phase and amplitude variation of the ransmitter/receiver circuits with AGC using LMS algorithm for DS-CDMA array antenna," tech. rep., IEICE Technical Report, RCS 2000-31, Jun. 2000.

- [30] M. S.Kobayakawa and Y.Tanaka, "A blind calibration method for an adaptive array antenna in DS-CDMA systems using and MMSE algorithm," in *IEEE Vehicular Technology Conference*, vol. 1, pp. 21 – 25, 2000.
- [31] J. S. Todd W.Nuteson, Jeffrey E.Stocker, "Performance characterization of FPGA techniques for calibration and beamforming in smart antenna applications," *IEEE Trans.Microwave Theory and Techniques*, vol. 50, pp. 3043 – 3051, 2002.
- [32] H. G. S. Drabowitch, A. Papiernik, *Modern Antennas*, ch. 11, pp. 378 – 382. Springer, 2nd ed., 2005.
- [33] N. Toyama, "A simple method of reducing grating lobes," in *Antennas and Propagation Society International Symposium, 2004. IEEE*, vol. 1, pp. 141 – 144, Jun. 2004.
- [34] H. Zhang and H. Xin, "Designs of dual-band wilkinson power dividers with flexible frequency ratios," in *Microwave Symposium Digest, 2008 IEEE MTT-S International*, pp. 1223 – 1226, Jun. 2008.
- [35] Agilent, *Agilent E8267D PSG Manual*, Aug. 2010.
- [36] Analog Devices, *0.8 GHz to 2.5 GHz Quadrature Modulator AD8346 Manual*, 2005.
- [37] Analog Devices, *Precision Micropower Low Dropout Voltage References Ref19x Series Manual*, 2010.
- [38] K. Morshed, D. Karmokar, and A. Numan-Al-Mobin, "Numerical analysis of impedance matched inverted-L antennas for Wi-Fi operations," in *Computers and Information Technology, 2009. ICCIT '09. 12th International Conference on*, p-p. 691 – 696, Dec. 2009.
- [39] J. Tie-hua, S. Dong-lin, D. Ke-jia, W. Guo-yu, and Z. yan, "Design of the low-profile inverted-f antenna with multi-parasitic elements," in *Antennas, Propagation EM Theory, 2006. ISAPE '06. 7th International Symposium on*, pp. 1 – 4, Oct. 2006.
- [40] Y. Ren and C. Lai, "Wideband antennas for modern radar systems," tech. rep., Advanced A&M Technologies, Inc. U.S.A, 2004.
- [41] H. G. S. Drabowitch, A. Papiernik, *Modern Antennas*, ch. 4, p. 86. Springer, 2nd ed., 2005.

- [42] K. Dandekar, H. Ling, and G. Xu, "Smart antenna array calibration procedure including amplitude and phase mismatch and mutual coupling effects," in *Personal Wireless Communications, 2000 IEEE International Conference on*, pp. 293 – 297, 2000.